



Modelling the  
mechanical behaviour  
of sodium borohydride  
before during and  
after time  
consolidation using  
DEM

A.A. Kalpoe



# MODELLING THE MECHANICAL BEHAVIOUR OF SODIUM BOROHYDRIDE BEFORE DURING AND AFTER TIME CONSOLIDATION USING DEM

by

ARVIND KALPOE

## Master Thesis

in partial fulfilment of the requirements for the degree of

**Master of Science**  
in Mechanical Engineering

at the Department Maritime and Transport Technology of Faculty Mechanical Engineering of Delft  
University of Technology

to be defended publicly on June, 5th, 2024, at 13:00 PM

Student number:	4726464	
MSc track:	Multi-Machine Engineering	
Report number:	2024.MME.8936	
Supervisors:	Ir. M.C. van Bente, Prof. dr. ir. D.L. Schott	
Thesis committee:	Prof. dr. ir. D.L. Schott, Ir. M.C. van Bente, Dr. L. Botto	TU Delft committee chair, ME TU Delft supervisor, ME TU Delft external member, ME
Date:	May 30, 2024	

An electronic version of this thesis is available at <http://repository.tudelft.nl/>

It may only be reproduced literally and as a whole. For commercial purposes only with written authorization of Delft University of Technology. Requests for consult are only taken into consideration under the condition that the applicant denies all legal rights on



# PREFACE

Dear reader,

This thesis is the final step for completing my Master of science in Mechanical Engineering at the faculty of Mechanical Engineering (previously known as 3mE) from Delft University of Technology. This master, track Multi-Machine Engineering, journey started in the middle of the covid-19 pandemic in 2020, but after successfully achieving a Master of Science in Science Education and Communication at the Faculty of Applied Science from Delft University of Technology, this master's thesis will be the final step towards completion of my academic career.

During the master my interest for bulk solids and DEM modelling was triggered after following two courses related to these topics. Therefore, I chose to do a research assignment related to DEM and this master thesis. Currently, a lot has been said about climate change and an energy transition (reduction of emissions) is necessary. The topic of this thesis gave me a great opportunity to contribute a small portion towards that goal.

I started my research under the supervision of Marcel van Bente, a PHD-researcher in the department of Maritime and Transport Technology. He was my daily supervisor and working together with him on this difficult topic was quite refreshing. He always had insightful comments and challenged me to search a bit deeper for explanations. My other supervisor Dingena Schott's input was related towards presenting the work and keeping me on the right track. Furthermore, I want to thank Gert-Jan van Selm for providing me with some insightful information and talks about DEM modelling.

Finally, I want to thank my parents, brother, family and friends for supporting me through not only the master thesis, but also throughout the almost 7-year journey at Delft University of Technology.

*Arvind Kalpoe  
Delft, June 2024*



# SUMMARY

Presently, global warming is more visible than ever and climate change is seen as an urgent problem, both socially and politically. A potential solution is the reduction of (carbon) emissions and a goal of carbon neutrality has been set for 2030. To ensure this goal an energy transition is required and alternative fuels can be considered. One of the promising fuels is hydrogen. Currently, hydrogen is already used, but not in large margins for multiple reasons such as safety risks, infrastructure problems, availability, efficiency and cost. Another new potential solution to store hydrogen is to use a hydrogencarrier. The main topic of this thesis is related to such a hydrogencarrier, sodium borohydride ( $\text{NaBH}_4$ ).  $\text{NaBH}_4$  is already known for years and the chemical properties are well documented, but the bulk behaviour is not well-known. From initial research and handling of the material in the lab, it became clear that  $\text{NaBH}_4$  is affected by humidity, temperature and time consolidation, but the exact effects are not described in the literature. Also, a model can be used to look more in detail at the particle level. In the literature, only one paper tried to model the behaviour of  $\text{NaBH}_4$  and this paper did not consider the effects of temperature, humidity and time consolidation. Therefore, this thesis focuses on modelling the effect of time consolidation on  $\text{NaBH}_4$ , to better understand the behaviour of  $\text{NaBH}_4$  for the use of alternative fuels in the maritime industry and provide a method to model time consolidation. More specifically, the goal of this thesis is to model the mechanical behaviour before, during and after time consolidation.

The main research question of this study is *How to model the mechanical behaviour of sodium borohydride ( $\text{NaBH}_4$ ) before, during and after time consolidation using the discrete-element method?*

To answer the main research question 5 subquestions, which can be seen below, were formulated:

1. What is time consolidation, and what are the causes and potential results of time consolidation?
2. What is a suitable method to measure time consolidation?
3. How can time consolidation be incorporated in DEM modelling?
4. How does time consolidation affect sodium borohydride?
5. What is a comprehensive method to capture time consolidation effects on  $\text{NaBH}_4$  using DEM?

The approach of this research was a literature study, followed by time consolidation experiments, modelling time consolidation for  $\text{NaBH}_4$  and calibrating and verifying the model. From the literature study, it became clear that limited research concerning the mechanical behaviour of  $\text{NaBH}_4$  was conducted. Therefore, measurements of time consolidation effects for  $\text{NaBH}_4$  need to be performed. In this thesis Schulze's Ring Shear Tester (RST) was used to measure these effects, this data is required for calibration and verification of the model. The method used for modelling time consolidation is the Discrete Element Method (DEM), and the selected contact model is the Edinburgh Elasto-Plastic Adhesive (EEPA) model. The model takes stress history of the particles into consideration and could potentially be used for modelling the effect of time consolidation on  $\text{NaBH}_4$ . It is important to note that the RST simulation model completely mimics the experimental procedure, except for the time consolidation, this is captured by changing different parameters of the simulation model to reduce the computational cost. Therefore, the particles do not need to be subjected to a load for a certain amount of consolidation time, but this method enables the instant creation of a time-consolidated particle bed. The relationships can be used to directly create a particle bed in a simulation model that mimics real-life applications and the influence in the process, for example, storing  $\text{NaBH}_4$  in a silo can be analysed.

The final results of this thesis are an approach to determine a relationship for the two most influential parameters in the model, the static friction and surface energy, over time and a relationship for these parameters for a bounded range. The found relationship is valid for the experimental time range of 0 to 1 hours of consolidation. With the relationships, it is possible to artificially create a particle bed after a certain consolidation time and use these particle beds to analyse a real-life situation such as storing of material in a silo.

Some recommendations are made for this thesis, the first one is to perform more experiments, using different preshear levels, normal stresses, consolidation stresses and consolidation times to get more insight into the influence of time consolidation on  $\text{NaBH}_4$ . These experimental results can be used in the model to gain a relationship for the most influential factors for  $\text{NaBH}_4$  over a longer time period. It is expected that for more data points an exponential fit for the parameters over time can be found, to support this claim more research with more experiments and simulations should be performed.

## SUMMARY (IN DUTCH)

Vandaag de dag zijn de resultaten van de opwarming van de aarde zichtbaar en zijn deze zowel een sociaal als politiek probleem. Het verlagen van de uitstoot (onder andere CO<sub>2</sub>) is nodig en het streven is om dit voor elkaar te krijgen voor 2030. Een energie transitie kan bijdragen aan de reductie van de uitstoot. Alternatieve brandstoffen kunnen een oplossing bieden voor het verlagen van de uitstoot en een hoopvol alternatief is waterstof. Waterstof wordt vandaag de dag al jaren gebruikt, maar er zijn diverse redenen waarom dit niet op grote schaal wordt gebruikt. Deze redenen zijn veiligheidsrisico's, problemen met de infrastructuur, beschikbaarheid van waterstof, efficiëntie en kosten. Een nieuwe methode om waterstof op te slaan is het gebruik van een waterstofdrager. In deze scriptie is het onderwerp een waterstofdrager, natriumboorhydride (NaBH<sub>4</sub>). NaBH<sub>4</sub> is al jaren beschikbaar en de chemische eigenschappen zijn bekend, maar het gedrag van het materiaal als het in bulk voorkomt is niet goed bekend. Uit het eerste onderzoek en omgang met het materiaal werd duidelijk dat NaBH<sub>4</sub> beïnvloed wordt door temperatuur, luchtvochtigheid en tijdsconsolidatie. De precieze effecten zijn niet gevonden in de literatuur. Een simulatie model kan worden gebruikt om het gedrag van een materiaal op deeltjes niveau te analyseren. In de literatuur is één poging gevonden om gedrag van NaBH<sub>4</sub> te modelleren. Deze studie hield geen rekening met het effect van tijdsconsolidatie. In deze scriptie wordt een poging gedaan om effecten van tijdsconsolidatie op NaBH<sub>4</sub> beter in kaart te brengen en een methode voorgesteld om deze tijdsconsolidatie effecten te modelleren.

Het doel van deze scriptie is het modelleren van het mechanisch gedrag van NaBH<sub>4</sub> voor, tijdens en na tijdsconsolidatie met het gebruik van de Discrete Element Method (DEM).

De methodologie die in deze scriptie is gebruikt begon met een literatuurstudie, gevolgd door tijdsconsolidatie experimenten, het modelleren van tijdsconsolidatie en het kalibreren en verifiëren van het DEM model. De conclusie van het literatuuronderzoek was dat er niet veel onderzoek is gedaan naar het mechanisch gedrag van NaBH<sub>4</sub>. Om deze reden zijn de tijdsconsolidatie experimenten een essentieel onderdeel van dit onderzoek, omdat deze informatie nodig is voor het kalibreren en verifiëren van het DEM model. Schulzes Ring Shear Tester (RST) is gebruikt om tijdsconsolidatie experimenten uit te voeren. Om DEM te kunnen gebruiken is het selecteren van een contact model essentieel. Het geselecteerde model is het Edinburgh Elasto-Plastic Adhesive (EEPA) model. Dit model houdt rekening met de spannings-geschiedenis van de deeltjes en zou hierdoor mogelijk gebruikt kunnen worden om het effect van tijdsconsolidatie (op NaBH<sub>4</sub>) te modelleren. Gedurende de tijdsconsolidatie experimenten zijn er drie stappen, preshearing, opslaan onder een bepaalde verticale spanning en afschuiving tot falen. In het DEM model vinden alleen de eerste en de derde stap plaats en wordt de tijdsconsolidatie nagebootst, door het aanpassen van de twee meest invloedrijke parameters is het mogelijk om direct een tijds geconsolideerd materiaal bed te creëren en dit zorgt voor een efficiëntere manier van tijdsconsolidatie modelleren. De relatie voor de twee meest invloedrijke parameters over de tijd zijn ook in deze scriptie onderzocht (en gevonden voor een consolidatie tijd tussen 0 en 1 uur) en deze relaties bieden de mogelijkheid om direct een tijds geconsolideerd materiaal bed te creëren. Dit materiaal bed kan worden gebruikt voor real-life toepassingen zoals het opslaan van NaBH<sub>4</sub> in een silo.



# CONTENTS

<b>Preface</b>	<b>5</b>
<b>Summary</b>	<b>7</b>
<b>Summary</b>	<b>9</b>
<b>Nomenclature</b>	<b>13</b>
<b>List of Figures</b>	<b>17</b>
<b>List of Tables</b>	<b>19</b>
<b>1 Introduction</b>	<b>1</b>
1.1 Background . . . . .	1
1.2 Problem definition and research questions . . . . .	2
1.3 Methodology . . . . .	3
1.4 Outline . . . . .	3
<b>2 Literature study</b>	<b>7</b>
2.1 Measuring time consolidation . . . . .	7
2.1.1 Measuring equipment time consolidation . . . . .	7
2.1.2 Defining time consolidation . . . . .	10
2.2 Caking . . . . .	13
2.2.1 Amorphous caking . . . . .	14
2.2.2 Humidity caking . . . . .	14
2.2.3 Mechanical caking . . . . .	15
2.3 Measuring bulk behaviour of sodium borohydride . . . . .	16
2.4 Modelling of time consolidation . . . . .	16
2.4.1 Discrete Element Method . . . . .	16
2.4.2 Hertzian repulsion, viscous damping and JKR cohesion model . . . . .	17
2.4.3 Edingburgh Elasto-Plastic Adhesive model . . . . .	18
2.5 Modelling of sodium borohydride (NaBH <sub>4</sub> ) . . . . .	20
2.6 Concluding remarks: literature gap . . . . .	20
<b>3 Time consolidation experiment</b>	<b>23</b>
3.1 Experimental setup . . . . .	23
3.2 Design of experiments . . . . .	24
3.3 Experimental results . . . . .	25
3.4 Concluding remarks . . . . .	28
<b>4 Modeling time consolidation</b>	<b>29</b>
4.1 Method for modelling time consolidation . . . . .	29
4.1.1 Calibration and verification framework . . . . .	31
4.2 The DEM model: Time consolidation ring shear test . . . . .	32
4.2.1 The contact model . . . . .	32
4.2.2 Scaling . . . . .	34
4.2.3 Simulation plan . . . . .	34
4.2.4 Reference case . . . . .	36
4.3 Sensitivity analysis . . . . .	37
4.3.1 Results sensitivity analysis . . . . .	37
4.4 Calibration and verification Rotation Restriction case . . . . .	40
4.4.1 Procedure calibration . . . . .	41
4.4.2 Results Rotation Restriction case and extrapolation . . . . .	44

4.5	Calibration and verification Rolling model type C case . . . . .	51
4.5.1	Results Rolling type C and extrapolation . . . . .	52
4.6	Concluding remarks . . . . .	53
<b>5</b>	<b>Discussion</b>	<b>55</b>
5.1	Discussion time consolidation experiment results . . . . .	55
5.2	Discussion DEM modelling results . . . . .	56
<b>6</b>	<b>Conclusion and recommendations</b>	<b>59</b>
6.1	Conclusion . . . . .	59
6.2	Recommendations . . . . .	61
<b>A</b>	<b>Scientific Paper</b>	<b>63</b>
<b>B</b>	<b>Experimental confidence intervals</b>	<b>65</b>
<b>C</b>	<b>Sensitivity analysis 2</b>	<b>69</b>
<b>D</b>	<b>Contour plots Rolling type C</b>	<b>73</b>
<b>E</b>	<b>Results Rotation Restriction case optimised parameter set search and extrapolation</b>	<b>75</b>
<b>F</b>	<b>Results Rolling type C case optimised parameter set search and extrapolation</b>	<b>81</b>
	<b>References</b>	<b>87</b>





# NOMENCLATURE

C	degree Celsius
$\phi_{lin}$	slope of linearized yield locus
$\phi_t$	angle of internal friction
$\rho_b$	bulk density
$\sigma$	normal stress
$\sigma_1$	Consolidation stress
$\sigma_c$	unconfined yield strength
$\sigma_{pre}$	Preshear stress
$\tau$	shear stress
CG	Coarse Graining
DEM	Discrete Element Method
DOE	Design Of Experiments
EEPA	Edinburgh Elasto-Plastic Adhesive
H <sub>2</sub>	hydrogen
K	Kelvin
KPI	Key performance indicator
KaBH <sub>4</sub>	potassium borohydride
NH <sub>3</sub>	ammonia
NaBH <sub>4</sub>	sodium borohydride
PSD	Particle Size Distribution
RC	Rolling model type C
RR	Rotation Restriction
RST	Ring Shear Tester
TYL	time yield locus
T <sub>g</sub>	glass temperature
YL	yield locus

e	coefficient of restitution
ff <sub>c</sub>	flow function / flowability
wt%	weight percentage

# LIST OF FIGURES

1.1	Experimental plan for research on sodium borohydride	2
1.2	Outline	5
2.1	Shear tester classifications	8
2.2	Schematic overview of Jenike shear cell	8
2.3	Ring shear tester	9
2.4	Uniaxial test	10
2.5	Schematic overview of stresses in ring shear test	11
2.6	Yield locus	11
2.7	Time yield locus	12
2.8	Schematic overview of stresses in time consolidation experiment	12
2.9	Flow function ranges	13
2.10	Different caking mechanisms and (possible) internal and external influential factors for lactose	13
2.11	Amorphous caking	14
2.12	Sintering	14
2.13	Moisture absorption vs Relative Humidity	15
2.14	Influential factors for amorphous, humidity and mechanical caking	15
2.15	General soft-particle DEM approach	17
2.16	Graphical representation of the (a) particle overlap $h$ (b) effective overlap parameter $h^*$ (c) scaling parameter $\alpha$ (d) total contact force model	19
2.17	Graphical representation of contact model for the normal contact force-displacement function (a) non-linear (b) linear	19
2.18	Contact model for sodium borohydride used by Nagar et al	20
3.1	Consolidation bench	23
3.2	Schulze's Ring shear Tester	23
3.3	General representation of Design Of Experiments for performed time consolidation experiment	24
3.4	Time yield locus all data points for sodium borohydride (N=3)	25
3.5	Time yield locus data points after filtering with the threshold value for sodium borohydride (N=3)	25
3.6	(Time) Yield Locus sodium borohydride constructed with all data points (N=3)	26
3.7	(Time) Yield Locus sodium borohydride constructed after filtering with the threshold value (N=3)	26
3.8	Final results for (time) yield loci with an 80 % confidence interval (N=3)	26
4.1	Generic flowchart for modelling time consolidation in DEM	30
4.2	Framework for calibration and verification of time consolidation for $\text{NaBH}_4$ using DEM	31
4.3	Filled shear cell in EDEM	32
4.4	Volume vs diameter for the powder (red) and granular form (blue) of $\text{NaBH}_4$	34
4.5	Simulation plan for calibration and verification of DEM model	35
4.6	Design Of Experiments for sensitivity analysis	37
4.7	Shear stress vs (a) static friction (b) surface energy (c) constant pull-off force (d) static friction and surface energy (e) static friction and constant pull-off force (f) constant pull-off force and surface energy	39
4.8	Calibration and verification for Rotation Restriction case	40
4.9	Contour plot KPI shear stress for normal stress 1600 Pa Rotation Restriction case	42
4.10	Contour plot shear stress for normal stress 3200 Pa Rotation Restriction case	43
4.11	Surface energy vs static friction parameter set optimisation for 1 hour consolidation Rotation Restriction case	43
4.12	Surface energy vs static friction parameter set optimisation for 0 hour consolidation Rotation Restriction case	44

4.13	Results potential fits of experimental data of 1600 Pa normal stress	45
4.14	Results potential fits of experimental data of 3200 Pa normal stress	45
4.15	Shear stress vs time second order polynomial fit for experimental data	47
4.16	Potential fits for static friction vs time Rotation Restriction case	47
4.17	Static friction/surface energy vs time fit Rotation Restriction case (scaled)	49
4.18	Static friction/surface energy vs time fit Rotation Restriction case (unscaled)	50
4.19	Calibration and verification for Rolling type C case	51
4.20	Static friction vs time fit Rolling type C case (scaled)	52
4.21	Static friction vs time fit Rolling type C case (unscaled)	53
B.1	Shear stress vs normal stress 400 Pa confidence intervals 80-95% for 0.5 and 1.0 hour of consolidation	65
B.2	Shear stress vs normal stress 800 Pa confidence intervals 80-95% for 0.5 and 1.0 hour of consolidation	66
B.3	Shear stress vs normal stress 1600 Pa confidence intervals 80-95% for 0.5 and 1.0 hour of consolidation	67
B.4	Shear stress vs normal stress 3200 Pa confidence intervals 80-95% for 0.5 and 1.0 hour of consolidation	68
C.1	Shear stress vs static friction (one-factor analysis)	69
C.2	Shear stress vs plasticity ratio (one-factor analysis)	70
C.3	Shear stress vs surface energy (one-factor analysis)	70
C.4	Shear stress vs static friction and surface energy (two-factor analysis)	71
C.5	Shear stress vs static friction and plasticity ratio (two-factor analysis)	71
C.6	Shear stress vs surface energy and plasticity ratio (two-factor analysis)	72
D.1	Contour plot Shear stress for normal stress 1600 Pa Rolling type C case	73
D.2	Contour plot Shear stress for normal stress 3200 Pa Rolling type C case	74
E.1	Surface energy vs static friction parameter set optimisation for 0.5 hour consolidation Rotation Restriction case	75
E.2	Shear stress vs time fit for experimental data	76
E.3	Surface energy vs time potential fits Rotation Restriction case	78
E.4	Static friction/surface energy vs time fit Rotation Restriction case (scaled)	78
E1	Surface energy vs static friction parameter set optimisation for 0 hour consolidation Rolling type C case	81
E2	Surface energy vs static friction parameter set optimisation for 0.5 hour consolidation Rolling type C case	82
E3	Surface energy vs static friction parameter set optimisation for 1 hour consolidation Rolling type C case	82
E4	Static friction vs time potential fits for Rolling type C case (optimised parameter set 1)	84
E5	Static friction vs time potential fits for Rolling type C case (optimised parameter set 2)	84
E6	Static friction vs time fit Rolling type C case (scaled)	85

# LIST OF TABLES

1.1	Volumetric and gravimetric density of energy carriers and different storing methods for hydrogen	2
2.1	Ring shear test results: influence of different moisture levels on NaBH <sub>4</sub> powder (preshear 4 kPa)	16
3.1	Time consolidation experiment input parameters	24
3.2	Flow properties for different consolidation times (N=3)	27
3.3	Angle of internal friction/slope of linearized yield locus (N=3)	27
4.1	Constant input parameters in DEM model	33
4.2	Variable input parameters in DEM	33
4.3	Scaling particle size with a scaling factor of 7	34
4.4	Rayleigh time step results	36
4.5	Reference simulation input parameters and result (in bold) 95% confidence interval	36
4.6	Levels (low, medium and high) for most influential parameters used in sensitivity analysis	37
4.7	Shear stress values for calibration of time consolidation	41
4.8	Calibration range Rotation Restricted case	41
4.9	Results parameter set optimisation Rotation Restriction case	44
4.10	Results $\zeta$ analysis for static friction Rotation Restriction case	48
4.11	Calibration range Rolling type C	52
4.12	Results parameter set optimisation Rolling type C case	52
5.1	Angle of internal friction/slope of linearized yield locus (N=3)	55
5.2	Flow properties for different consolidation times (N=3)	56
5.3	Ring shear test results: influence of different moisture levels on NaBH <sub>4</sub> powder (preshear 4 kPa)	56
5.4	Final results Rotation Restriction and Rolling type C cases (scaled)	57
5.5	Final results Rotation Restriction and Rolling type C cases (unscaled)	57
E.1	Results parameter set optimisation Rotation Restriction case	75
E.2	Results $\zeta$ analysis for surface energy Rotation Restriction case	77
E1	Static friction vs time potential fits for Rolling type C case	83



# 1

## INTRODUCTION

### 1.1. BACKGROUND

Currently, climate change is one of the main challenges that humanity is facing. Climate change is partly caused by the emission after usage of fossil fuels [1, 2], hence an energy transition (reduction of carbon emissions) is required. The political goal is to have carbon neutrality in 2030. To fulfill this goal it can help to find renewable energy sources to replace fossil fuels with. The maritime sector is responsible for 3% of the global greenhouse gas emissions [3] and the International Maritime Organization (IMO) formulated a goal to reduce the emissions by 70% in 2050 with respect to the levels of 2008 [4]. One of the most promising alternative energy sources (in the maritime sector) is hydrogen ( $H_2$ ) [5].

There are three methods to store hydrogen: compressed, liquefied and a combination of the two cryo-compressed. The first method stores hydrogen as a gas, using pressures up to 700 bar at ambient temperature. To this end, high-strength storage tanks are required, and this is not without safety risks [6]. Liquefied hydrogen storage provides some benefits in comparison to the compression of hydrogen. It has a higher volumetric and gravimetric density and no safety risks due to high pressures. However, it still has some challenges. For liquifying hydrogen it is required to cool it down to  $-253\text{ }^\circ\text{C}$  and also to store the hydrogen ortho-para-hydrogen conversion is a major challenge [7]. Cryo compression storage is a combination of both compressed and liquefied hydrogen storage. It uses the benefits of both methods and also avoids some downfalls. For cryo-compression storage, the hydrogen is stored in a compression tank at a lower pressure than for compressed hydrogen storage (up to 350 bar) and with higher temperatures in comparison to liquefied hydrogen storage (up to 63 K). Cryo-compression storage provides the possibility to store hydrogen with a higher density than both liquid hydrogen and compressed hydrogen gas [8, 9]. Cryo-compression showed more potential and had fewer safety hazards in comparison to the first two methods. However, three major challenges remain infrastructure, availability, and cost [10].

A more promising approach, to the three mentioned methods for storing hydrogen, is using a hydrogen carrier. An example of a hydrogen carrier is ammonia ( $NH_3$ ), which is the most proposed by researchers and companies [11]. There are more potential hydrogen carriers such as  $NaBH_4$  and  $KBH_4$ . In Table 1.1 the gravimetric and volumetric density of the different processes and hydrogen carriers can be seen. Sodium borohydride ( $NaBH_4$ ) showed promising theoretical results (10% wt [12, 13]) in storing hydrogen and can therefore be used as an alternative fuel for the future [14]. In the maritime sector it can be used to replace fossil fuels [15]. However, to this day researchers are searching for a way to commercialize the usage of  $NaBH_4$  in material science, environmental fields, and energy-based applications [16].

$NaBH_4$  is a deliquescent hygroscopic material, it is soluble in water [18].  $NaBH_4$  is initially used as a reagent in the chemical industry for the reduction of aldehydes and ketones into alcohols [19, 20].

Bulk behaviour of  $NaBH_4$  in both powder and granular form remains unknown. Despite this, knowledge regarding bulk behaviour is important for designing storing and transporting equipment. Modelling of bulk behaviour using the Discrete Element Method (DEM) can speed up the process of optimization for design of equipment and make more accurate decisions for storing and handling  $NaBH_4$ . However, limited research

Table 1.1: Volumetric and gravimetric density of energy carriers and different storing methods for hydrogen [17]

Storage Method	Volumetric Energy Density [MJ/L]	Gravimetric Energy Density [MJ/L]
Compressed	4.9	6.8
Liquefied	6.4	9.0
Cryo-compressed	4	6.5
NaBH <sub>4</sub>	27.3 <sup>1,2,3</sup>	25.6 <sup>1,2</sup>
KBH <sub>4</sub>	20.1 <sup>1,2,3</sup>	17.8 <sup>1,2</sup>

<sup>1</sup> Theoretical value. The practical energy density depends on the process used to extract hydrogen

<sup>2</sup> In case hydrolysis is used for dehydrogenation

<sup>3</sup> Depends on the particle size distribution

has been conducted regarding modelling of NaBH<sub>4</sub> to predict the behaviour for different environmental circumstances. In 2016, Nagar et al [21] published a paper where several experimental tests were conducted, and for each experiment, a DEM simulation model was created and tested. However, Nagar et al neglected permanent bonding between particles. Initial research of van Bente [17] showed that when subjecting NaBH<sub>4</sub> to a normal load, for example when storing the material in a silo, time consolidation can occur and after sufficient time and/or with a sufficient normal load caking might occur. The definition used in this thesis for caking is: "caking is the phenomenon by which a low moisture, the free-flowing powder is first transformed into lumps, then into an agglomerated solid" [22]. In research conducted by van Bente observations were made that time consolidation affects NaBH<sub>4</sub> and a potential results is caking. Time consolidation and caking are known phenomena and are present for handling other materials such as flour, fine tea, whey and mannitol [23, 24]. Currently, van Bente et al [17] are researching the potential effect of time consolidation, humidity and stress-history on the mechanical behaviour of NaBH<sub>4</sub>. In figure 1.1 the relevant parameters and experimental test that will be conducted can be seen. In this study, the focus is on the influence of stress history, more specifically of time consolidation on NaBH<sub>4</sub> in powder form.

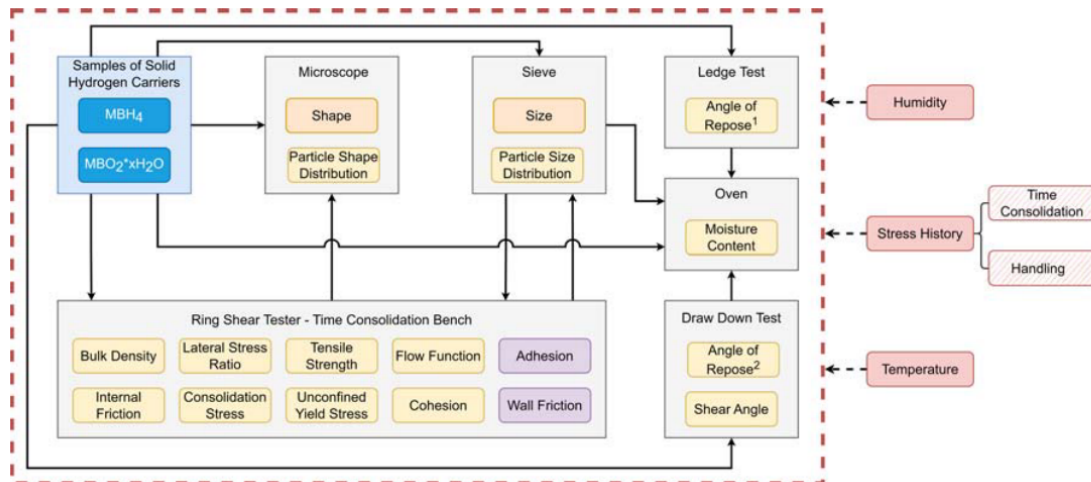


Figure 1.1: Experimental plan for research on sodium borohydride [17]

## 1.2. PROBLEM DEFINITION AND RESEARCH QUESTIONS

The possibility of time consolidation and caking occurring, makes storage of NaBH<sub>4</sub> challenging. When NaBH<sub>4</sub> is stored in a silo, the material is compressed under its own weight for a longer period of time due to gravitational forces. This causes time consolidation and a potential result of caking when storing the materials for longer time periods. How time consolidation affects NaBH<sub>4</sub> and what critical storing times might be are yet unknown, so in this research, the effect of time consolidation on NaBH<sub>4</sub> will be investigated. This leads to the following problem definition: *Formulate, calibrate, and verify a predictive model that mimics the mechanical behaviour of sodium borohydride (NaBH<sub>4</sub>) before, during, and after time consolidation using the Discrete Element Method*

Main research question: *How to model the mechanical behaviour of sodium borohydride ( $\text{NaBH}_4$ ) before, during, and after time consolidation using the Discrete Element Method?*

To answer the main research question 5 subquestions, which can be seen below, were formulated:

1. What is time consolidation, and what are the causes and potential results of time consolidation?
2. What is a suitable method to measure time consolidation?
3. How can time consolidation be incorporated in DEM modelling?
4. How does time consolidation affect sodium borohydride?
5. What is a comprehensive method to capture time consolidation effects on  $\text{NaBH}_4$  using the DEM?

### 1.3. METHODOLOGY

First, a uniform definition, measurement and modelling options for time consolidation need to be gathered. Second, measuring time consolidation is required to gather data on how time consolidation affects  $\text{NaBH}_4$ . Schulze's Ring Shear Tester (RST) is selected to measure the increase in shear strength of  $\text{NaBH}_4$  after time consolidation. The procedure for time consolidation experiments described by Schulze in [25] will be used. The relevant parameters are the shear stress, flowability, unconfined yield strength, and cohesion of  $\text{NaBH}_4$ . The shear stress results are used in the next step of the methodology.

Third, modelling of time consolidation using a DEM model is proposed in this study. The contact model used to model contacts between particles is the Edinburgh Elasto Plastic Adhesive (EEPA) model, this model considers stress-history. The DEM model mimics a regular ring shear test, where preshearing and shear to failure occur. The experimental procedure for the time consolidation experiments is preshearing, storing under consolidation stress for a certain time and shear to failure. Modelling the storing procedure is computationally expensive, so by changing the most influential parameters of the simulation to create a particle bed that mimics the behaviour after a specific consolidation time, time consolidation can be modelled more efficiently. To select the two most influential parameters a sensitivity analysis is performed using the Design of Experiments (DOE), more specifically full factorial design. At last, the final result of the thesis will be relationships of the two most influential parameters of  $\text{NaBH}_4$  in DEM over time and with these results a particle bed can be created. To determine these relationships, the model is calibrated and verified using the shear stress data gathered from the RST measurements. The found relationships make it feasible to simulate a particle bed after consolidation for a certain period in a practical scenario and this can help design equipment such as a silo.

### 1.4. OUTLINE

In this section the outline of the study will be discussed and a generic overview can be seen in Figure 1.2. First, in Chapter 1 the background, motivation and scope of this research is discussed. Next, the problem definition is formulated and with the problem definition, the main research question and sub-questions are formulated and Chapter 1 closes with an overview of the methodology of this study.

To answer the main research question a couple of steps need to be taken. First, a literature study is done, this can be found in Chapter 2. From the literature study, no data regarding the effect of time consolidation on  $\text{NaBH}_4$  was found. To select the relevant parameters and determine material behaviour during time consolidation for calibration of the model, experiments need to be performed. The experiment and the results can be found in chapter 3. The experiments will measure the shear stress and unconfined yield strength e.g. strength before and after time consolidation of  $\text{NaBH}_4$ . More relevant parameters are the change in flowability and cohesion. The experiments will give more insight into the behaviour of the material and are used to select the suitable contact model for modelling  $\text{NaBH}_4$ . In this study, Schulze's time consolidation test procedure, described in [25] will be used. A sufficient amount of repetitions for the experiments is required for accurate results, the number of trials is set to be three. It should be noted that the interest of this thesis is to find a trend. The experiments are not conducted in a climate chamber, so it is possible to measure an increase in weight and connect this with the moisture intake of  $\text{NaBH}_4$ , because it is affected by humidity. The increase in weight is caused by absorption of water. Therefore, the weight of  $\text{NaBH}_4$  before and after every trial is monitored.

In Chapter 4 DEM modelling of time consolidation is done for  $\text{NaBH}_4$ . Different considerations need to be

made to model  $\text{NaBH}_4$  using DEM. In DEM a contact model needs to be selected for both bulk-bulk interactions and bulk-equipment interactions. The available options in the literature were limited. The only explicit option for modelling time consolidation for the bulk-bulk interactions is the Hertzian repulsion, viscous damping, and JKR cohesion model, which is described in section 2.4.2. Another possible option to model time consolidation is the Edinburgh-elasto plastic adhesive (EEPA) model described in section 2.4.3, because similar to the first model it takes into consideration the stress-history and cohesiveness of the material. It requires some extra steps to use the model for time consolidation. In this study, EEPA is selected as the contact model, because it is used to model the mechanical behaviour of cohesive materials successfully by Mohajeri [26]. The newly proposed method in this study is to use a DEM model using EEPA where time consolidation is captured by artificially changing the most influential parameters of  $\text{NaBH}_4$  in the DEM model.

Other, general (chemical) parameters such as the Solid density, particle size, etc. of  $\text{NaBH}_4$  are important for the model. When modelling the material it is vital to scale up the material to limit the computational power that is needed [27]. In this study three parameters are considered in the sensitivity analysis, these are the static friction, the constant pull-off force, and the surface energy. From the sensitivity analysis, it is possible to determine the two most influential parameters. Design Of Experiments (DOE) is used for the sensitivity analysis.

After selecting the most influential parameters, calibration and verification of the model is required. The method used for calibration is referred to as the *Bulk calibration method* and in this method an output response (Key performance indicator (KPI)) is experimentally determined. The next step is to change the influential parameters in the simulation to match the experimental value with the simulation output response and when this is successfully achieved a parameter set for the two most influential parameters is found [28] and the model is calibrated and verified.

In Chapter 5 both experimental and simulation results are discussed and reflected on. The final chapter, Chapter 6 provides an answer to the main research question, the conclusion of this thesis, and recommendations for future research regarding measuring, modelling time consolidation and bulk behaviour of  $\text{NaBH}_4$ .

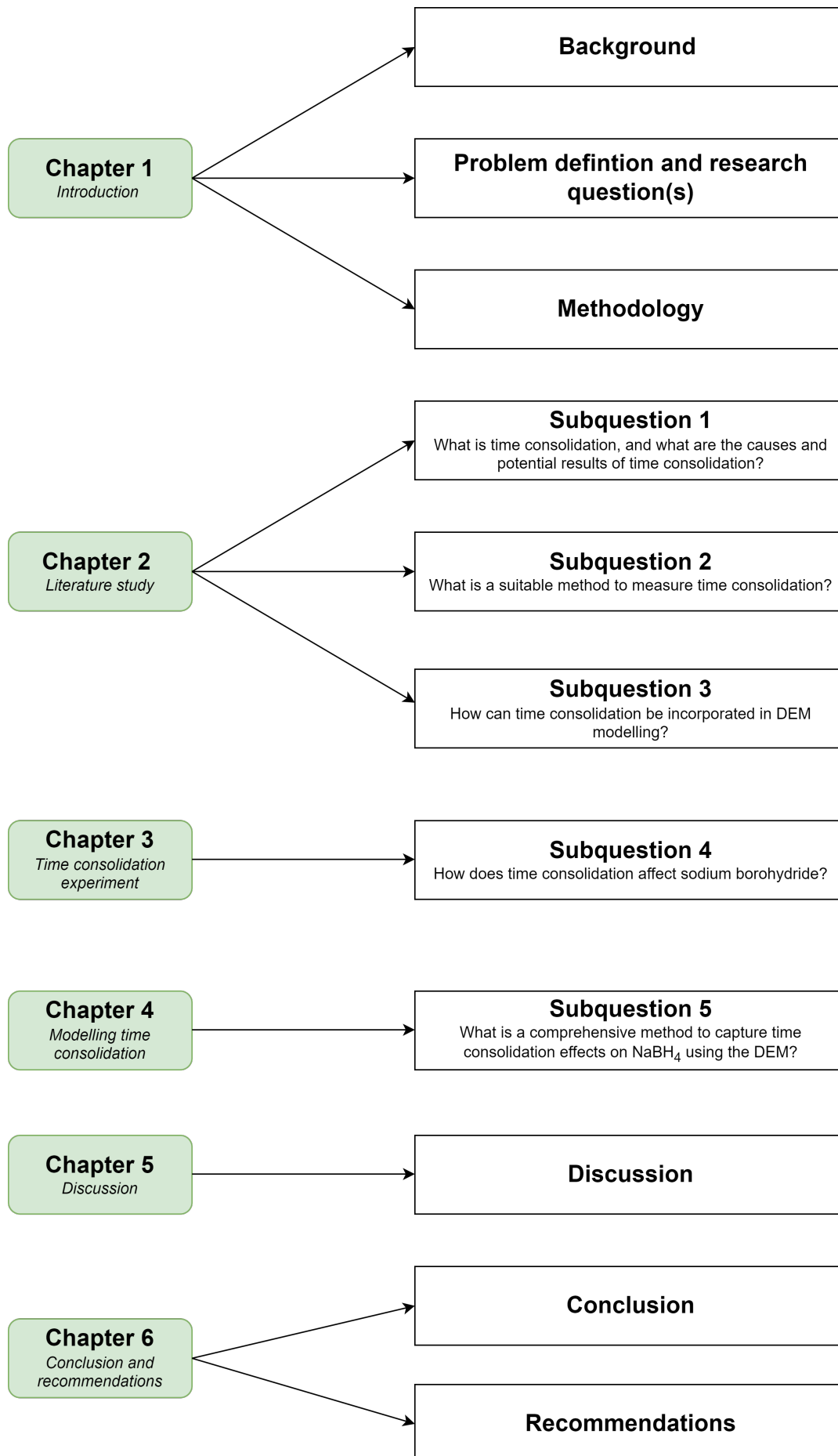


Figure 1.2: Outline

# 2

## LITERATURE STUDY

In this chapter the literature study can be found. It should be noted that there is no uniform definition for time consolidation and caking in the literature, but these are application-specific and sometimes share the same definitions. Therefore, in Section 2.1, time consolidation, how it is measured and characterised are presented and a definition for time consolidation is selected. Section 2.2, provides an overview of what is caking and the different forms of caking will be discussed together with the underlying mechanisms. In Section 2.3 findings of a paper that measured the impact of humidity on the mechanical behaviour of NaBH<sub>4</sub> are presented. In Section 2.4 (potential) methods for modelling time consolidation can be found. In Section 2.5 a study is presented that modelled NaBH<sub>4</sub> and in Section 2.6 the literature gap and concluding remarks are presented.

### 2.1. MEASURING TIME CONSOLIDATION

Time consolidation is the main focus of this study and has no uniform definition. According to Schulze, caking and time consolidation share the same definition: "the increase in strength if bulk solids are stored for a period of time at rest under a compressive stress (e.g. in a silo or an intermediate bulk containers (IBC))". The definition of Schulze will be used in this study when referring to time consolidation, the definition of mechanical caking describes a potential effect of time consolidation. The next step is to measure time consolidation, this can be done by measuring the increase in shear strength of the material. The shear strength can be measured by using different equipment, this will be further discussed in this section.

#### 2.1.1. MEASURING EQUIPMENT TIME CONSOLIDATION

Shear testers are used for shear strength measurements and in Figure 2.1 the general classification of shear testers direct and indirect shear testers can be seen. A difference between both shear testers is the location of the shear zone, for direct shear testers is it dependent on the design of the equipment and for indirect shear testers, it is only dependent on the applied stress. Another difference is the direction of the principal stress during the test, for indirect shear testers the major principal stress remains constant throughout the whole test, and for the direct shear testers, the major principal stress radiates, so is not constant [29]. The most popular shear testers are the Jenike shear cell and the ring shear testers. The Jenike shear cell even became an industry standard [30].

Most used equipment for strength measuring/(time) consolidation testing

- Jenike shear cell used in multiple studies [31, 32], the complete procedure can be found in [33]
- Schulze's ring shear tester, most used equipment for measuring time consolidation [23, 34, 35], the procedure can be found in [25].
- Uniaxial test, the complete procedure can be found in [29]

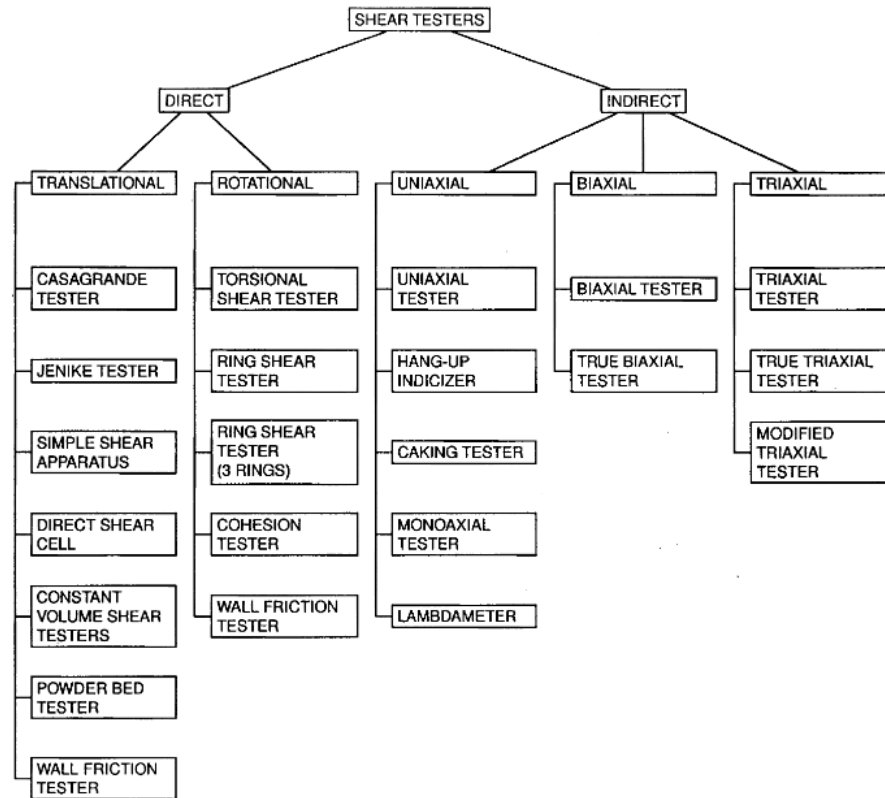


Figure 2.1: Shear tester classifications [29]

### JENIKE SHEAR CELL

The Jenike shear cell is a direct translational shear tester. A schematic overview of the shear cell can be seen in Figure 2.2. The procedure for this shear cell consists of two steps the first one is the pre-shear step where first a sample is critically consolidated which results in steady-state flow of the shear cell. The second step is to measure a shear stress for a normal load that is applied and smaller than the normal stress for preshearing. The material will yield and after that, the shear stress is obtained [36]. A more elaborate description of the procedure can be found in [33].

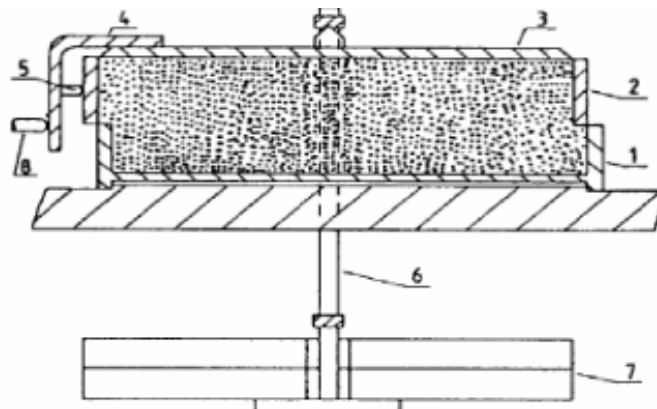


Figure 2.2: Schematic overview of Jenike shear cell [36]

### RING SHEAR TESTER

In Figure 2.3 a schematic overview of Schulze's ring shear tester (RST) can be seen. The RST test consists of two procedures, first preshearing and second subsequent shearing (shear to failure). Preshearing happens under a normal stress  $\sigma_{pre}$  until steady state flow occurs and the shear strength reaches  $\tau_{pre}$ . The second step subsequent shearing happens when a normal stress  $\sigma < \sigma_{pre}$  is applied and the peak shear stress is obtained. With this result, the first point of the yield locus is determined. To get the next point of the yield locus preshearing needs to happen again and when steady-state flow is reached another normal stress  $\sigma < \sigma_{pre}$  can be applied [29].

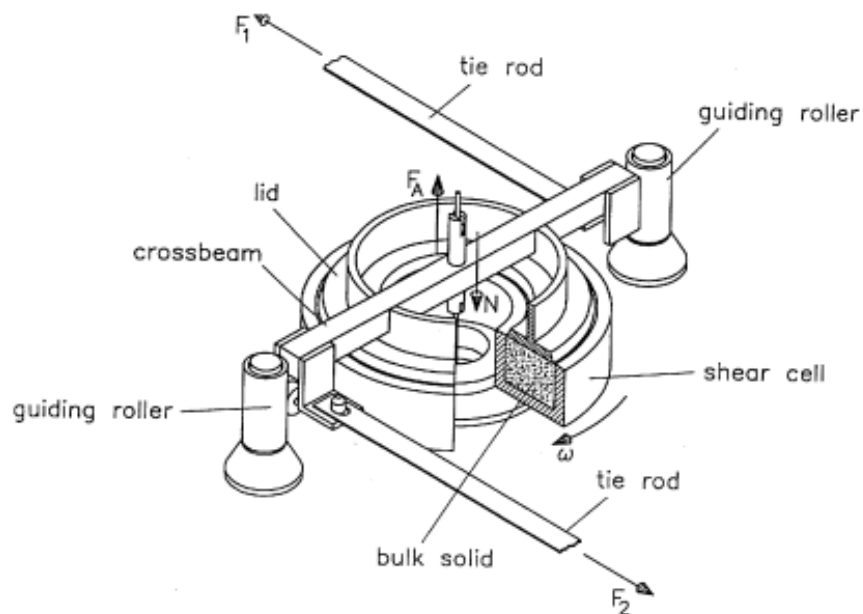


Figure 2.3: Ring shear tester [29]

### UNIAXIAL TESTER

A schematic representation of the uni-axial test can be seen in Figure 2.4. This is an example of an indirect shear test. The test is performed with a cylinder filled with a sample. The walls of the cylinder are considered to be frictionless. Consolidation of the sample is done under a normal stress  $\sigma_{1,c}$ . After this step, the cylinder is removed and the point of failure will be determined. The stress at which the sample fails is called the unconfined yield strength ( $\sigma_c$ ). When using the uniaxial test steady-state flow of the material cannot be reached which results in a smaller Mohr circle,  $\sigma_c$ , and bulk density ( $\rho_b$ ) than using a ring shear tester [25, 29].

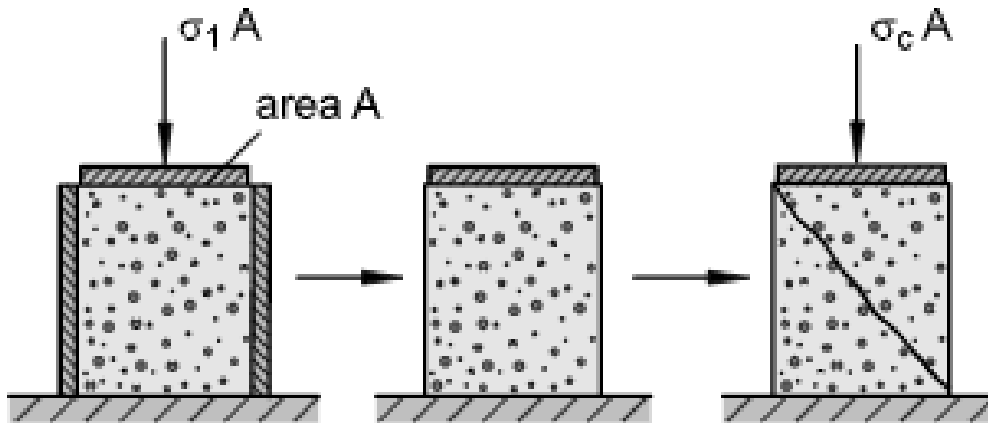


Figure 2.4: Uniaxial test [25]

### SELECTING SHEAR TESTER

The three testers that were selected are the Jenike shear cell, ring shear and uniaxial tester, these tests are the most popular tests used to measure consolidation effects. Schwedes [29] compared different testers and recommended using a ring shear test or uniaxial test to perform time consolidation experiments. However, the uniaxial test underestimates the strength of the material. The remaining options are the Jenike shear cell and Schulze's ring shear test, Schulze described the procedure for time consolidation experiments in [25] using his RST and in recent years different researchers have successfully used ring shear tests and time consolidation tests using Schulze's ring shear tester [23, 26, 34, 37, 38]. Therefore, the time consolidation experiments of Schulze will be performed using Schulze's ring shear test.

#### 2.1.2. DEFINING TIME CONSOLIDATION

##### YIELD LOCUS

In Figure 2.5 a schematic overview of the stress development in a regular ring shear test can be seen. The results of this test will be a yield locus. If one wants to determine the unconfined yield strength and the consolidation stresses a circle of Mohr is used. In Figure 2.6 an example of a Mohr circle can be seen together with the yield locus. The Mohr circle and yield locus are represented in the diagram with on the vertical axis the shear stress ( $\tau$ ) and on the horizontal axis the normal stress ( $\sigma$ ). From preshearing the first point of the Mohr circle can be found, which is the preshear-point ( $\sigma_{pre}$ ) indicated in Figure 2.6. The intersection of the Mohr circle and the yield locus is at a point  $\sigma < \sigma_{pre}$ . The endpoint of the yield locus is indicated as point 'e' in Figure 2.6. The yield locus is unique for every consolidation stress.  $\sigma_1$  is the major principal stress during steady-state flow and  $\sigma_2$  is the minor principal stress during steady-state flow, these are the highest and lowest stresses present in the material [25].

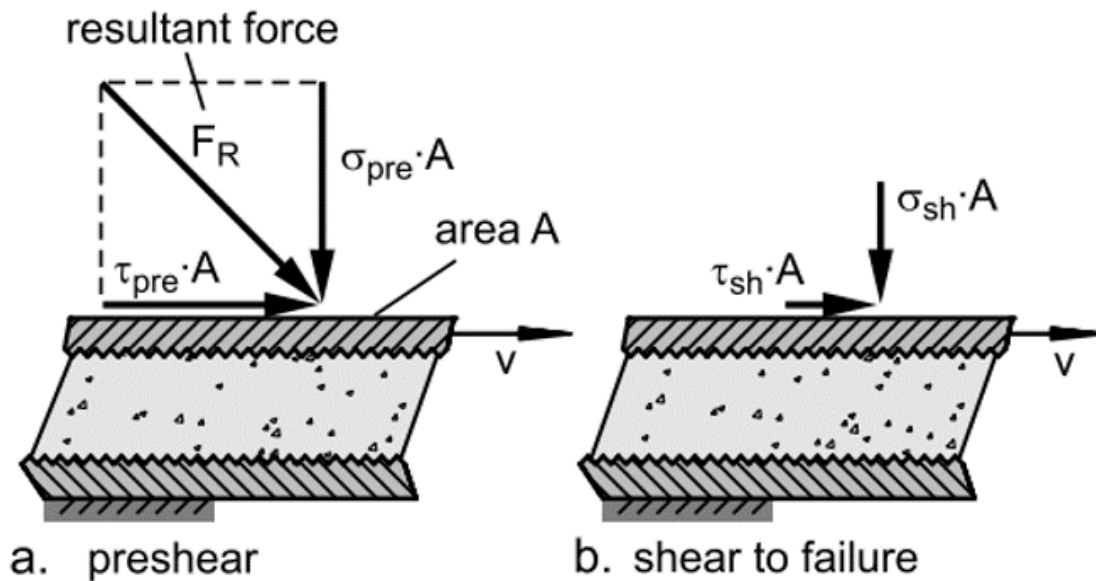


Figure 2.5: Schematic overview of stresses in ring shear test [25]

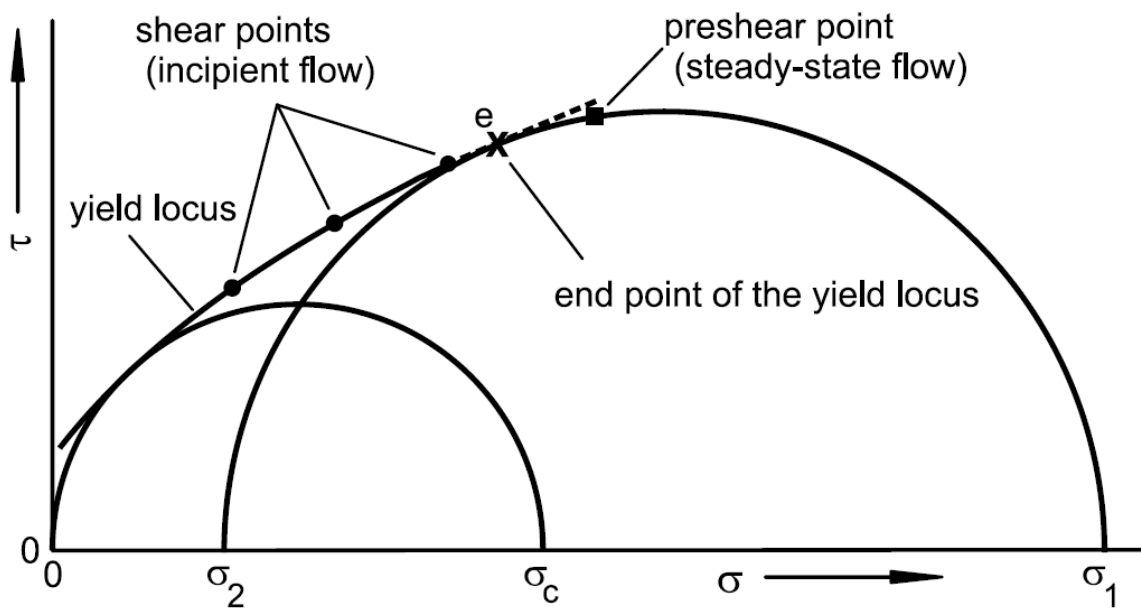


Figure 2.6: Yield locus [25]

### TIME YIELD LOCUS

When dealing with time consolidation effects the construction of the yield locus is similar. After preshearing the major principal stress is used as the consolidation stress ( $\sigma_1$ ). The test specimen is stored for a period of time under a normal stress equal to  $\sigma_1$  as can be seen in the second step of Figure 2.8, this is called time consolidation. After this period the specimen is sheared till failure for a normal stress  $\sigma_{sh} < \sigma_{pre}$ . The result is a time yield locus, this can be repeated for multiple consolidation times ( $t$ ). As indicated in Figure 2.7 the longer a specimen is consolidated the larger the shear strength becomes. With the yield loci, the angle of internal friction ( $\phi_t$ ) can be determined. The angle of internal friction is the local angle between the time yield locus and the  $\sigma$ -axis. The angle is mostly non-constant over the time yield locus, however, linearization of the yield locus to determine a constant value is commonly done and useful for most applications [25].

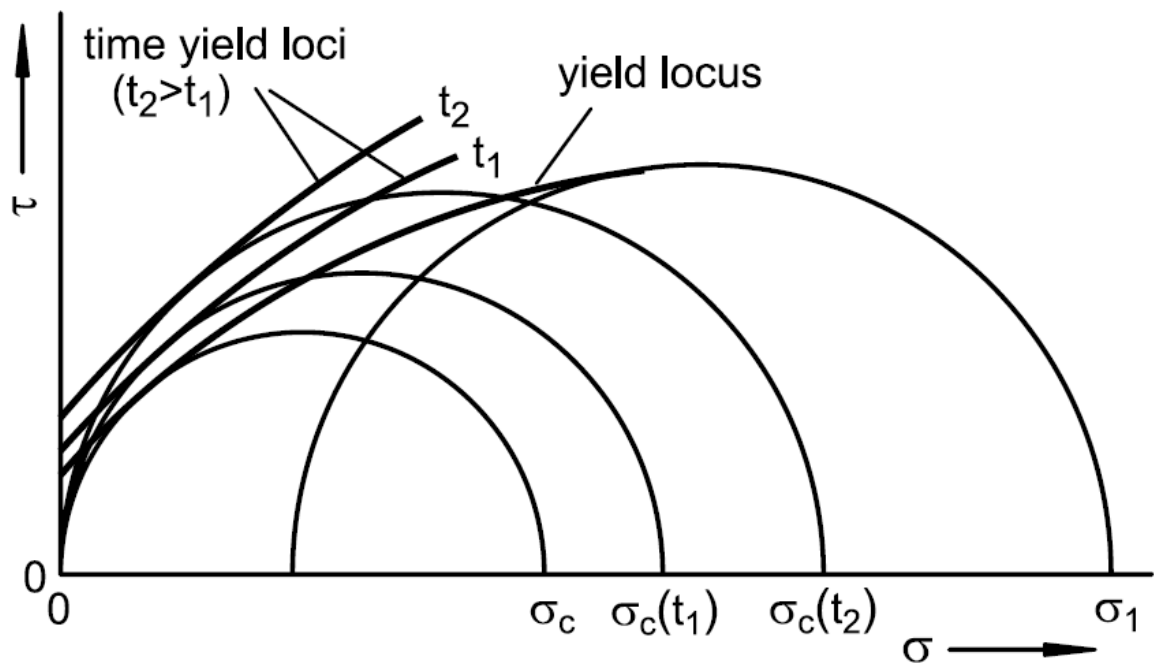


Figure 2.7: Time yield locus [25]

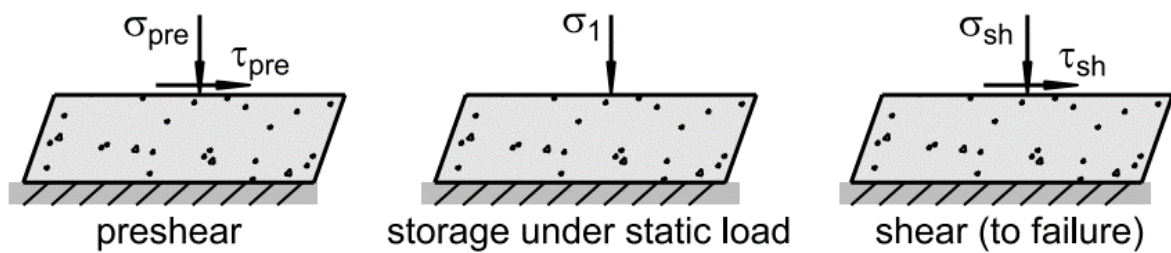


Figure 2.8: Schematic overview of stresses in time consolidation experiment [25]

### FLOW FUNCTION

The result of time consolidation causes a decrease in flowability. The flowability or flow function is defined as the ratio between the consolidation stress and the unconfined yield strength, this can be seen in Equation 2.1 [25].  $\sigma_c$  increases during time consolidation as can be seen in Figure 2.7 leading to a smaller flow function.

$$ff_c = \frac{\sigma_1}{\sigma_c} \quad (2.1)$$

In Figure 2.9 the characterization of the numerical value for the flowability can be seen. In this graph, it can be seen that the material is free-flowing when the flow function is above 10, not flowing when it is below 1 and all classifications between 1 and 10.

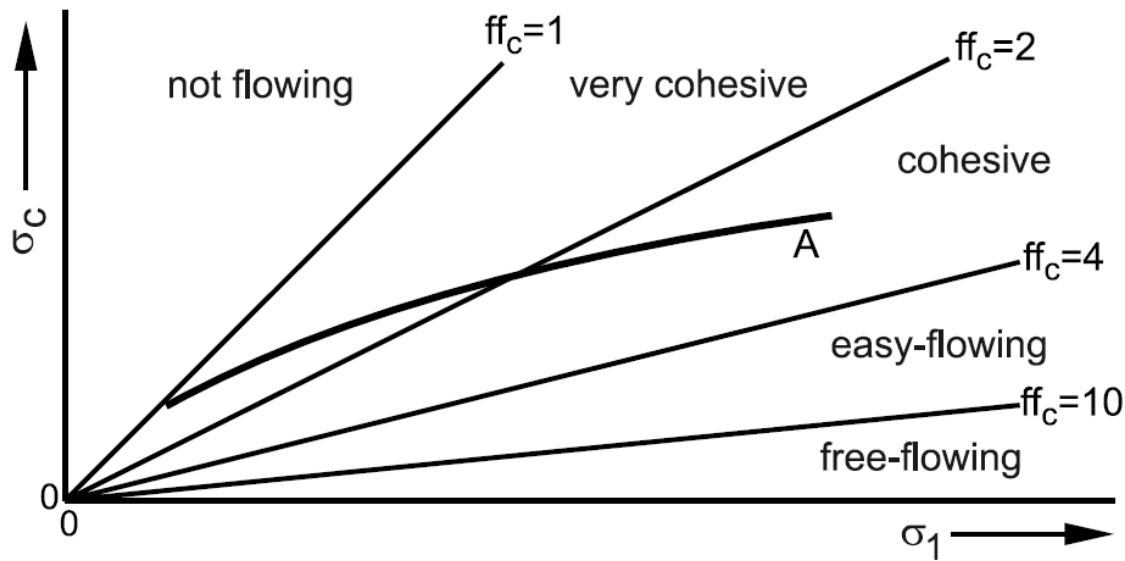


Figure 2.9: Flow function ranges [29]

## 2.2. CAKING

The process that is referred to as caking has multiple definitions in the literature and can be considered as a potential result of time consolidation. According to Schulze ([25]): "caking is the increase in strength if bulk solids are stored for a period of time at rest under a compressive stress (e.g. in a silo or an intermediate bulk container (IBC))". Caprin et al [39] showed two different definitions for caking. The first one is blockage of a spiral conveyor due to the creation of hard crusts from powders. The second one is "the formation of both loose and hard agglomerates of various sizes in a bag after storage". From these three definitions, it becomes clear that it is difficult to formulate one universal definition for caking. One reason is that the definitions seem application-specific. Another reason is that there are three caking mechanisms, amorphous, humidity, and mechanical caking, which are all triggered during different circumstances [40]. For example, amorphous caking cannot occur in crystalline powders. In Figure 2.10 the three caking mechanisms and the relevant parameters affecting the caking mechanism for lactose can be seen.

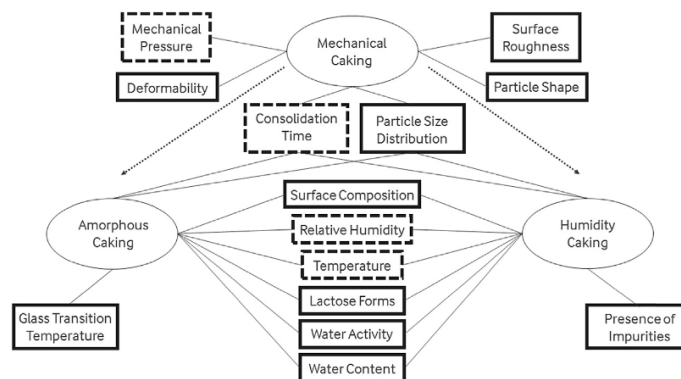


Figure 2.10: Different caking mechanisms and (possible) internal and external influential factors for lactose [39]

Increase of cohesive forces can cause caking. There are three cohesion forces involved during the caking process. The first one is the electrostatic force, this force is present when particles are charged. The electrostatic force can be both attractive or repulsive. The second force is the van der Waals force between the particles, these are electromagnetic forces between the molecules [41]. The third force type is capillary forces as a result of liquid bridges. This occurs when the particles are subjected to humidity and the material can absorb moisture. This moisture causes the material to form liquid bridges between the particles [21].

For this thesis a general definition for caking and time consolidation is required. The general definition for caking, used in this study is the one of Chen et al [40]: "caking is the phenomenon by which a low moisture, free-flowing powder is first transformed into lumps, then into an agglomerated solid." The cohesive forces between particles increase over time due to different mechanisms. Four possible mechanisms are deformation, solid bridge formation, chemical processes, or biological processes.

### 2.2.1. AMORPHOUS CAKING

Amorphous powders are vulnerable to amorphous caking, examples of powders that are amorphous are dairy milk powder, onion powder, and fish protein. Amorphous caking occurs when a free-flowing material is heated to a temperature above the glass temperature  $T_g$ , this causes the amorphous material to change from a glassy (hard) state to a rubbery (soft) state [42]. When the material is cooled down to a temperature below the glass temperature, the state is reversed back to the glassy state. In the time when the material had a temperature above the glass temperature, viscous properties caused the individual particles to stick together. The bond that is formed between the particles is called sintering, this is a stable powder structure [40]. The procedure for this bond to form can be seen in Figure 2.11.

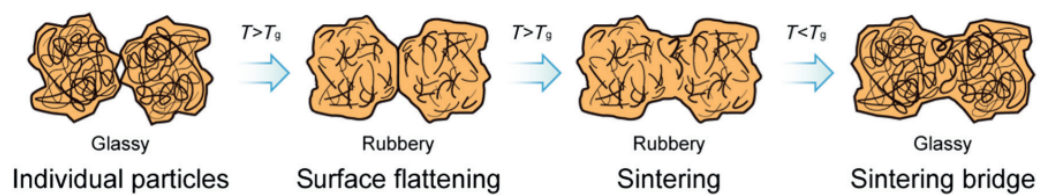


Figure 2.11: Amorphous caking [40]

Sintering bridges can collapse after a certain amount of time due to a non-stable inner structure of some particles. After this, a melt takes place that results in a highly viscous and foam-like amorphous powder e.g. the "cake" [43]. In Figure 2.12 the complete process after forming the sinter bonds can be seen.

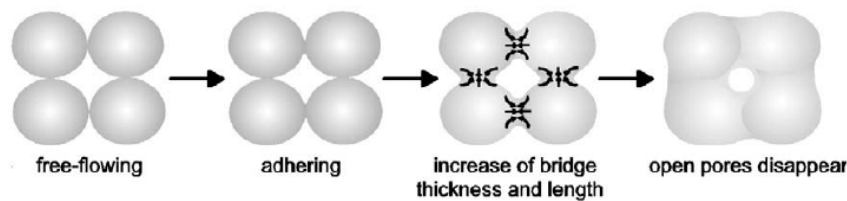


Figure 2.12: Sintering [43]

### 2.2.2. HUMIDITY CAKING

Humidity caking is dependent on environmental conditions such as temperature and humidity conditions. Hygroscopic powders are affected by these conditions and humidity caking can occur for these types of powders. Crystalline powders can have humidity caking, which is dependent on the relative humidity (RH), there is a point which is called the deliquescence point,  $RH_0$ . For RH below the deliquescence point absorption of moisture is slow, but when the RH is greater than  $RH_0$  absorption of moisture increases rapidly as can be seen in Figure 2.13. In Figure 2.13 another point of interest can be seen, which is the  $RH_{cc}$ , this point represents the RH where capillary condensation will lead to liquid bridging. Capillary condensation is the phenomenon where moisture is condensed at the contact points of particles [22].

Capillary condensation requires water that can be absorbed by the material. Hygroscopic powders have a water activity for which the critical capillary radius increased exponentially, this is called the Kelvin radius [44]. The critical capillary radius can be predicted using Kelvin's equation [45]. When the critical capillary radius is reached liquid bridging can occur.

Deliquescence is the process where a crystalline powder is exposed to humidity for a longer period of time and dissolves into a sorbed liquid, for  $\text{NaBH}_4$  it is sorbed water [39, 46]. Deliquescence and capillary condensation

can both or individually be the cause of humidity caking in hygroscopic powders depending on the RH [22, 39].

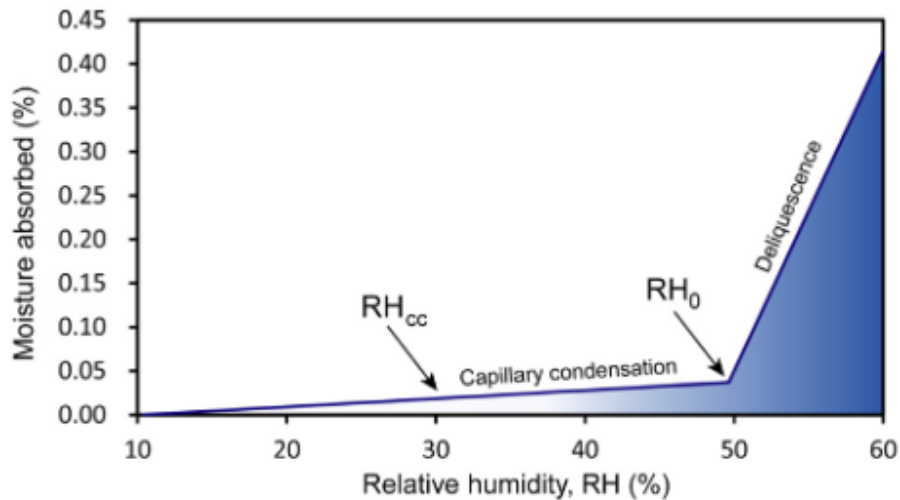


Figure 2.13: Moisture absorption vs Relative Humidity [22]

Figure 2.14 shows the key (orange), potential (blue) and other (green) influential factors for amorphous, humidity and mechanical caking. Also, it can be noted that for amorphous powders it is difficult to make a distinction between amorphous and humidity caking because the increase in temperature also triggers humidity caking. Liquid bridge forming is the main cause of humidity caking for a crystalline powder [40].

### 2.2.3. MECHANICAL CAKING

Carpin et al [39] gave a definition for mechanical caking and it is: "powder consolidation due to mechanical pressure". This definition is similar to the definition of time consolidation used by Schulze. As mentioned before in this thesis caking is referred to as the agglomeration of solid particles, so this definition is not used for caking but for time consolidation. It is important to note that liquid bridging is the most influential force for caking, but this is caused by moisture, and for mechanical caking, a dry powder is used. Schulze [25] discovered that the van der Waals forces are the most influential forces when dealing with mechanical caking [25]. In Figure 2.14 the most influential factors for mechanical caking can be seen.

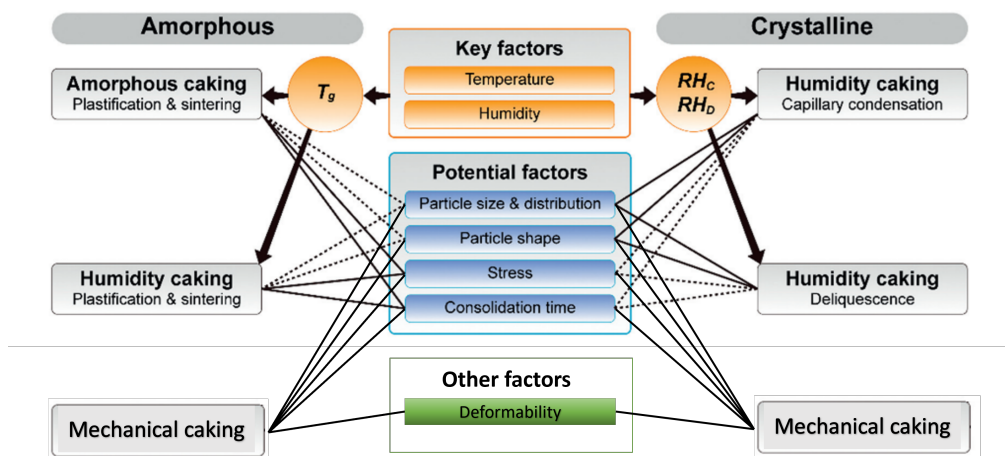


Figure 2.14: Influential factors for amorphous, humidity and mechanical caking [39, 40]

### 2.3. MEASURING BULK BEHAVIOUR OF SODIUM BOROHYDRIDE

Romijn [38] performed several tests to determine the influence of (ambient) humidity on the bulk properties of  $\text{NaBH}_4$  (both powder and granules) during storage and handling. Four tests were performed the Dynamic Vapor Sorption, Moisture Depth, Ring Shear and Dry-Wet-Dry test. Tests were performed for different preshear levels (4, 8 and 16 kPa) to investigate how the consolidation stress and moisture affect the bulk properties. Both material forms show similar bulk properties for zero moisture content, but show different bulk behaviours when higher moisture content levels were analysed. The granules are easier to handle, because the flowability is better for higher moisture content levels in comparison to the powders. Also, the moisture sorption of  $\text{NaBH}_4$  is affected by the relative humidity rather than the moisture level of the material. The conclusion is that for storing and handling the granules are preferred and enclosed handling is required because the bulk properties are more affected at high moisture content levels. Romijn also tried to evaporate the moisture from the material by drying the samples in the oven, this resulted in a giant brick of material making this not a valid option for extracting the moisture content from  $\text{NaBH}_4$ .

Table 2.1: Ring shear test results: influence of different moisture levels on  $\text{NaBH}_4$  powder (preshear 4 kPa) [38]

Moisture [wt%]	Cohesion [Pa]	$\sigma_c$ [Pa]
2	$468 \pm 34$	$1860 \pm 73$
4	$451 \pm 49$	$1813 \pm 194$
6	$555 \pm 29$	$2283 \pm 129$

In Table 2.1, results of the ring shear test performed with  $\text{NaBH}_4$  powder for a preshear of 4 kPa can be seen and these results will be used to make a comparison between the influence of moisture levels (humidity) and time consolidation.

## 2.4. MODELLING OF TIME CONSOLIDATION

### 2.4.1. DISCRETE ELEMENT METHOD

DEM modelling is used in this thesis and the soft-particle approach seems to be the most fitting one, because the particle deformation is taken into account in the form of overlap between particles. This approach is time-driven, because small time-steps are used for the calculations. In these calculations, both the particle-particle and particle-wall interactions are calculated. The approach depends on force-displacement relationships. These relationships together with the overlap are used to determine the forces on every individual particle.

With the forces the second law of Newton is applied and eventually the positions and velocities for every particle are determined. The iterative process can be seen in Figure 2.15 and continues until the simulation is finished.

The contact model is a significant aspect of DEM modelling, the contact model provides equations to calculate the particle-particle and particle-wall interactions. It is not necessary to use the same model for both the particle-particle and the particle-wall interaction. The contact model makes a distinction between normal and tangential components of forces. To carry out the calculations material properties are required such as the solid density, coefficient of restitution ( $e$ ), Coefficient of rolling friction, static friction etc [47].

The software that will be used in this study is EDEM, within EDEM two categories of basic models, the elastic and the elasto-plastic models can be found. Examples of elastic models are Hertz-Mindlin and Linear spring. Examples of elasto-plastic models are hysteric spring and the Edinburgh Elasto-Plastic Adhesive model. The difference between the two types is a residual overlap after unloading, which is present for the elasto-plastic models and not for the elastic models. Therefore, the elastic models are used for most of the dry bulk solids, and the elasto-plastic models for bulk materials that are compressible. After selecting a base contact model an additional model can be used when for example cohesion is not taken into account in the base model a linear cohesion model can be added depending on the application.

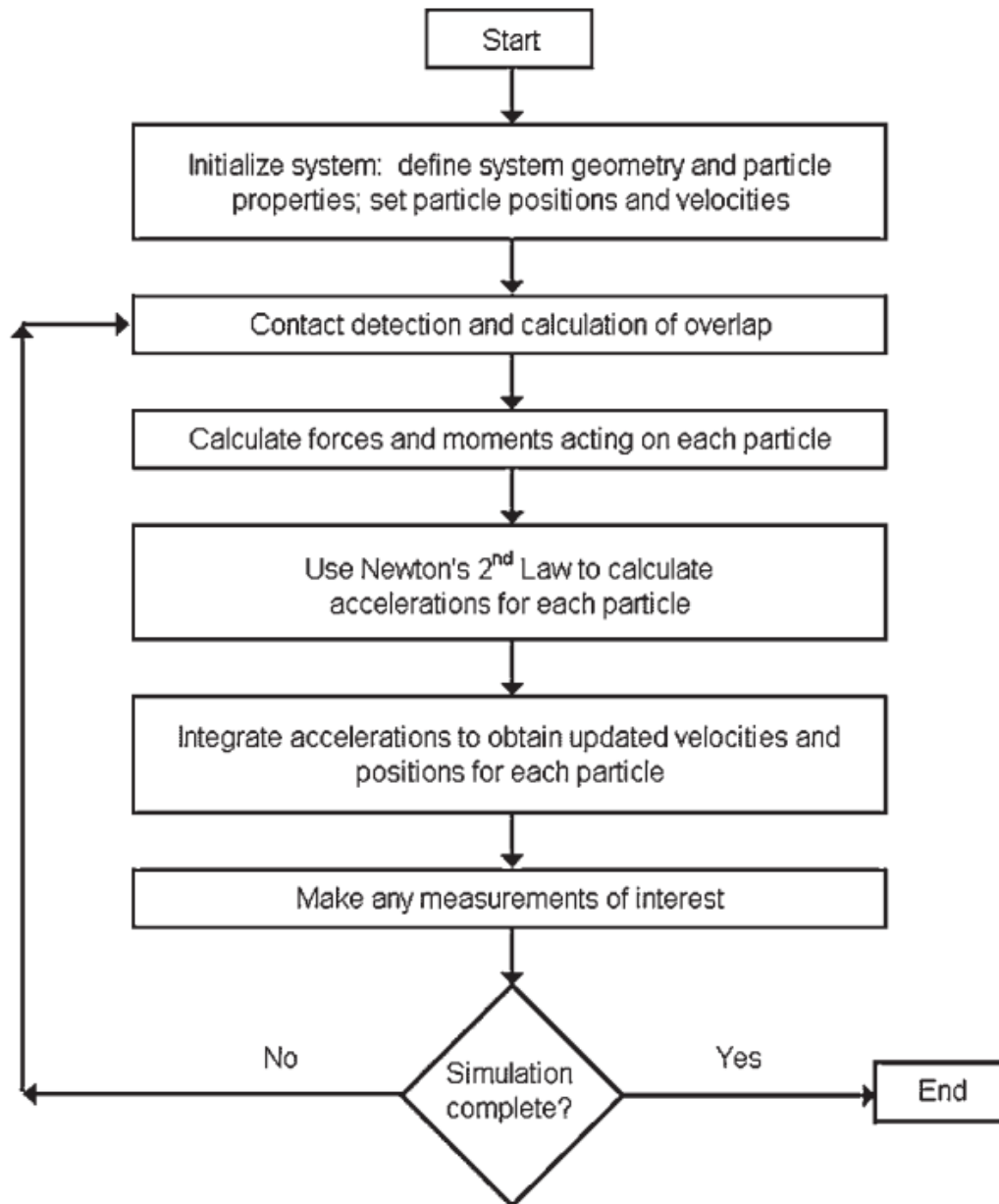


Figure 2.15: General soft-particle DEM approach [47]

Modelling of time consolidation has not explicitly been done. Therefore, two history-dependent models are selected as possibilities to model time consolidation. The two selected models "Hertzian repulsion, viscous damping and JKR cohesion model" and the "Edinburgh Elasto-Plastic Adhesive contact model", are explained in Subsections 2.4.2 and 2.4.3.

#### 2.4.2. HERTZIAN REPULSION, VISCOUS DAMPING AND JKR COHESION MODEL

The first history-dependent model that is selected is the Hertzian repulsion, viscous damping and JKR cohesion model, proposed by Hasibon et al[48] and in that study, a mesoscopic study was performed by using Hertzian repulsion, viscous damping, and JKR for the cohesion. The equations to determine these three forces can be found in Equations 2.2-2.4. In these equations the effective Young's modulus  $\bar{E}$  is defined as  $\frac{E}{1-\nu^2}$  with the Young's modulus  $E$  and the poisson ratio  $\nu$ . The overlap of two particles  $i$  and  $j$  at positions  $\mathbf{r}$ ,  $h_{ij}$  is defined as  $R_i + R_j - |\overrightarrow{r_{ij}}|$  with radius  $R$ , an effective particle radius  $\bar{R} = \frac{R_i R_j}{R_i + R_j}$  and  $\mathbf{r}_{ij}$ .  $\mathbf{r}_{ij}$  is defined as  $\mathbf{r}_i - \mathbf{r}_j$ .

Furthermore, "w" is defined as the surface energy,  $\gamma_n$  is the contact viscosity which is an empirical damping parameter and v is the velocity of the particle. A picture of the overlap parameter h can be seen in Figure 2.16a [48].

2

$$F^{rep} = \left( \frac{2}{3} \bar{E} \sqrt{\bar{R}} h_{ij}^{3/2} \right) \vec{r}_{ij} \quad (2.2)$$

$$F^{coh} = \left( \sqrt{4\pi w \bar{E} \bar{R}^{3/4}} h_{ij}^{3/4} \right) \vec{r}_{ij} \quad (2.3)$$

$$F^{vis} = \left( \gamma_n \sqrt{\bar{R}} h_{ij} (v_i - v_j) \cdot \vec{r}_{ij} \right) \vec{r}_{ij} \quad (2.4)$$

With this model the cohesion is time-dependent and to take this into account the surface energy  $w$  and effective Young's modulus  $\bar{E}$  are scaled similarly by a linear factor to keep the ratio constant. This linear assumption only takes into account elastic deformation, for plastic deformation a different ratio between the surface energy and effective Young's modulus should be used. To store the stress history a new parameter is introduced as the effective loading time ( $\tau$ ). This parameter is dependent on a normalized overlap parameter  $h^*$  that can be seen in Equation 2.5 and a graphical representation can be seen in Figure 2.16b. In the Equation,  $h_0$  is defined as  $(9\pi \frac{w}{\bar{E}})^{2/3} \bar{R}^{1/3}$  which is the overlap between the particles when they are in equilibrium [48].

$$h^* = \begin{cases} h/h_0 - 1 & \text{when } 0 < h \leq 2h_0 \\ 1 & \text{when } h > 2h_0 \end{cases} \quad (2.5)$$

The effective overlap can be both positive and negative according to Equation 2.5. When the overlap is negative ( $0 < h < h_0$ ) then the particles are in the cohesive region and when the overlap is positive ( $h > h_0$ ) the particles are in the repulsion region.

The definition for the effective loading time ( $\tau$ ) can be seen in Equation 2.6. It is referred to as the contact time.

$$\tau = \begin{cases} \int_0^T h^* dt & \text{when } \tau < \tau_{max} \\ \tau_{max} & \text{when } \tau \geq \tau_{max} \end{cases} \quad (2.6)$$

Previously it was mentioned that there are two regions, the cohesive and repulsion regions. The final step is to define a scaling factor  $\alpha(\tau)$  for the cohesive region and this scaling factor will be used to scale the effective Young's modulus and surface energy. It should be noted that the scaling factor can be different, but for simplicity in this study, a linear form is used. The definition of the scaling factor can be seen in Equation 2.7 and a graphical representation can be seen in Figure 2.16c. In Figure 2.16d the difference between a non-scaled Hertz-JKR model in black and the scaled model proposed in the study in green.

$$\alpha(\tau) = \begin{cases} \frac{\alpha_{max}-1}{\tau_{max}} \cdot \tau + 1 & \text{when } \tau < \tau_{max} \\ \alpha_{max} & \tau \geq \tau_{max} \end{cases} \quad (2.7)$$

### 2.4.3. EDINBURGH ELASTO-PLASTIC ADHESIVE MODEL

Another possible contact model to model time consolidation is the Edinburgh Elasto-Plastic adhesive (EEPA) model, because it takes into account stress history and cohesion. It is a relatively new model and was proposed by Morrissey et al in 2014 [49]. The assumption is made that when the plastic contact area increases also the pull-off strength increases. In the model, both elastic and plastic deformation is accounted for. Five parameters describe the non-linear model of Figure 2.17a. When the fifth parameter, the stiffness exponent is set to  $n = 1$ , the model becomes linear and the model can be simplified to the model of Figure 2.17b.

The five parameters that describe EEPA are [49]:

- $k_1$ , the virgin loading stiffness

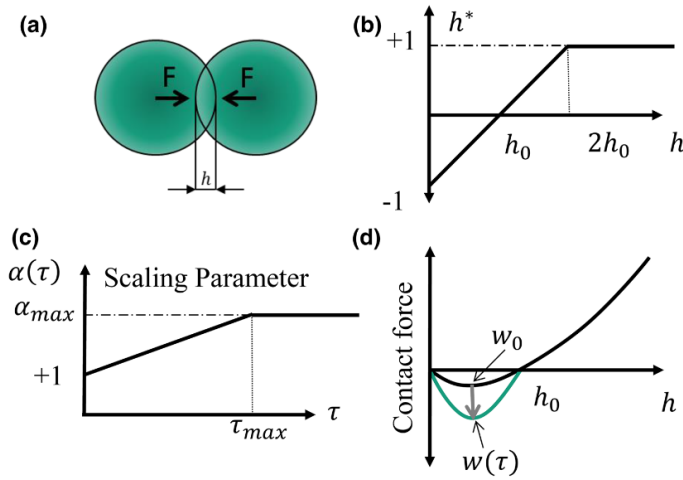


Figure 2.16: Graphical representation of the (a) particle overlap  $h$  (b) effective overlap parameter  $h^*$  (c) scaling parameter  $\alpha$  (d) total contact force model [48]

- $k_2$ , the unloading and reloading stiffness
- $f_0$ , the constant adhesive strength (pull-off force)
- $k_{adh}$ , the adhesive stiffness
- $n$ , the stiffness exponent

The pull-off force  $f_0$  is a constant in the model. In Figure 2.17 three parts can be distinguished. The first part is the branch that follows the virgin stiffness  $k_1$ . When loading occurs and contact between particles happens, the model follows the branch of the virgin stiffness. Contact is defined as the moment when the distance between the centerpoints of the particles is equal to the sum of the radii of the two particles. When unloading and reloading the stiffness will switch to the unloading and reloading stiffness  $k_2$ . This is because of the plastic deformation. When reloading occurs the model will follow the trajectory of  $k_2$  until the force reaches the same value as the force that was experienced during the first time loading. After this, the model switches back to the branch of  $k_1$ . The third part is the adhesive force and it is triggered when unloading occurs and the trajectory of  $k_2$  is followed below the plastic overlap  $\delta_p$ .

The history of the model is erased when the particles are no longer in contact with each other. This happens when unloading occurs and the adhesive force exceeds the maximum value at  $\delta_{min}$ . The normal overlap and the adhesive force will both reduce until the separation condition of  $\delta = 0$  has been reached [49].

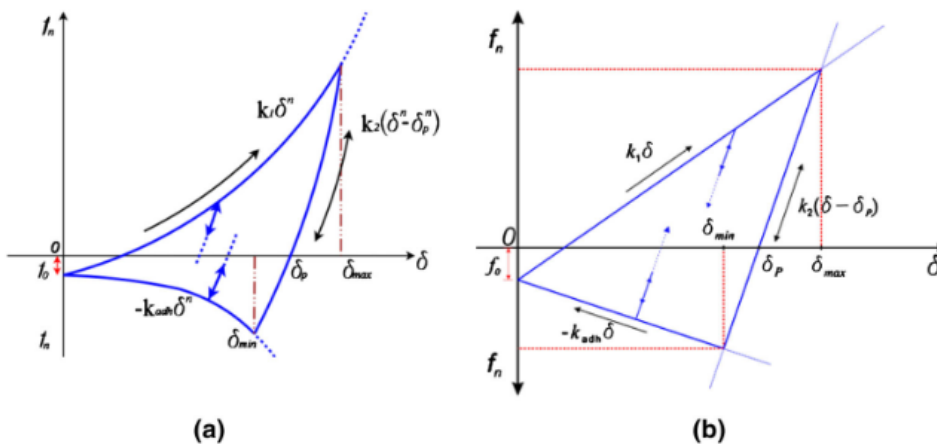


Figure 2.17: Graphical representation of contact model for the normal contact force-displacement function (a) non-linear (b) linear [49]

Researchers successfully used EEPA to model bulk behaviour [50, 51]. Mohajeri et al [52] showed that EEPA is better at capturing stress-history in comparison to Hertz-Mindelin, the material used in Mohajeri's research was iron ore. Mohajeri et al [51] also successfully calibrated and modelled both cohesiveness and stress history dependency for moist coal with this model. The researchers used Schulze's ring shear tester and the EEPA model. Also, a scaling method for EEPA has been developed by Mohajeri et al [53] to reduce the computational cost.

### 2.5. MODELLING OF SODIUM BOROHYDRIDE ( $\text{NaBH}_4$ )

Nagar et al [21] performed several experiments and modelled these in a DEM environment to model the mechanical behaviour of  $\text{NaBH}_4$ . Two experimental tests were conducted and modelled in DEM: a shear strength experiment and a wedge penetration experiment. A linear elastic contact model was used to mimic the mechanical behaviour, this was done to determine the physical governing parameters of the powder form of  $\text{NaBH}_4$ . A schematic overview of the contact model together with the governing parameters can be seen in Figure 2.18.

$$F_n = -k_n h_n \quad (2.8)$$

$$F_s = \begin{cases} k_s h_s & \text{when } k_s h_s \leq \mu F_n \\ F_n \mu_s & \text{when } k_s h_s > \mu F_n \end{cases} \quad (2.9)$$

In the model  $k_n$  and  $k_s$  represent the normal and tangential stiffness. The normal force and tangential force can be seen in Equations 2.8 and 2.9, which remain constant in this study. The adhesive force is proportional to  $k_p$  during contact of particles. The contact in this model is defined as the distance between two particles equal to or less than 1.1 times the radii of the particles. The viscous damping coefficient ( $\mu_g$ ) is used for the energy loss in both the normal and tangential directions. The coulomb friction is described as  $\mu_s$  and works against the moving direction of the particles.

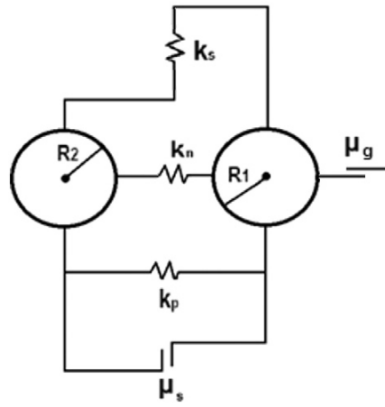


Figure 2.18: Contact model for sodium borohydride used by Nagar et al [21]

### 2.6. CONCLUDING REMARKS: LITERATURE GAP

In this chapter, the first, second, and third subquestions: "What is time consolidation, and what are the causes and potential results of time consolidation?", "What is a suitable method to measure time consolidation?" and "How can time consolidation be incorporated in DEM modelling?" are answered, with a literature study.

For time consolidation in this study the definition of Schulze [25] is used and it is: "the increase in strength if bulk solids are stored for a period of time at rest under a compressive stress (e.g. in a silo or an intermediate bulk container (IBC))". Caking can occur when this happens, in this thesis a dry powder will be used so mechanical caking is likely to happen. The definitions for mechanical caking and time consolidation look similar, however these are not exactly the same. Therefore, in this thesis, caking (mechanical and humidity)

is considered as the result of time consolidation where particles become lumps. In Figure 2.10 a complete overview of the caking mechanisms can be found and this needs to be considered when performing experiments outside a climate chamber.  $\text{NaBH}_4$  is affected by humidity and temperature, so it is difficult to make a distinction between mechanical and humidity caking, and therefore the strength increase in the material can be caused by both time consolidation and liquid bridge forming. To monitor this the weight of the particle bed is measured before and after the test to give an insight into the sorption of water.

Studies that analysed the bulk behaviour of  $\text{NaBH}_4$  are limited. Romijn [38] investigated the effect of humidity on the bulk behaviour of  $\text{NaBH}_4$ . Nagar et al performed two experiments and modelled these experiments, but all the findings in both studies were never confirmed by other studies. The experiment that will be performed is the time consolidation experiment described in Section 2.1.2 using Schulze's RST. This test is an industry standard and several researchers successfully measured bulk behaviour with Schulze's RST.

Next, modelling the mechanical behaviour of  $\text{NaBH}_4$  is done by Nagar et al, but this model is not able to model  $\text{NaBH}_4$  during and after time consolidation. During time consolidation the material will be subjected to a load, particles will come closer to each other, and plastic deformation of particles will happen, which affects the mechanical properties of  $\text{NaBH}_4$ . In the model of Nagar et al plastic deformation is not accounted.

The literature gap is a lack of knowledge of how  $\text{NaBH}_4$  is affected by time consolidation and modelling  $\text{NaBH}_4$  before, during, and after time consolidation. In the literature, no data was available on the effect of time consolidation on  $\text{NaBH}_4$ , so to calibrate the model a time consolidation experiment will be performed. Therefore, in this study, the time consolidation will be measured and modelled for 0, 0.5, and 1 hour consolidation using time consolidation experiments in Schulze's RST. The end goal is to determine a relationship between the two most influential parameters over time in DEM, similar to the relationship of the shear stress over time for  $\text{NaBH}_4$  that is found from the time consolidation experiments. The DEM model that is used mimics the complete process of a normal RST test, to be more specific no time consolidation happens in the DEM model. The contact model that is used is EEPA, because it considers stress-history. When a relationship between the most influential parameters over time is found it is possible to instantly create a time-consolidated particle bed for a certain consolidation time and stress e.g. a particle bed after time consolidation occurred.

# 3

## TIME CONSOLIDATION EXPERIMENT

The literature study presented in Chapter 2 consisted of three major parts. One of the parts was measuring and characterization of time consolidation. In the literature study no data for time consolidation of  $\text{NaBH}_4$  was found, the solution is to perform experiments for  $\text{NaBH}_4$ . In this study Schulze's RST is used and in this chapter the experimental setup (3.1), the design of experiments (3.2), and the experimental results (3.3) are presented. The chapter finishes with concluding remarks on the experiments in Section 3.4.

### 3.1. EXPERIMENTAL SETUP

The combination of Schulze RST and a consolidation bench will be used to conduct experiments. The procedure described in [25] for time consolidation testing will be used. More specifications on the RST can be found in Section 2.1.1. In Figure 3.1 the setup for time consolidation using the consolidation bench can be seen. First, preshearing will be done in the RST and after that, the shear cell will be transferred to the consolidation bench. The weights on top of the bench, provide the consolidation stress and will remain on the shear cell for the specific consolidation time (0.5 or 1.0 hour). After this time the shear cell will be transferred back to the RST and shear to failure of the particle bed occurs. In Figure 3.2 a filled shear cell in the RST can be seen. The shear cell can also be time-consolidated in the RST. After the preshear process the time consolidation will take place and after the appropriate time has passed shearing of the particle bed will occur and the shear stress for one point on the time yield locus will be found.



Figure 3.1: Consolidation bench



Figure 3.2: Schulze's Ring shear Tester

### 3.2. DESIGN OF EXPERIMENTS

Design of experiments (DOE) is a statistical approach to determine the relationship between input parameters and output response(s). It is preferable over other approaches such as a one-variable-at-a-time or trial-and-error approach. The input (independent) variables and output responses (dependent variables) need to be selected to use DOE. The input variables can be both controlled and uncontrolled, the controllable variables can be changed during the experiment as opposed to the uncontrollable ones, which are difficult to control and cannot be kept constant at all times [54, 55].

In Figure 3.3 a schematic overview of the DOE for the experiment can be seen. The experiment that will be performed is the time consolidation experiment, with the input variables normal stress and consolidation time and output response shear stress. Uncontrollable variables in this experiment are for example the humidity, packing, and temperature. To control the humidity and temperature one needs to use a climate chamber, unfortunately, this was not available.

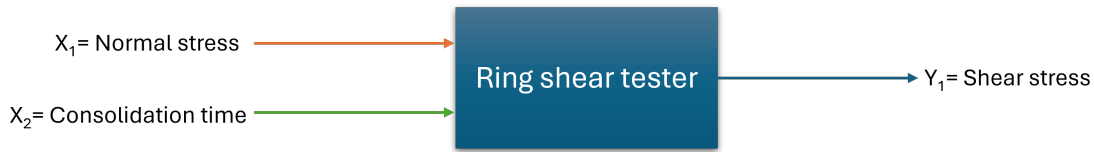


Figure 3.3: General representation of Design Of Experiments for performed time consolidation experiment

With the input variables and output response a suitable DOE-method should be selected. In this study, full factorial design will be used, because of the limited number of input variables and the main and joint effects of the factors on the KPI(s) can be investigated [54]. The number of experiments ( $N$ ) can be determined by using equation 3.1. In this equation  $n$  is related to the number of levels in this study equal to 3 for one factor and 4 for the other factor.  $k$  is the number of factors which is 2 in this study. However, when using different levels for the factors, Equation 3.1 changes a bit and the factors are decoupled as can be seen in Equation 3.2. In this equation, the  $n$  refers to the number of levels for factor A, which is equal to three and the  $m$  refers to the number of levels for factor B which is four. Therefore, the number of experiments is equal to 12. To improve the reproducibility of the results every experiment is repeated three times, making the total amount of separated trials 36.

$$N = n^k \quad (3.1)$$

$$N = n \cdot m \quad (3.2)$$

The preshear for all experiments is constant and equal to 4 kPa. After preshearing, the Mohr circle can be constructed and the major principal stress can be found. This value will be used for the consolidation stress ( $\sigma_1$ ) during the time consolidation. After the time consolidation is finished a normal stress of 400 Pa, 800 Pa, 1600 Pa, or 3200 Pa will be used to determine the shear stress of the material after time consolidation.

Table 3.1: Time consolidation experiment input parameters

Parameter	Unit	Value(s)
$\sigma_{pre}$	kPa	4
$\sigma_{sh}$	Pa	400, 800, 1600 and 3200
$\sigma_1$	Pa	8611
Consolidation time	h	0, 0.5 and 1.0

### 3.3. EXPERIMENTAL RESULTS

The results from the conducted experiments for 0.5 and 1 hour consolidation can be seen in Figure 3.4. The experiments are conducted by using an external bench and a Ring Shear Tester. From Figure 3.4 it can be noticed that the data on the bottom left is much lower. These data points were determined by using both the RST and time consolidation bench. During the experiments, the shear cell is transferred from the RST to the time consolidation bench and afterwards transferred back. During the transfer process bumps or other vibrational disruptions can influence the particle bed, these disruptions can cause small defects in the particle bed and it can result in a particle bed that reaches failure at a lower shear stress than the actual shear stress of the material after time consolidation. Therefore, these data points will be filtered by comparing the values with the values for the yield locus. The threshold value is set to be 2000 Pa and all data points below the threshold will be left out. The plot with the remaining data points (without the values below the threshold) can be seen in Figure 3.5.

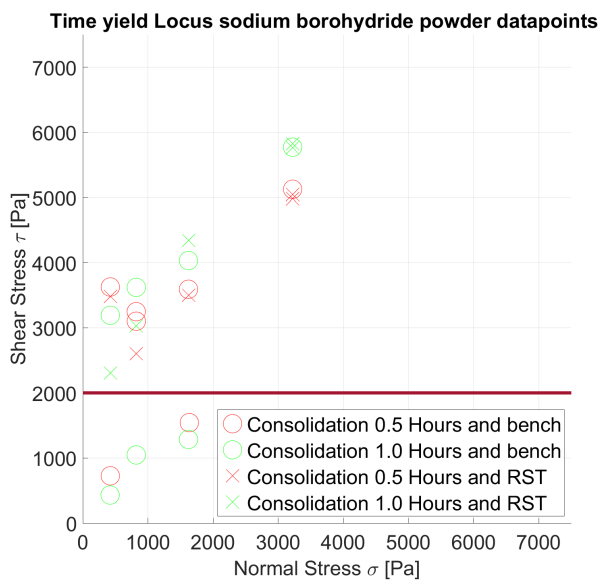


Figure 3.4: Time yield locus all data points for sodium borohydride (N=3)

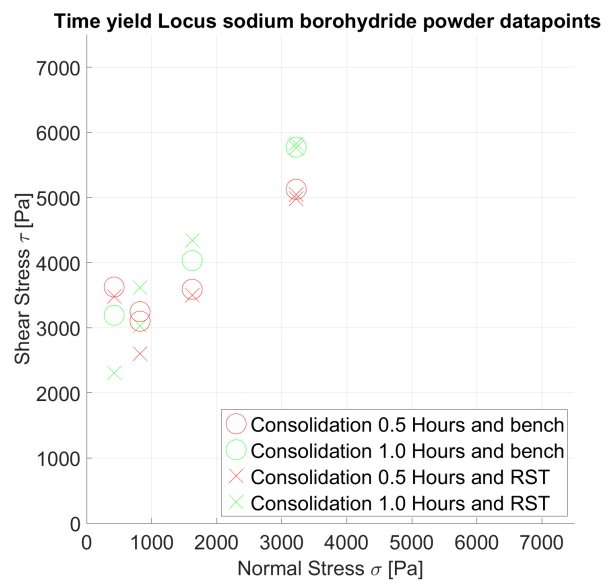


Figure 3.5: Time yield locus data points after filtering with the threshold value for sodium borohydride (N=3)

With the filtered and unfiltered data from Figure 3.4 and 3.5 the mean can be determined. The mean TYL for both cases can be seen in Figure 3.6 and 3.7. In these figures also the yield locus for 0 hours can be seen. The filtered data in Figure 3.7 shows a higher shear stress for 0.5 hours of time consolidation in comparison to 1.0 hours when looking at a normal stress of  $\sigma = 400$  Pa. This is not expected but can be due to a larger fluctuation for lower normal stresses. The lower normal stress can fluctuate so much that the shear stress ranges overlap each other. This phenomenon is not visible for higher normal stresses as can be seen from the results for  $\sigma = 3200$  Pa. Therefore, it is decided to remove the data point of  $\sigma = 400$  Pa for the final TYL, this TYL will be used for calibration of the DEM model. To confirm the conclusion that fluctuations for the shear stress are higher at lower normal stress more experiments and repetitions should be performed.

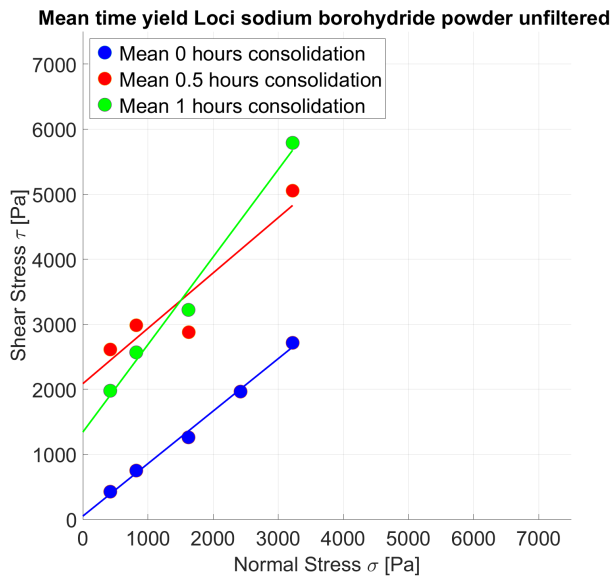


Figure 3.6: (Time) Yield Locus sodium borohydride constructed with all data points (N=3)

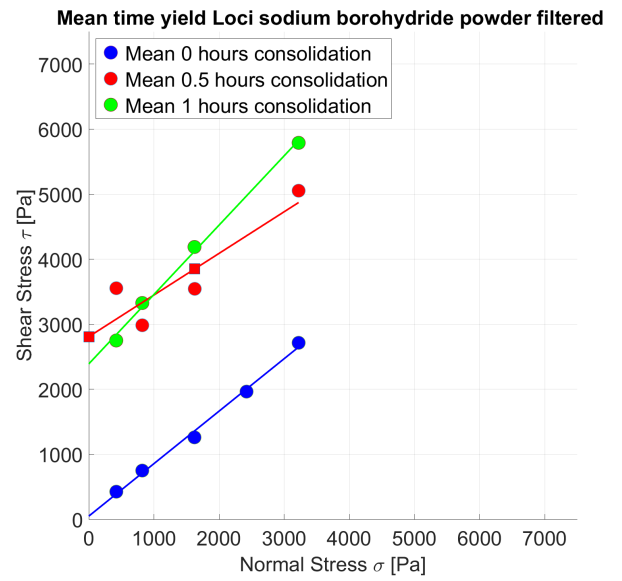


Figure 3.7: (Time) Yield Locus sodium borohydride constructed after filtering with the threshold value (N=3)

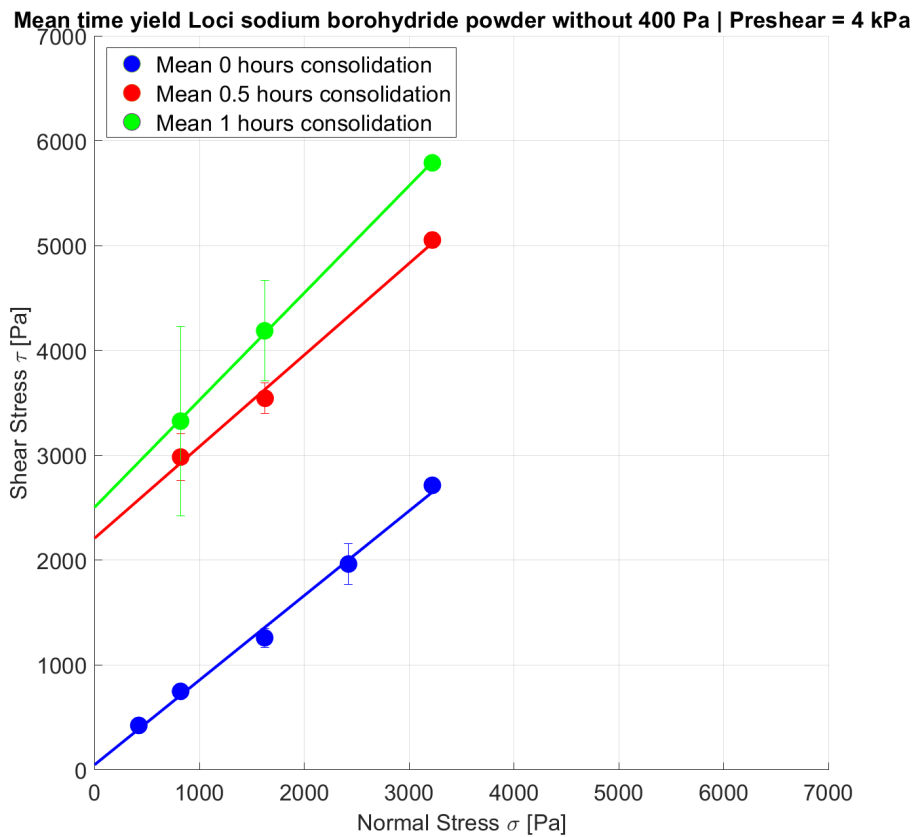


Figure 3.8: Final results for (time) yield loci with an 80 % confidence interval (N=3)

### FLOWABILITY

The flowability is affected by the strength of the material. When looking at Table 3.2 the flowability of the material for no consolidation (0 hours consolidation) is 21.4. In Table 3.2 the flow function for 0.5 and 1.0 hours of consolidation is much lower, which changes the material state from a free-flowing to a non-flowing material. The decrease is caused by an increase in the strength of the material  $\sigma_c$ , which is expected from the literature and the two influential factors are the consolidation time and  $\sigma_1$  [25]. The increase in  $\sigma_c$  of NaBH<sub>4</sub> is a factor 24 for 0.5 hours of consolidation and a factor 33 for 1.0 hours of consolidation.

Table 3.2: Flow properties for different consolidation times (N=3)

Time consolidation [h]	Cohesion [Pa]	Cohesion factor [-]	$\sigma_1$ [Pa]	$\sigma_c$ [Pa]	$\sigma_c$ factor [-]	$ff_c$ [-]
0	49	1	8611	403	1	<b>21.4</b>
0.5	2209	44	8611	9785	24	<b>0.88</b>
1.0	2504	50	8611	12132	33	<b>0.71</b>

The cohesion is another parameter that increases with a higher consolidation time, from Table 3.2 an increase in cohesion of a factor 44 after 0.5 hour of consolidation and an increase with a factor 50 for 1.0 hours of consolidation can be seen. This suggests that there is an upper limit for the increase in strength e.g. after a certain consolidation time the material does not increase more in strength and the cohesive forces between the particles have a maximum magnitude. The material changes during time consolidation, which causes a change in the cohesion and other flow properties.

The initial packing for testing of powders becomes more influential when the state is changed by for example consolidation [56]. The distance between the particles becomes smaller e.g. the powder becomes more compact and the contact surface between the particles increases. This can happen because of particle re-arrangement and plastic deformation [57]. The increase in cohesion can be due to the increase in friction between the particles. An increase in surface area between particles causes the particles to slide over each other and leads to an increase in inter-particle forces.

The experiments were performed in a lab without a climate chamber, so potentially both humidity and mechanical caking occurred similar to a practical situation. The increase in mass was measured and was within the range of the manufacturer indicating that the sorption of water was limited. The tests were performed with different samples to limit the effect of humidity on the samples. However, to measure the effect of the two caking mechanisms separately it is necessary to use the suggested climate chamber.

The slope of the time yield locus, the internal angle of friction  $\phi_t$  is often assumed to be similar to the slope of the linearized yield locus  $\phi_{lin}$  to reduce the number of experiments for the time yield locus [25]. One point on the time yield locus is measured and the slope  $\phi_{lin}$  is used to create the time yield locus. In the case of these experiments, the slope angle increases with a higher consolidation time as can be seen from Table 3.3 which could be an indication that the material acts differently under time consolidation circumstances and the increase in shear stress is higher for higher consolidation times. These results show that the assumption of  $\phi_t$  is equal to  $\phi_{lin}$  is not always valid. However, more trials and experiments should be performed to make that conclusion. Several factors can influence the results, the first one is the packing of the material. The influence of the packing is related to the voids between the particles. Initial voids between the particles can become smaller during consolidation due to a favourable orientation of particles. The increase in overlapping area causes higher inter-particle forces and a higher  $\sigma_c$  of the material, the opposite can be the case in a following trial and the result would be deviations in the results. This effect is not controllable despite a similar filling process, because it is dependent on the individual particle sizes and orientation of the particles. Another option is the sorption of water, more specifically the contribution of humidity caking to the increase in strength. Liquid bridge forming can occur when moisture sorption happens. This can cause the angles to increase and it is important that the experiments should be performed in a climate chamber.

Table 3.3: Angle of internal friction/slope of linearized yield locus (N=3)

Time consolidation [hours]	0	0.5	1.0
$\phi_t / \phi_{lin}$ [°]	38.9	41.4	45.6

### 3.4. CONCLUDING REMARKS

In this chapter the fourth subquestion: "How does time consolidation affect sodium borohydride?" is answered, with the results of the time consolidation tests.

It can be noted that the powder form of  $\text{NaBH}_4$  is affected significantly by time consolidation. The experiment shows an increase in cohesion, shear stress, and unconfined yield stress, the flowability shows the opposite and decreases. The state of  $\text{NaBH}_4$  changed from a free-flowing to a non-flowing material. The increase in strength of the material shows signs of an upper limit, it is potentially influenced by the consolidation stress, initial packing, voids between the particles, and the particle size. The experiments were not conducted in a climate chamber, so it should be noted that the increase in strength is potentially due to both mechanical and humidity caking. Repercussions were made to limit the influence of humidity caking, but it is not possible to eliminate that without a climate chamber. Further research regarding both caking mechanisms can provide more insight into the influence of humidity on time consolidation and  $\text{NaBH}_4$ . Despite, these remarks the results from Chapter 3 will be used as a basis for the calibration and verification in Chapter 4. More specifically, the constructed yield locus and two-time yield loci of  $\text{NaBH}_4$  will be used.

# 4

## MODELING TIME CONSOLIDATION

In Chapter 3, experiments with the ring shear tester were carried out, and the effects of time consolidation were identified. The behaviour will be modelled in this chapter, using DEM. The following procedure is used. First, the method for time consolidation modelling is introduced in Section 4.1. In Section 4.2 the RST setup is replicated in DEM, and a suitable contact model is chosen to simulate the observed behaviour. Then, in Section 4.3, a sensitivity analysis to determine the most influential parameters is executed. Finally, the most influential parameters are calibrated and verified, and this is discussed in Sections 4.4 and 4.5.

### 4.1. METHOD FOR MODELLING TIME CONSOLIDATION

In the literature no uniform method is found for modelling of time consolidation, so in Figure 4.1 a generic flowchart for time consolidation modelling that is used in this thesis can be seen. To model time consolidation, data on the effect of time consolidation on the material is required and it is obtained experimentally. The test that is performed is a time consolidation experiment in Schulze's RST. The experimental data that will be used to calibrate and verify the model are the yield locus and the time yield loci.

The next step is to develop a model setup of the experiment and it must mimic the time consolidation experiment. The goal is to match the experimental value for the KPI shear stress with the simulation model to mimic the material behaviour. Also, in this step, the overlap between particles in DEM should be defined by selecting a contact model and the particle properties such as the solid density, Poisson ratio, particle shape etc of the material should be found. The particle shape needs to be modelled, often when dealing with an irregularly shaped particle it is possible to use a spherical shape and still obtain similar bulk behaviour [26, 58]. The final part of this step is to make sure that the computational time is not unpractical high, so scaling might be necessary to achieve that.

To describe the behaviour of the material KPI(s) (at least one) and input parameters (most influential parameters) of the model and material need to be selected. The most influential parameters (at least three) and the KPI(s) are used in a sensitivity analysis that consists of a statistical approach. DOE can be performed as described in Section 3.2 and one of the options is full factorial design. In this study, three factors will be analysed in the sensitivity analysis, so full factorial design is suitable to determine the two most influential factors. When dealing with 5 or more factors full factorial design can be time-consuming so a different method can be used such as fractional factorial design [59]. The KPI(s) should be similar to the experimental data to match the experimental data with the output response(s) of the simulation model.

The next step is to calibrate and verify the model using the experimental data and find a unique parameter set for different consolidation times. The method to verify and calibrate the model will be discussed in detail in Subsection 4.1.1. The final step is to determine if a relationship for the two most influential parameters over time can be found and these relationships enable the instantaneous creation of a time-consolidated particle bed that mimics the material behaviour after a consolidation time.

4

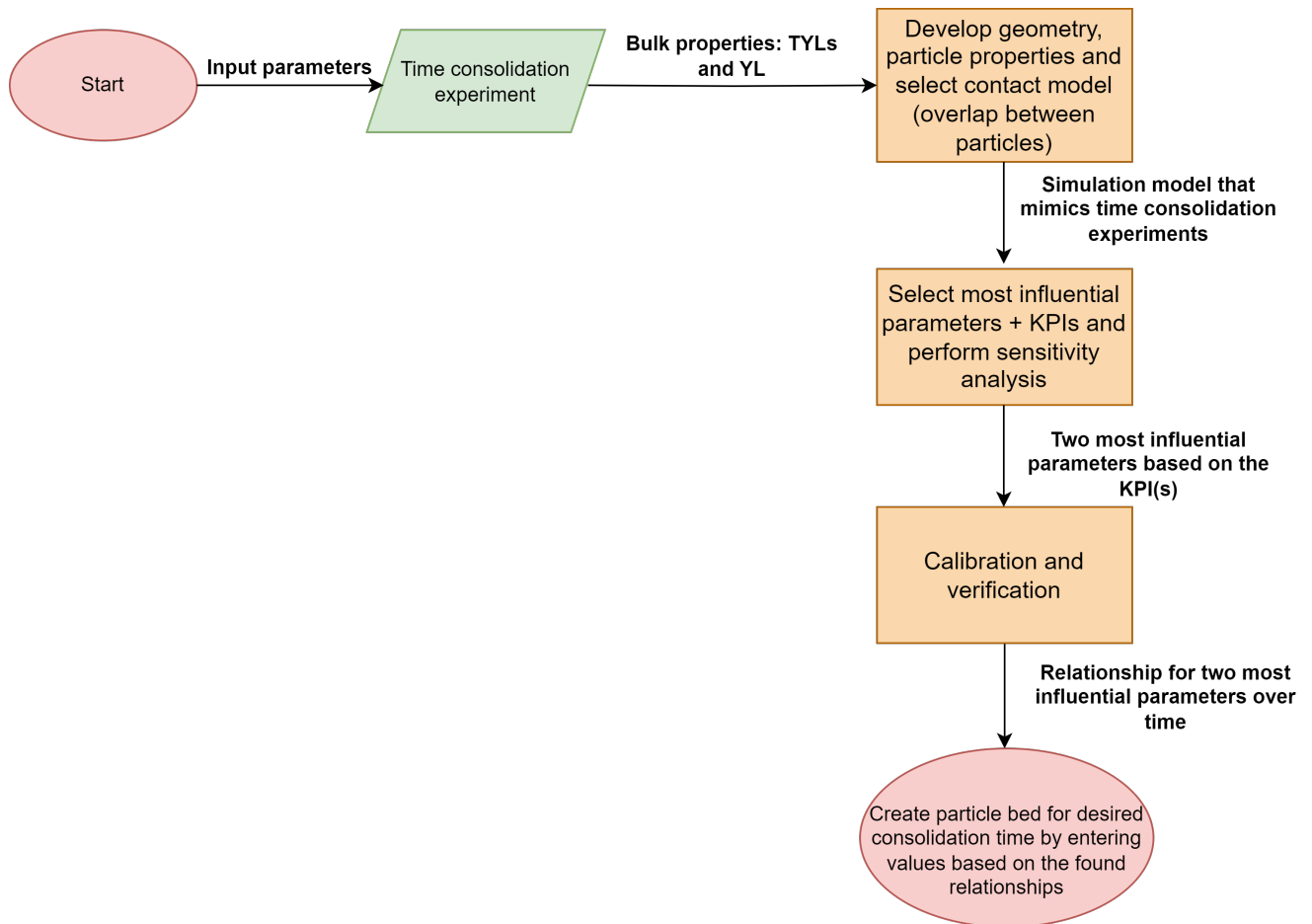


Figure 4.1: Generic flowchart for modelling time consolidation in DEM

4.1.1. CALIBRATION AND VERIFICATION FRAMEWORK

The calibration and verification step consists of two steps. With the two most influential parameters and one KPI for example the shear stress a contour plot can be made with on the x-axis one parameter and the y-axis the other parameter. The contour plot represents combinations of the two parameters and the corresponding KPI value for that specific combination. The process described above will be done in simulation B and the following step is to search for the KPI value of experiment B ( $t=0.5$  hour &  $\sigma = 1600$  Pa) in the contour plot and a parameter set (line) with combinations of the two most influential parameters is found indicated in the next square as B set 1-B Set j. Similarly, this is done in simulation and experiment C ( $t=0.5$  hour &  $\sigma = 3200$  Pa) and a parameter set, C Set 1-C Set j is found. To verify the model and find a parameter set for one consolidation time an overlap between these two parameter sets is searched for and the overlap is considered as the optimised parameter set for one consolidation time. In this thesis, the process is repeated for two consolidation times of 0.5 and 1.0 hours with two normal stress levels of 1600 and 3200 Pa.

After the optimised parameter set for 0.5 and 1.0 hour consolidation is found, the value for 0 hours of time consolidation is extrapolated and with this final data point, the relationship for the parameters over time can be fitted for the range of  $0 \leq t \leq 1$ .

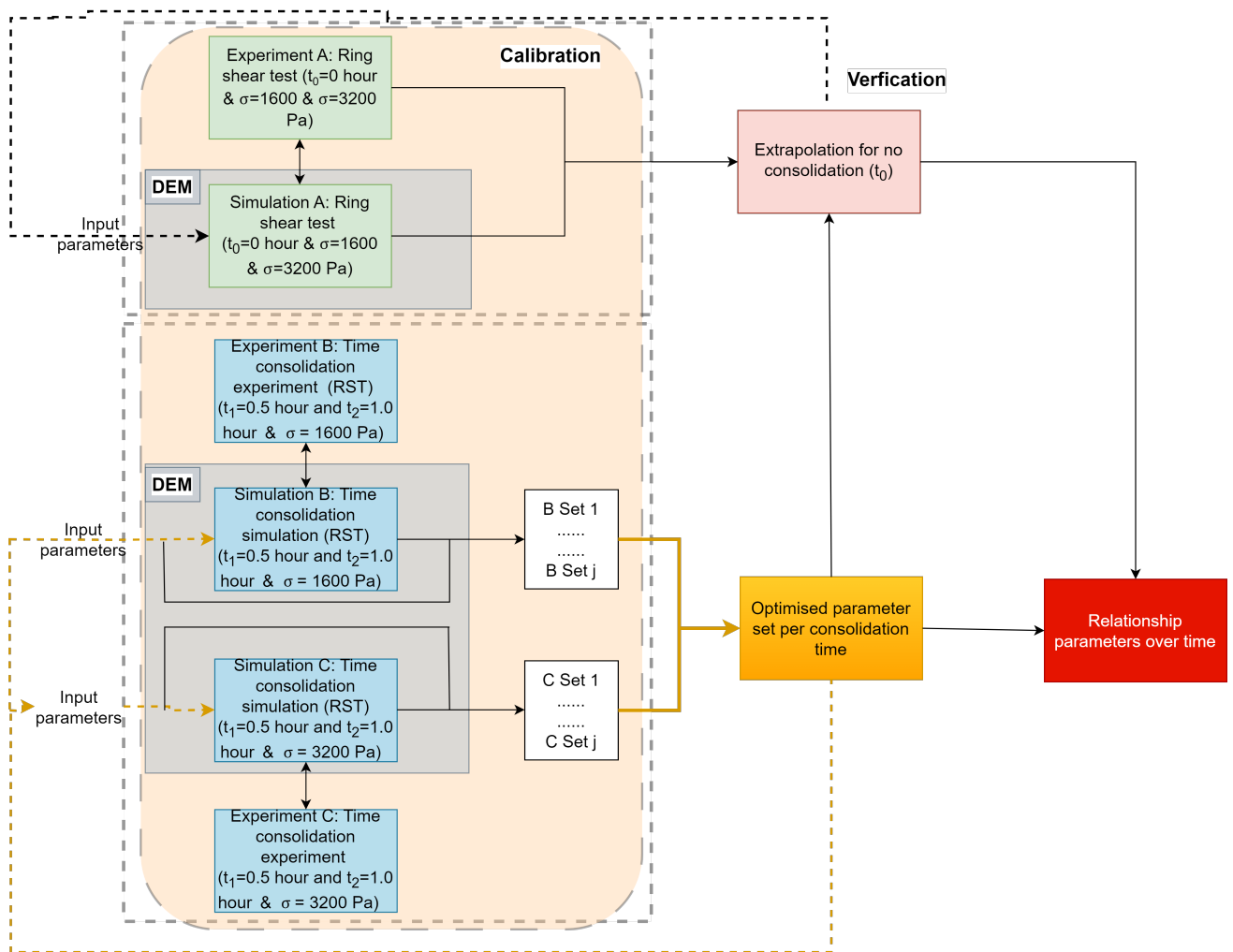


Figure 4.2: Framework for calibration and verification of time consolidation for NaBH<sub>4</sub> using DEM

## 4.2. THE DEM MODEL: TIME CONSOLIDATION RING SHEAR TEST

In this study the effect of time consolidation on sodium borohydride is investigated. The method presented in Section 4.1 shows the complete procedure. Previously, experiments were conducted to determine the strength of the material when it is subjected to a vertical load e.g. time consolidation. Experiments were conducted using Schulze's RST and to mimic the test, modelling of the RST is required. In this study the model of Mohajeri [51] will be used, developed to model the behaviour of cohesive iron ore (8.7% moisture content). The model uses a simplification with a quarter of the shear cell filled, this can be seen in Figure 4.3. Mohajeri concluded that the simulation shows similar results as for a filled shear cell with a significant benefit of a reduced computation time by at least 50 %. The RST model represents a normal RST test, so no time consolidation occurs. In this study, time consolidation is not modelled explicitly, but captured by artificially changing the most influential parameters for  $\text{NaBH}_4$  in the simulation. The result is a DEM model with varying input parameters that can be used to instantly create a time-consolidated particle bed that can be used for the simulation of a real-life application.

4

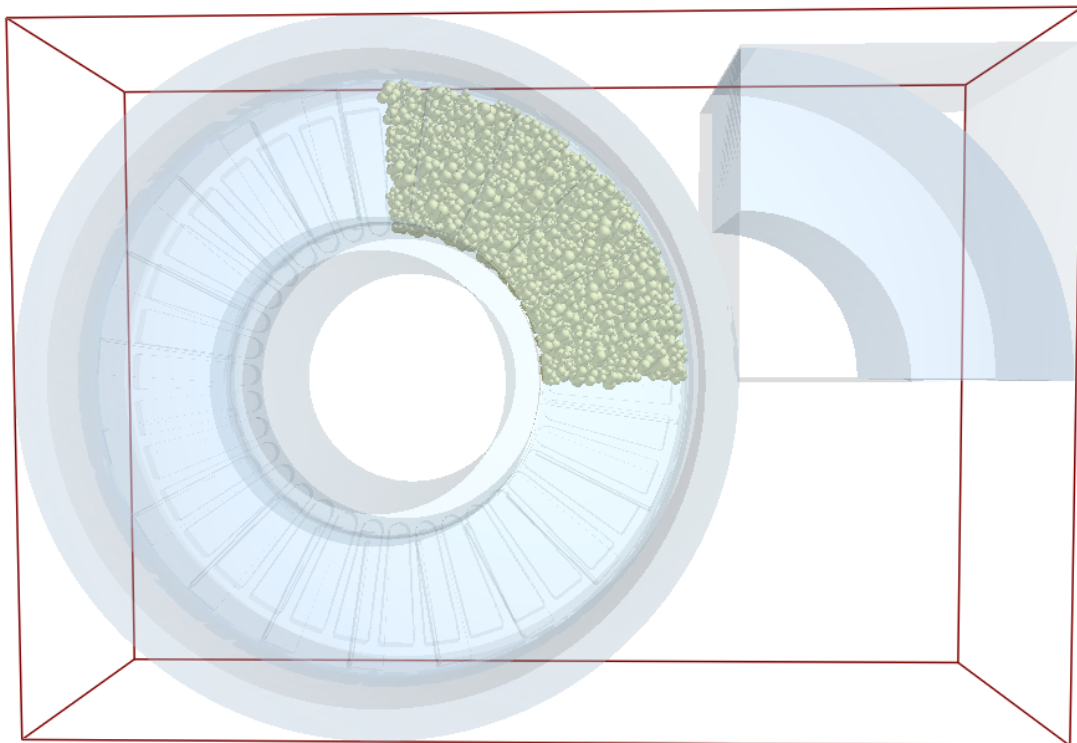


Figure 4.3: Filled shear cell in EDEM

### 4.2.1. THE CONTACT MODEL

The contact model used for modelling of the particle-particle interactions is the Edinburgh Elasto Plastic Adhesive model described in Subsection 2.4.3, the same contact model that Mohajeri used to calibrate the simulation model for cohesive iron ore.  $\text{NaBH}_4$  can be considered a cohesive or even a non-flowing material after time consolidation and the stress history needs to be captured to model this. For the particle wall interactions, the contact model Hertz-Mindlin (no slip) is selected. In Mohajeri's work [51], the model was applied under the assumption of negligible adhesive strength. Furthermore, based on the practical observations regarding material handling and storage in containers, it is assumed that the particle-wall interactions are also considered negligible.

In Table 4.1 the parameters that remain constant during the simulations can be seen. First, the chemical properties of  $\text{NaBH}_4$  such as the shear modulus, Poisson ratio, and particle density are listed. Next, the particle-particle interaction and particle-wall interactions can be seen.  $\text{NaBH}_4$  particles are not irregularly shaped, so modelling the particle shapes is challenging and leads to unpractical computational times.

Therefore, a more simple model with spherical particles is used, it is still important that the rotational torque

Table 4.1: Constant input parameters in DEM model [26, 60]

Parameter	symbol	unit	value
Shear modulus	$G_p$	GPa	10
Poisson ratio	$\nu$	-	0.28
Particle density	$\rho$	$kg/m^3$	1070
Rolling friction coefficient	$\mu_{r,p-p}$	-	Rotation restriction (RR) / 0.9
Coefficient of static friction (wall-particle)	$\mu_{r,w-p}$	-	0.1
Coefficient of restitution	$e$	-	0.1
Particle shape	$\Psi_p$	-	sphere
Particle size distribution (PSD)	$d_p$	$\mu m$	$289 \pm 94$
Plasticity ratio	$\lambda_p$	-	0.75
Slope exponent	$n$	-	1.5
Tensile exponent	$\chi_{p-p}$	-	7.7

Table 4.2: Variable input parameters in DEM

Parameter	symbol	unit	range
Coefficient of static friction (particle-particle)	$\mu_{r,p-p}$	-	0.1-1.0
Surface energy	$\Delta\gamma$	$J/m^2$	1-100
Constant pull-off force	$-f_0$	N	0.0005-0.05

is considered. This can be done by either using a non-spherical shape or restricting the rotational freedom. In this study, a spherical shape is selected, so rotation restriction is required. There are two methods to restrict the rotational freedom, the first one is by restricting the particle rotation and the second one is to artificially do so and use a rolling friction module. Mohajeri [51] used both methods and made a comparison where some advantages were found by using rotation restriction over using a rolling friction model (type C) [61]. One advantage of restricting the rotational freedom is a lower computational time, because lower cohesive and friction forces can be used for the calibration and this reduces the simulation time and a second benefit is the reduction of the number of input variables. Multiple researchers used this principle to mimic real-life material behaviour [51, 62]. The particle diameter and Particle Size Distribution (PSD) are determined by data acquired from Delft Solid Solutions (DSS).

The final three parameters are required for the contact model: the plasticity ratio, slope exponent, and tensile exponent. The plasticity ratio captures the virgin loading stiffness  $k_1$  and the tangential stiffness  $k_2$ , which can be seen in Equation 4.1.

$$\lambda_p = 1 - \frac{k_1}{k_2} \quad (4.1)$$

The virgin loading stiffness and tangential stiffness are equal for a plasticity ratio of 0, which results in an elastic model. When the plasticity ratio is equal to 1 the model is completely plastic. In this study, a plasticity ratio of 0.75 is used. Mohajeri [51] showed that this value was sufficient for a cohesive material and when looking at the experiments NaBH<sub>4</sub> showed cohesive/non-flowing behaviour according to the flow function. This suggests that the plasticity ratio should be the same or a bit higher when dealing with a non-flowing material. In the same study, Mohajeri used for the cohesive material iron ore a slope exponent and tensile exponent of 1.5 and 7.7 respectively, so these values will also be used in this study.

In Table 4.2 the three variable inputs of the simulation can be seen. The internal shear strength is highly dependent on the sliding coefficient between particles for non-cohesive materials [63] and Mohajeri [51] showed that it was the most influential parameter for the cohesive material iron ore. Therefore, this parameter is taken into consideration for the sensitivity analysis. The other two parameters surface energy and constant pull-off force were also considered influential factors for iron ore in the study of Mohajeri, but these were not the most influential. The three levels for the parameters are selected to simulate with a "low", "medium" and "high" value and will be used for the sensitivity analysis in the next section.

### 4.2.2. SCALING

To reduce the computational time of the simulation multiple possibilities exist. They can be categorized into two categories. The first one is the computational techniques, for example, it is possible to reduce the stiffness of the model to reduce the computational time of the simulation. Lommen et al [64] showed that a reduction of the shear modulus up to  $10^6$  Pa gave similar responses as for using a value of  $10^{11}$  for a ledge test.

The second group is related to scaling the geometry or particle properties. This is the most commonly used group to reduce computational cost [65]. Scaling of the particle size had several consequences for other particle properties. The sliding friction and the surface energy are scaled with the same factor as the particle size and the constant pull-off force needs to be scaled with the square of the scaling factor for the particle size in the EEPA contact model according to Mohajeri [26].

In this study the particles are scaled by using Coarse Graining (CG) with a scaling factor of 7 as proposed by Mohajeri [26]. In Table 4.1 the PSD can be seen and is  $0.289 \pm 0.094$  mm. In Figure 4.4 the results of the test of DSS can be seen for the particle size distribution (PSD), the PSD was determined and with the figure, the assumption was made to limit the maximum and minimum particle size of the distribution to 10 % and 90 % of the distribution and a cap was used in the simulation to reduce the computational time. The computational time is dependent on the smallest particle, so by using a cap, the computational time is reduced significantly. In Table 4.3 the real values and scaled values for the particle size can be seen. The cap provides a reduction of the computational time and when looking at Figure 4.4 the curve shows a narrow PSD indicating that the PSD shows low deviations from the mean particle size.

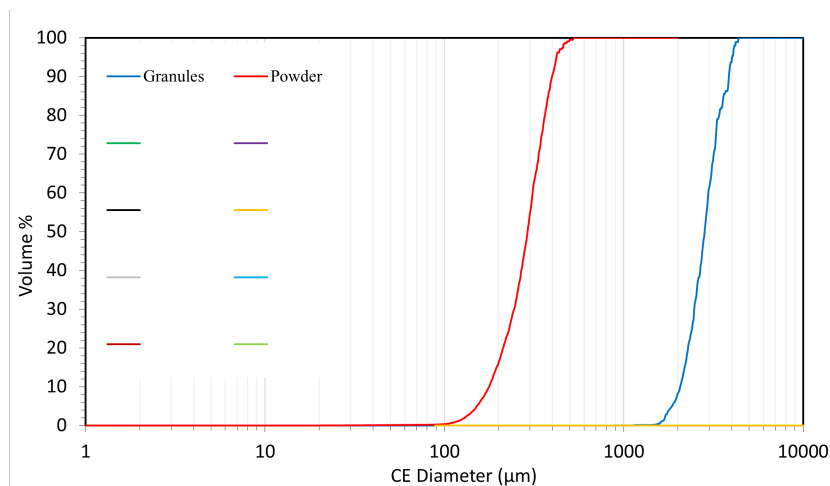


Figure 4.4: Volume vs diameter for the powder (red) and granular form (blue) of  $\text{NaBH}_4$

Table 4.3: Scaling particle size with a scaling factor of 7

	Mean diameter [mm]	Standard deviation [mm]	Minimum [mm]	Maximum [mm]
Real (1)	0.289	0.094	0.10	0.5285
Scaled (7)	1.015	0.658	0.70	3.70

### 4.2.3. SIMULATION PLAN

In this section the simulation plan of this thesis is presented.  $\text{NaBH}_4$  is irregularly shaped and trying to replicate these shapes leads to unpractical high computational times. Two methods where spherical particles can be used will be analysed in this thesis, the first one is to use a rolling friction model (type C) and the second is to restrict the rotation of particles. 4.5 shows the general procedure for the simulations, so this procedure is used twice for both individual cases. The procedure is a causal iterative process where the previous step is required to advance to the next step. The simulation plan starts with a sensitivity analysis to determine the most influential parameters of  $\text{NaBH}_4$  by literature search and modelling. In the sensitivity analysis, the two most influential parameters are selected to advance to the next step and calibrate the model. For the calibration, contour plots of the desired output response are necessary and with experimental data or data from the literature an optimised parameter set for every consolidation time is searched for. In this thesis, 0, 0.5 and 1.0

hour of consolidation are analysed and for 0.5 and 1.0 hour of consolidation, the method mentioned above is used. To find the value for no consolidation (0 hour of consolidation) extrapolation with the data points of 0.5 and 1.0 hour of consolidation is done. The extrapolation is based on the fit used to determine the relationship of the experimental data over time. The final step is to compare the two cases to see the similarities and pros and cons of using the specific method for modelling irregular particle shapes as spherical particles.

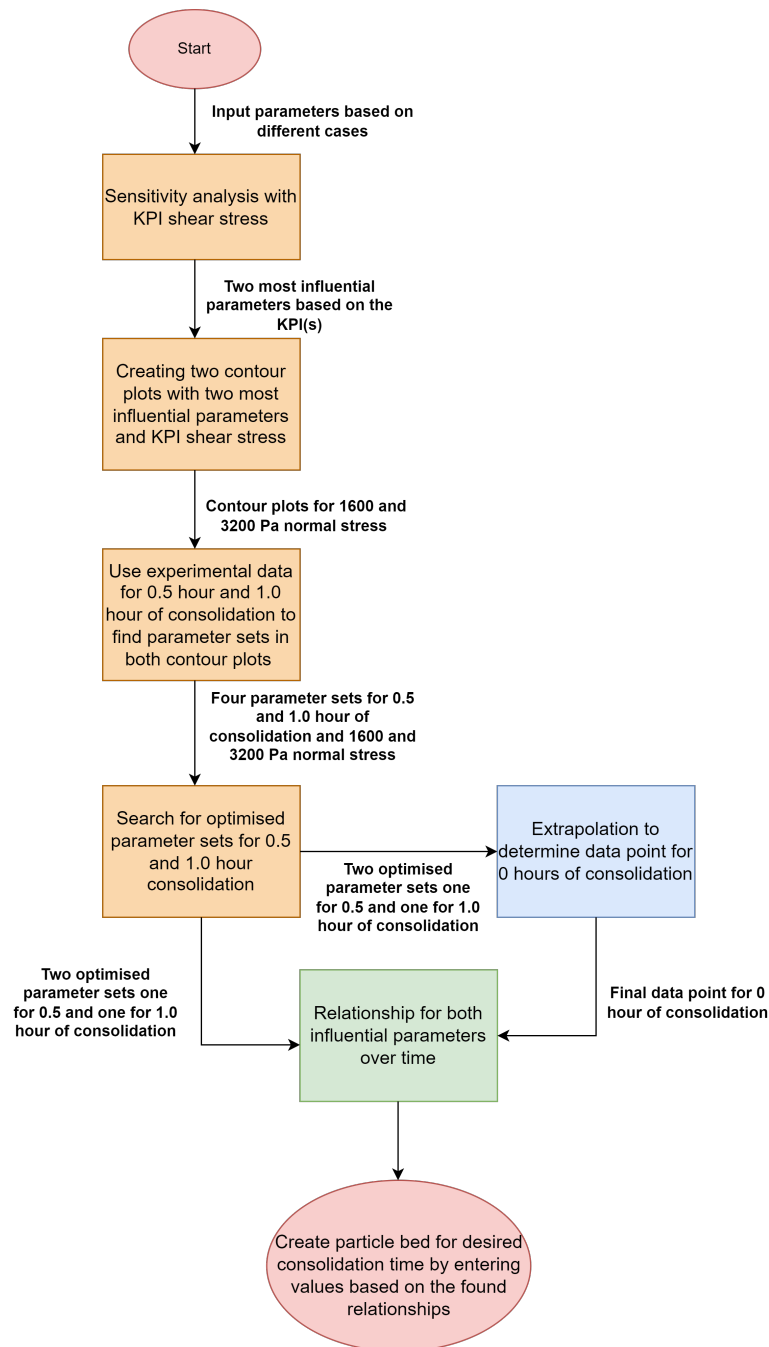


Figure 4.5: Simulation plan for calibration and verification of DEM model

#### 4.2.4. REFERENCE CASE

For the sensitivity analysis of the model, it is important to select a Rayleigh time step for the simulations, the Rayleigh time step is selected by varying the value and the results are compared to see the influence of the time step. In table 4.4 the results for varying the time step can be seen and from the results, it can be noticed that varying the time step above 10% shows a lot of deviation in the output response. Therefore, a time step higher than 10% will result in a non-stable simulation. To ensure a stable simulation the time step that will be used in this study is 10%. In Table 4.5 the input parameters and the results with a 95 % confidence interval are presented. The results are based on four trials and a Rayleigh time step of 10%.

Table 4.4: Rayleigh time step results

Rayleigh time step [%]	Rayleigh time step * 10 <sup>-6</sup> [s]	Shear stress [kPa]	Deviation shear stress in comparison to 5 % Rayleigh time step [%]
5	4.095	2.910	0
7.5	6.142	2.857	-1.86
10	8.190	3.081	+5.88
15	12.28	3.231	+11.0
20	16.38	3.109	+6.84
30	24.57	3.086	+6.05
40	32.76	3.501	+20.3
50	40.95	1.751	-39.8

Table 4.5: Reference simulation input parameters and result (in bold) 95% confidence interval

Input parameters	Symbol	unit	Value
Rayleigh time step	$t_{ray}$	%	10
Coefficient of static friction	$\mu_{r,p-p}$	-	0.3
Constant pull-off force	$-f_0$	N	-0.01
Surface energy	$\Delta\gamma$	J/m <sup>2</sup>	40
Normal stress	$\sigma_{shear}$	kPa	3.2
<b>Shear stress (95%) CI</b>	$\tau_{shear}$	<b>kPa</b>	<b>3.505 ± 0.147</b>

### 4.3. SENSITIVITY ANALYSIS

In the sensitivity analysis the same method is used as for the experimental plan, DOE presented in Section 3.2. This method provides the benefit of investigating the main and joint effects of the different factors. Initially, there were six parameters to describe the physics of the material using the EEPA model.

The six parameters are the

- Static friction
- Rolling friction
- Coefficient of Restitution
- Plasticity ratio
- Surface energy
- Constant pull-off force

The six parameters mentioned above can be separated into a category independent of the contact model the three parameters that fall into this category are static friction, rolling friction and coefficient of restitution. The three parameters specifically for the EEPA model are the plasticity ratio, surface energy and constant pull-off force. From these six parameters, three are assumed based on the literature. The value for the rolling friction is estimated by van Bente to be 0.9 and a second case with the rolling friction is used where the rotation is restricted and no value for the rolling friction is required [61]. Next, the coefficient of Restitution and plasticity ratio are based on the study of Mohajeri [26].

This leaves the static friction, surface energy and constant pull-off force for the sensitivity analysis as can be seen in Figure 4.6. The output response in this study is the shear stress and in the sensitivity analysis, a normal stress of 3200 Pa is used to determine the two most influential factors.



Figure 4.6: Design Of Experiments for sensitivity analysis

Table 4.6: Levels (low, medium and high) for most influential parameters used in sensitivity analysis

Labels	Factor	Units	Low level (-1)	Medium level (0)	High Level
A	Static friction	-	0.1	0.5	1.0
B	Surface energy	J/m <sup>2</sup>	1	10	100
C	Constant pull-off force	N	0.0005	0.005	0.05

In Table 4.6 the levels for all three parameters can be seen and in the sensitivity analysis all combinations of these three levels will be analysed for the KPI shear stress, making the total amount of simulations 27.

#### 4.3.1. RESULTS SENSITIVITY ANALYSIS

The results of the sensitivity analysis can be seen in Figure 4.7. Figure 4.7a-c on the left shows the results of the individual parameters versus the KPI (output response) shear stress.

In Figure 4.7a it can be seen that for the static friction, the shear stress increases from approximately 3 kPa to approximately 7 kPa. For the surface energy the shear stress increases from 4 kPa to 5.5, as can be seen in Figure 4.7b. The last figure, Figure 4.7c shows an increase from 4.5 kPa to 4.7 kPa for the shear stress. The two most influential parameters based on these three figures are the static friction and surface energy.

In the Figures 4.7d-f the coupled influence from two of the three parameters can be seen. In Figure 4.7d the influence of the static friction and surface energy on the shear stress can be seen. When comparing the three coloured dots for one static friction value vertically, it can be seen that for increasing surface energy the shear stress increases. The increase of the shear stress is at minimum 1 kPa up to a maximum of 2 kPa.

The increase by looking at the three levels of the static friction can be seen by individually looking at the three coloured lines. The lines show a higher increase in shear stress in comparison to the surface energy, the shear stress increases by a minimum of 3.5 kPa upto a maximum of 4.5 kPa.

Figure 4.7e shows the influence of the static friction and the constant pull-off force. The increase in shear stress for the static friction can be seen by looking at the individual lines, the increase is at least 3.5 kPa and has a maximum of 4.5 kPa. When looking at the constant pull-off force the individual coloured points for one static friction level (vertical direction) must be compared. When looking at these points the minimum increase is 0.5 kPa and a maximum of 1.5 kPa.

The final figure, Figure 4.7f shows the influence of the constant pull-off force and the surface energy. The constant pull-off force is approximately constant when looking at the individual lines, showing no significant increase in shear stress. The surface energy can be compared by the vertical coloured points for one level of the constant pull-off force and the increase in shear stress has a minimum of approximately 1 kPa and a maximum of 1.5 kPa.

From these results it can be concluded that the static friction is the most influential factor, followed by the surface energy and the least influential parameter is the constant pull-off force. As expected from the literature, static friction is the most influential parameter for non-cohesive materials and the cohesive material iron-ore [51, 63].

The input parameter for the constant pull-off force is chosen to be the value where the most deviation can be found and that is for a value of  $-0.005$ . The other two parameters, static friction and surface energy are used to calibrate and verify the DEM model.

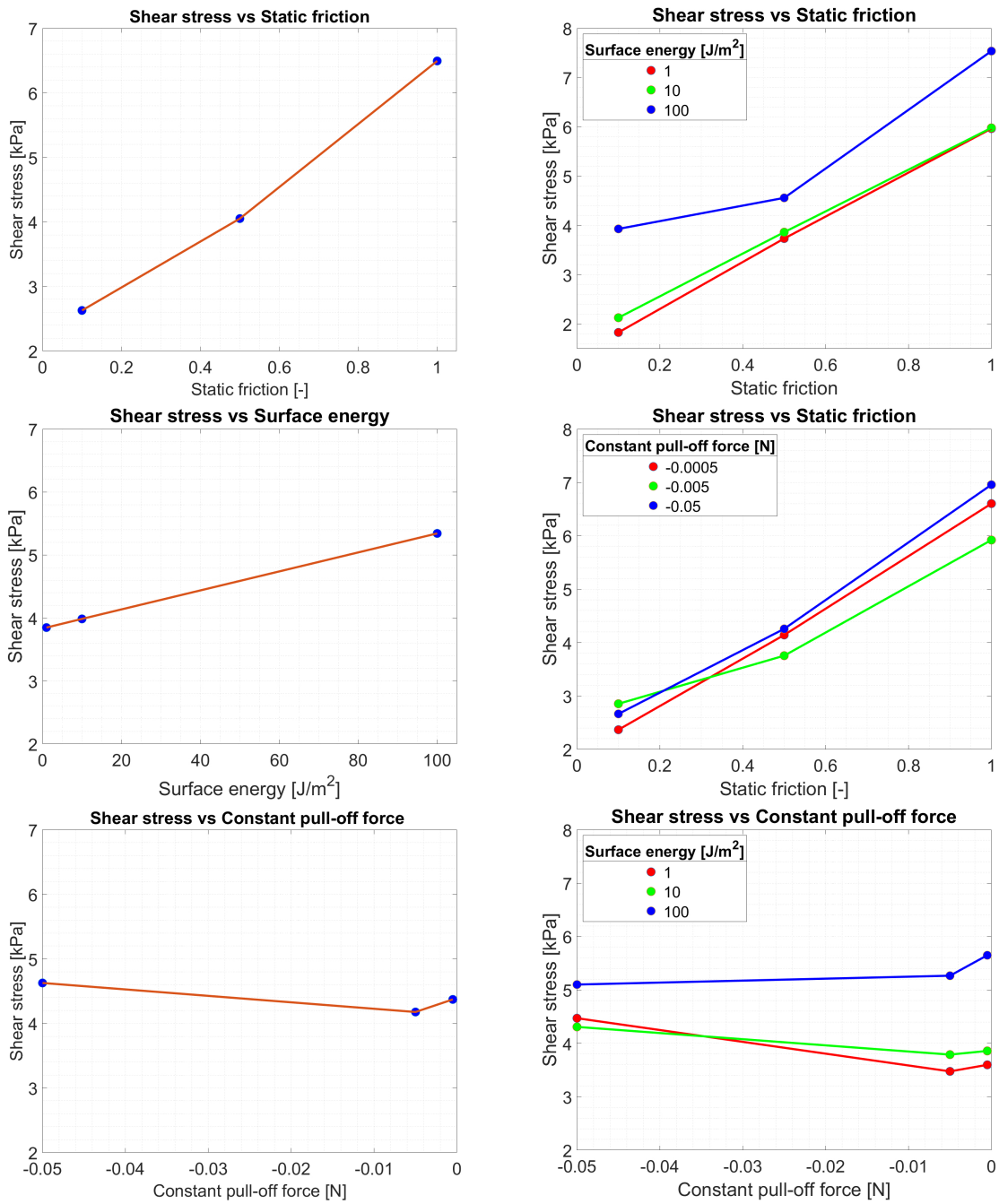


Figure 4.7: Shear stress vs (a) static friction (b) surface energy (c) constant pull-off force (d) static friction and surface energy (e) static friction and constant pull-off force (f) constant pull-off force and surface energy

#### 4.4. CALIBRATION AND VERIFICATION ROTATION RESTRICTION CASE

In Chapter 3 experiments were performed with the RST for a preshear of 4 kPa. From the experiments, the yield locus and the time yield loci for 0.5 and 1.0 hour of consolidation were determined. These time yield loci will be used as a basis for the calibration of the model in DEM. In Table 4.7 the relevant points of the yield loci for 0, 0.5 and 1.0 hours of consolidation and for the two normal stresses 1600 and 3200 Pa can be seen, these values will be used to calibrate the coefficient of static friction and surface energy. Figure 4.8 shows the complete procedure to determine the relationships for both the static friction and surface energy over time.

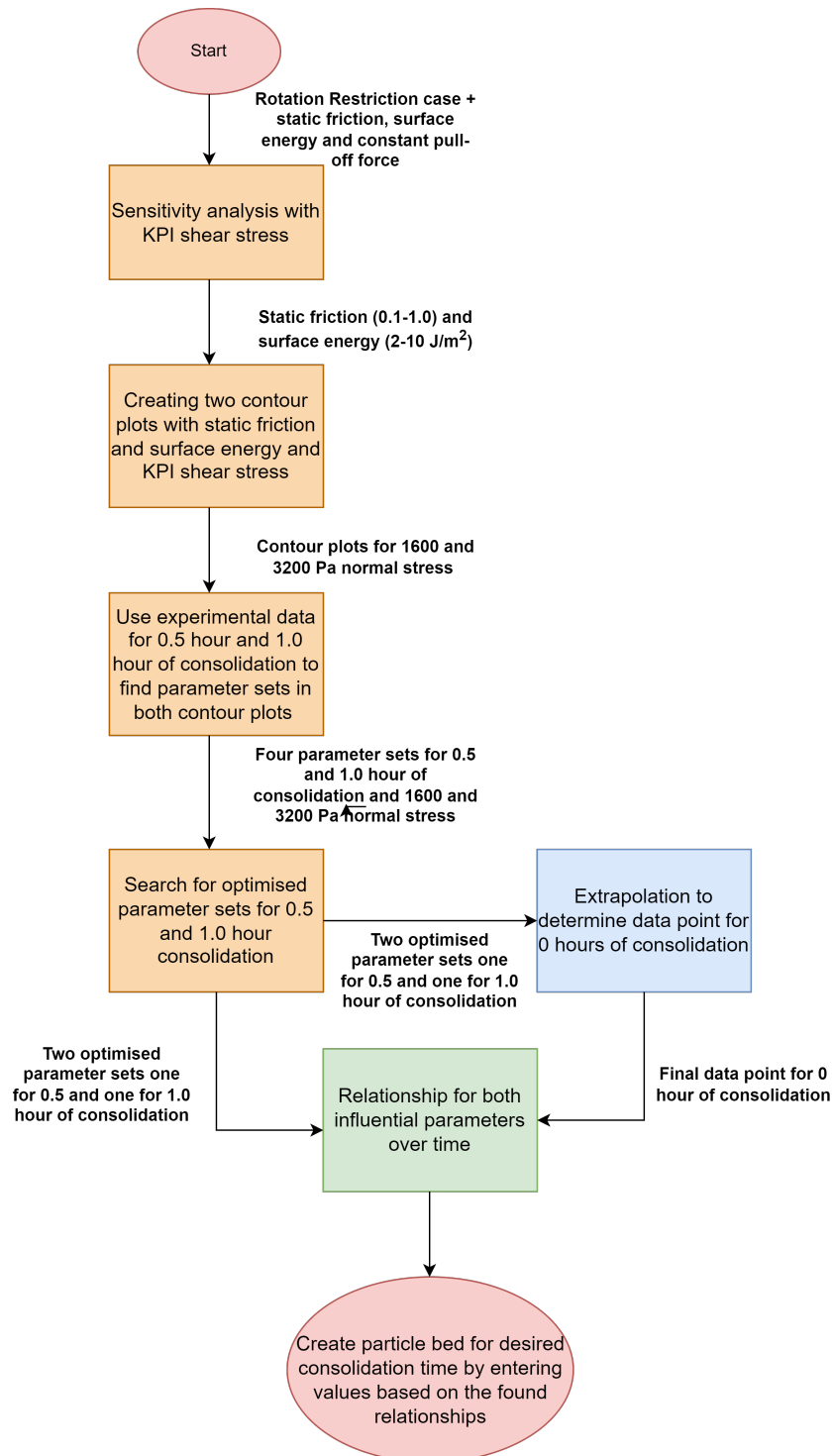


Figure 4.8: Calibration and verification for Rotation Restriction case

Table 4.7: Shear stress values for calibration of time consolidation

Normal stress [Pa]	Shear stress 0 hours TC [kPa]	Shear stress 0.5 hours TC [kPa]	Shear stress 1.0 hours TC [kPa]
1600	1.3	3.6	4.2
3200	2.6	5.0	5.8

In the calibration two parameters will be used to calibrate the DEM model, these parameters were selected in Section 4.3 and are the static friction and surface energy. In Table 4.8 the range and increments for both factors can be seen for the Rotation Restriction case. The goal is to find a trend/correlation between static friction and surface energy over time. This correlation in combination with the model can be used to instantly create a time-consolidated particle bed.

Table 4.8: Calibration range Rotation Restricted case

Parameter	Unit	Values
$\mu_{r,p-p}$	-	0.1, 0.2, 0.4, 0.6, 0.8 and 1.0
$\Delta\gamma$	J/m <sup>2</sup>	2, 4, 6, 8 and 10

#### 4.4.1. PROCEDURE CALIBRATION

The calibration process involves evaluating shear stress for different normal stresses, represented by contour plots. More specifically, in this study contour plots corresponding to normal stresses 1600 (seen in Figure 4.9) and 3200 Pa (seen in Figure 4.10). To calibrate the model, the aim is to match specific shear stress values corresponding to consolidation times. For instance, for a consolidation time of 1 hour, a shear stress of 4.2 kPa within the contour plot of 1600 Pa (Figure 4.9) is searched for. Subsequently, a shear stress of 5.8 kPa within the contour plot of 3200 Pa (Figure 4.10) is targeted. Upon obtaining these shear stress values, overlapping regions in the two contour plots are identified to determine an Optimised parameter set for the static friction and surface energy. These parameters represent the material's behaviour during 1 hour of consolidation. This process is repeated for consolidation times of 0 and 0.5 hours.

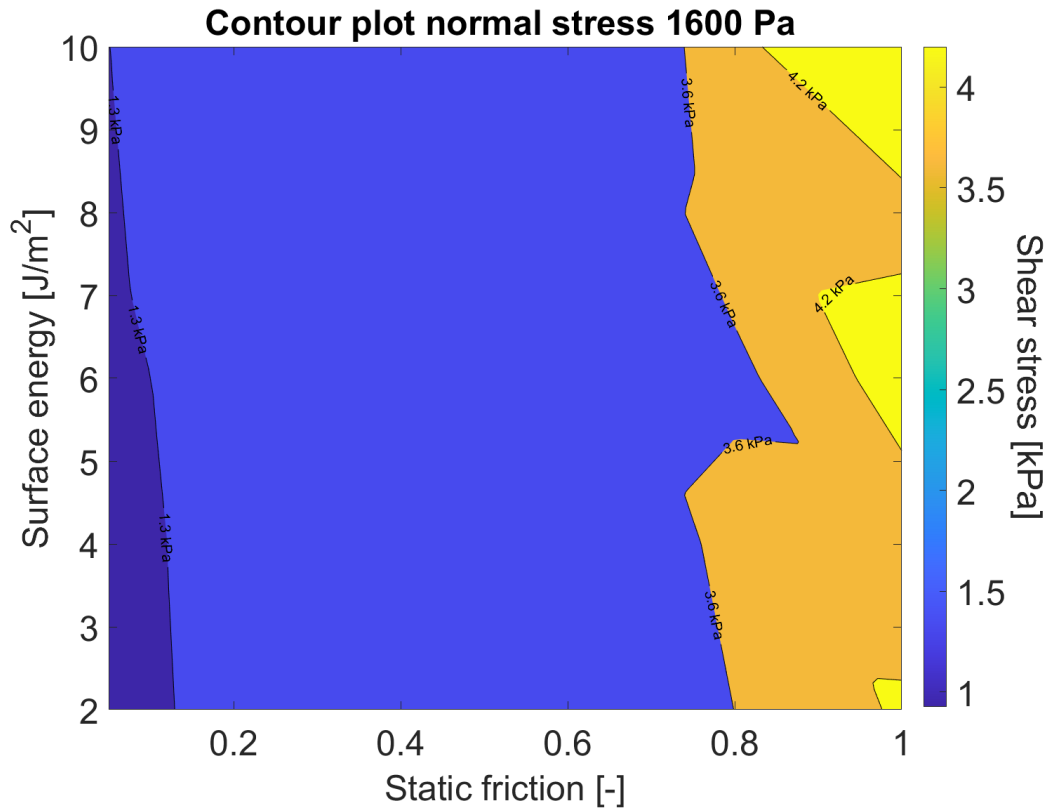


Figure 4.9: Contour plot KPI shear stress for normal stress 1600 Pa Rotation Restriction case

In Figure 4.11 a blue line can be seen, this line represents all the combinations of surface energy and static friction from the contour plot of 3200 Pa resulting in a shear stress of 5.8 kPa. Similarly, the red line shows all the combinations of surface energy and static friction from the contour plot of 1600 Pa that result in a shear stress of 4.2 kPa. An overlap can be found at a static friction of 0.744 and a surface energy of 7.90 J/m<sup>2</sup>. This process is done for 0 (see Subsection 4.4.2), 0.5 (see Appendix E), and 1.0 hours of consolidation. For 0 hours of consolidation, no result was found, in the next Subsection 4.4.2 an extrapolation method is introduced to determine the value for no consolidation.

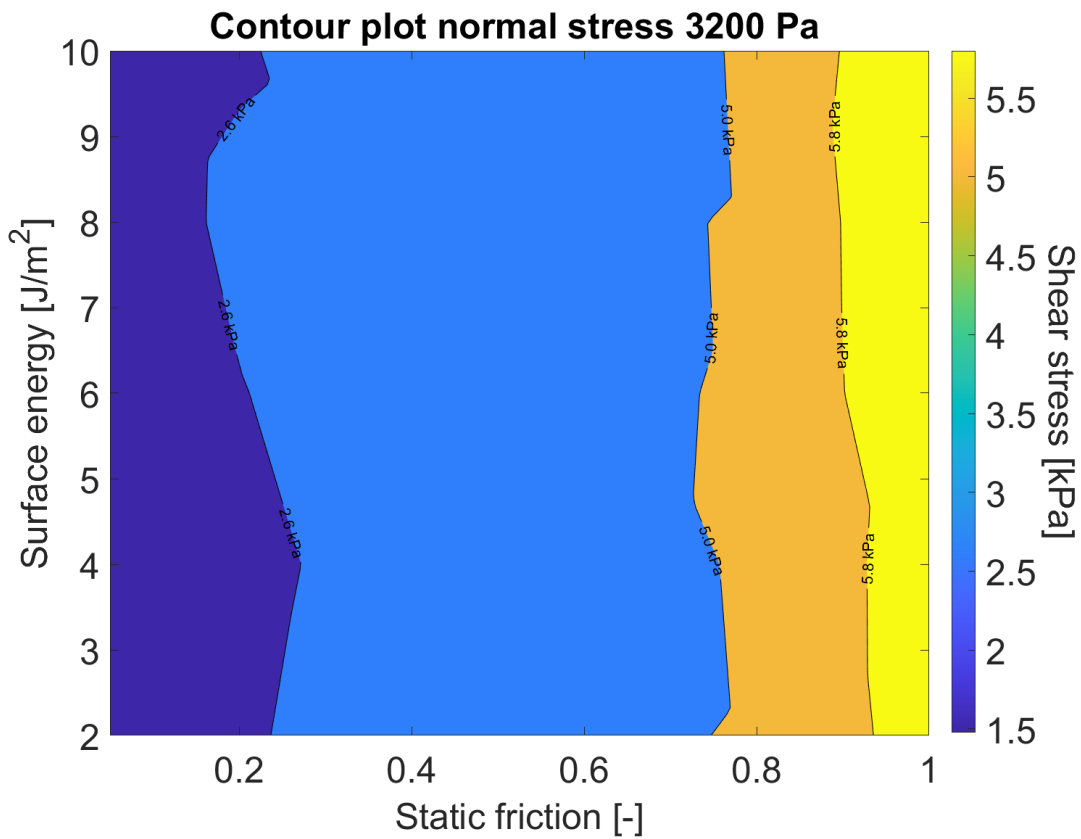


Figure 4.10: Contour plot shear stress for normal stress 3200 Pa Rotation Restriction case

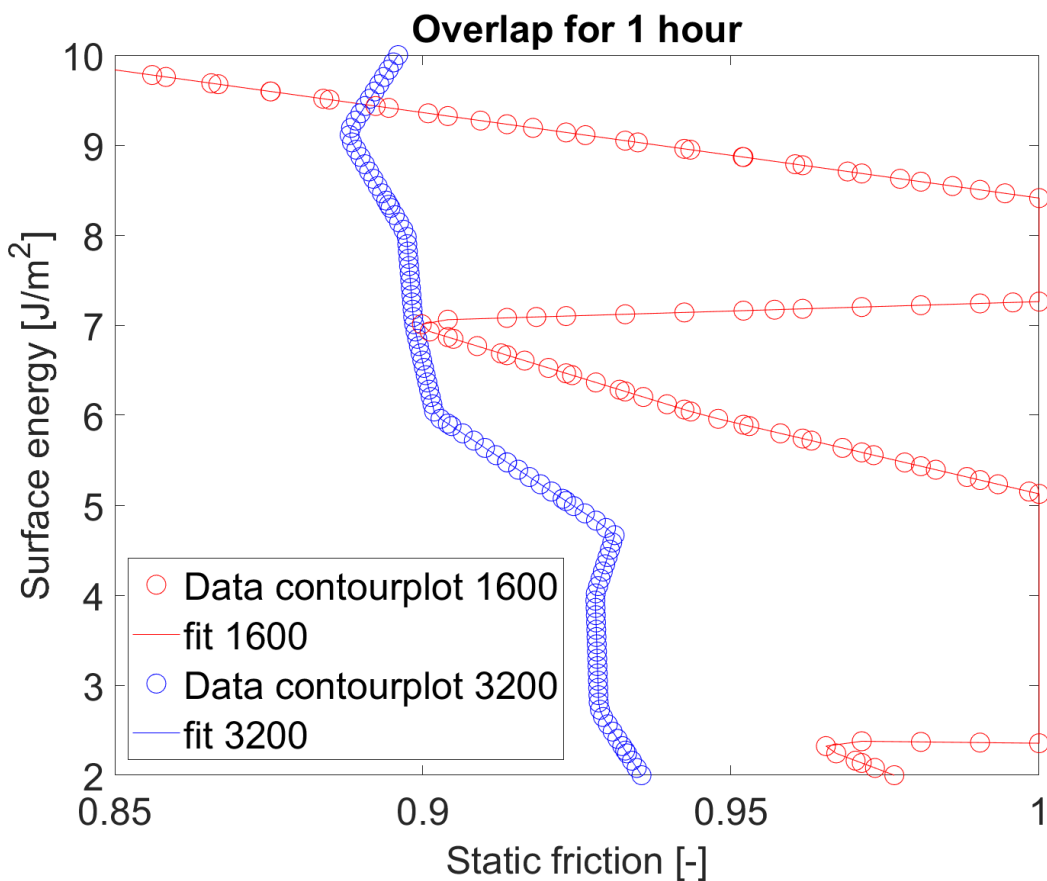


Figure 4.11: Surface energy vs static friction parameter set optimisation for 1 hour consolidation Rotation Restriction case

#### 4.4.2. RESULTS ROTATION RESTRICTION CASE AND EXTRAPOLATION

Table 4.9: Results parameter set optimisation Rotation Restriction case

Time consolidation [hours]	Static friction [-]	Surface energy [J/m <sup>2</sup> ]
0	non	non
0.5	0.744	7.90
1.0	0.891	9.47

In Table 4.9 the results of the RR case can be seen. An overlap is found for the consolidation times of 0.5 and 1.0 hours. For 0 hours of consolidation no overlap is found as shown in Figure 4.12. An extrapolation method is used to determine the values for 0 hours of consolidation. It is assumed that the values for the static friction are bound between the red (normal stress 1600 Pa) and blue line (normal stress 3200 Pa) in Figure 4.12, so a range of 0.05 – 0.27 will later be used to extrapolate for the static friction and for the surface energy the range is 1 – 5 J/m<sup>2</sup>.

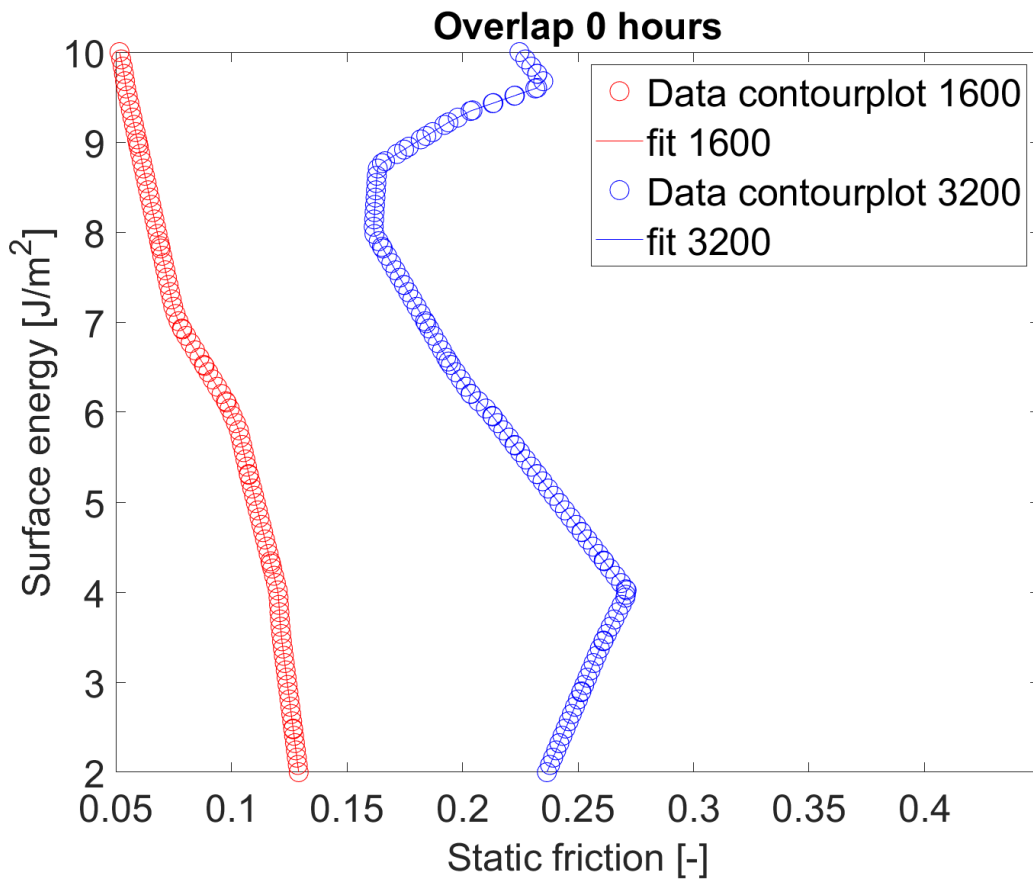


Figure 4.12: Surface energy vs static friction parameter set optimisation for 0 hour consolidation Rotation Restriction case

#### EXTRAPOLATION FOR PARAMETER OVER TIME

To determine the datapoint for 0 hours of consolidation a different method was required, extrapolation will be done with the two datapoints. The extrapolation is based on the data of the time consolidation experiments discussed in Chapter 3.

The first step is to fit the experimental results according to different fits and select the best option for the range of  $0 \leq t \leq 1$  hours consolidation. In Figure 4.13 four different fitting plots, a square root, logarithmic, second order polynomial and exponential function for the experimental data of 1600 Pa normal stress, can be seen. From these results, it can be seen that the data is best fitted using the second order polynomial function. A similar conclusion can be given when looking at the data for 3200 Pa normal stress in Figure 4.14. Therefore, the second order polynomial function is selected for the extrapolation of the most influential parameters.

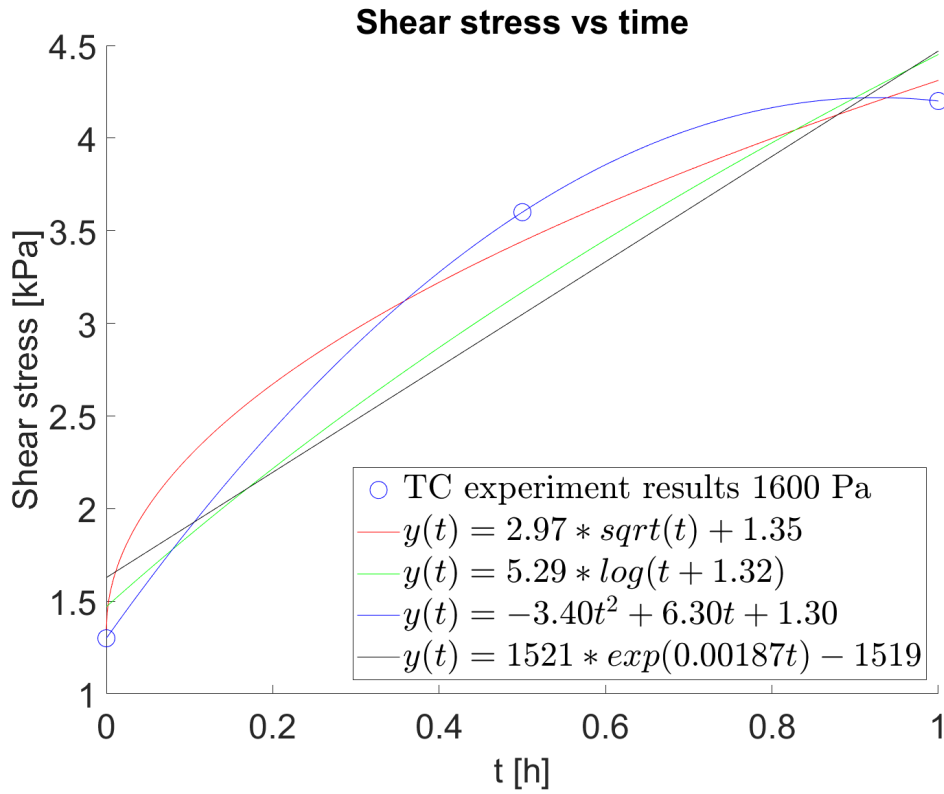


Figure 4.13: Results potential fits of experimental data of 1600 Pa normal stress

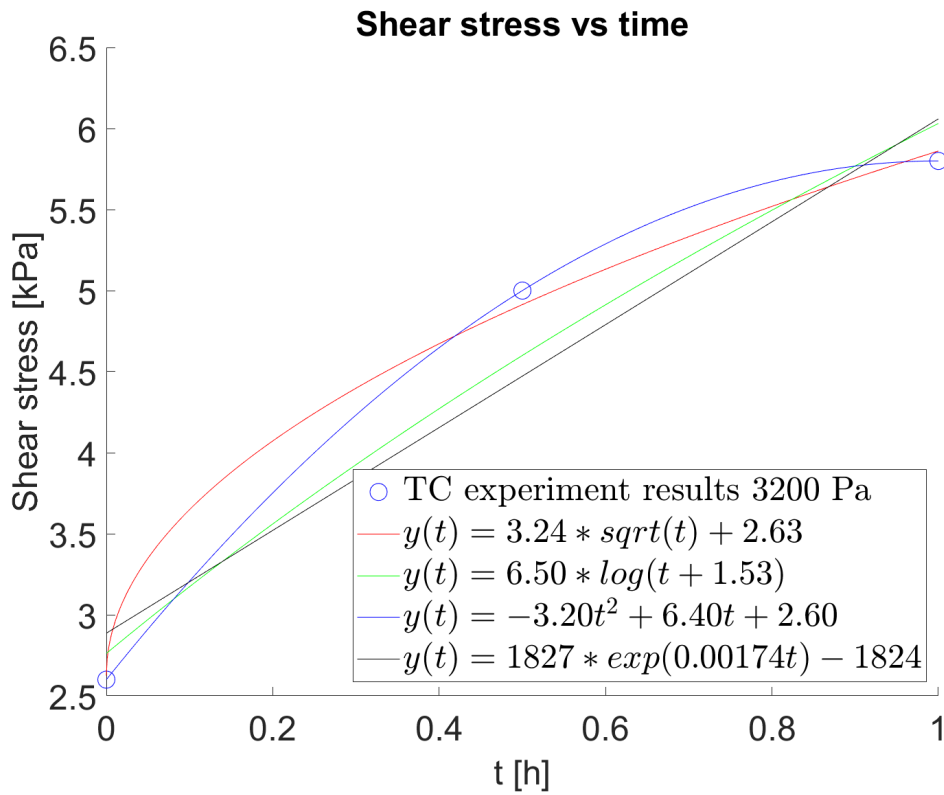


Figure 4.14: Results potential fits of experimental data of 3200 Pa normal stress

Equation 4.2 represents a second order polynomial fit used to model the temporal evolution of a certain variable  $y(t)$  over time  $t$ . The parameters  $\alpha, \beta$  and  $C$  are coefficients determined through the fitting process, capturing the quadratic and linear behaviour of the data. The experimental data will be fitted by using the second-order polynomial of Equation 4.2 [66].

$$y(t) = \alpha t^2 + \beta t + C \quad (4.2)$$

where:

$y$  = Relevant parameter

$t$  = time (h)

$\hat{\alpha}$  = Coefficient 1 (quadratic)

$\hat{\beta}$  = Coefficient 2 (linear)

$C$  = startpoint

Equation 4.3 provides a definition for  $\zeta$ , the ratio between  $\alpha$  and  $\beta$ , which shows the relationship between the quadratic and linear terms in the fit [66].

$$\zeta = \frac{\alpha}{\beta} \quad (4.3)$$

Equation 4.4 and 4.5 are fitted curves for the experimental data for normal stresses 1600 and 3200 Pa. The equations describe the shear stress for a consolidation time between  $0 \leq t \leq 1$

$$shear\ stress_{1600}(t) = -3.4t^2 + 6.3t + 1.3 \quad \text{for } 0 \leq t \leq 1 \quad (4.4)$$

$$shear\ stress_{3200}(t) = -3.2t^2 + 6.4t + 2.6 \quad \text{for } 0 \leq t \leq 1 \quad (4.5)$$

Equation 4.6 presents the mean value for the  $\zeta$  of both normal stress values from Equations 4.4 and 4.5. This value  $\zeta_{mean}$  provides an understanding of the relationship across multiple levels and this value will be used for fitting the static friction and surface energy over time.

$$\zeta_{mean} = \frac{\frac{-3.4}{6.3} + \frac{-3.2}{6.4}}{2} = -0.52 \quad (4.6)$$

With the two data points of 0.5 and 1.0 hours of consolidation from Table 4.7 and the  $\zeta_{mean} = -0.52$  an extrapolation to find the point for 0 hours of consolidation is performed. The range for the static friction, previously determined by the results from Figure 4.12 to be 0.05–0.27, is iteratively used to fit the data. In Figure 4.16 the result can be seen and for every fit in the figure, the ratio  $\zeta$  is determined.  $\zeta_{mean}$  is matched with the results to determine the appropriate fit for the static friction. In Table 4.10 the results can be seen and for a value of  $\zeta = -0.52$  a static friction of 0.24–0.25 is required. Similarly, for the surface energy, the same procedure is performed, this can be seen in Appendix E.

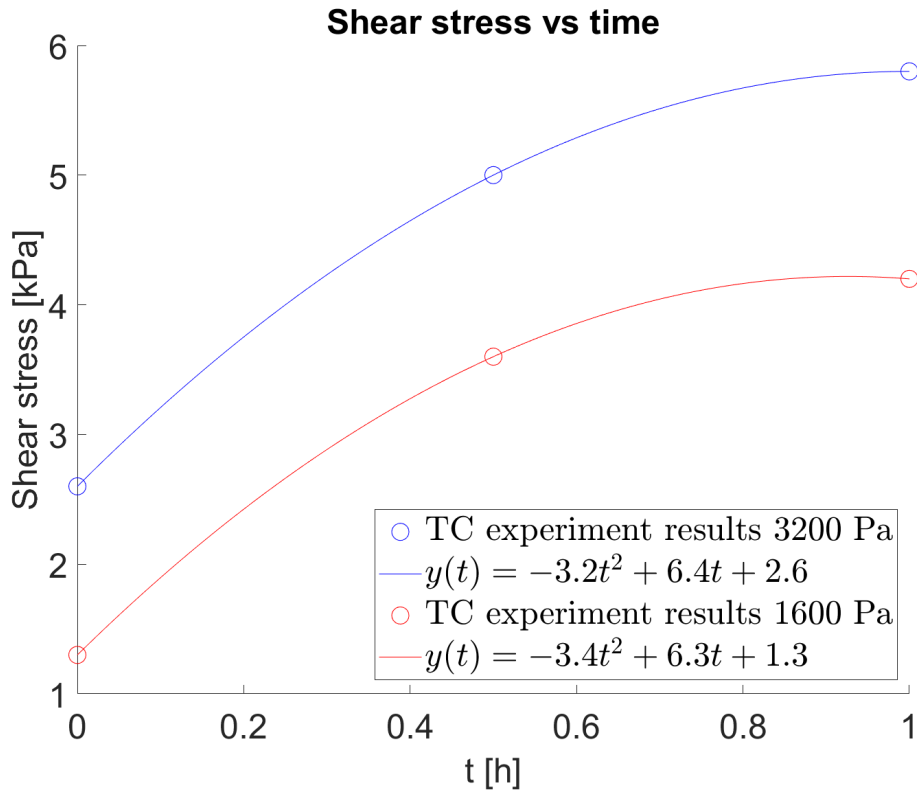


Figure 4.15: Shear stress vs time second order polynomial fit for experimental data

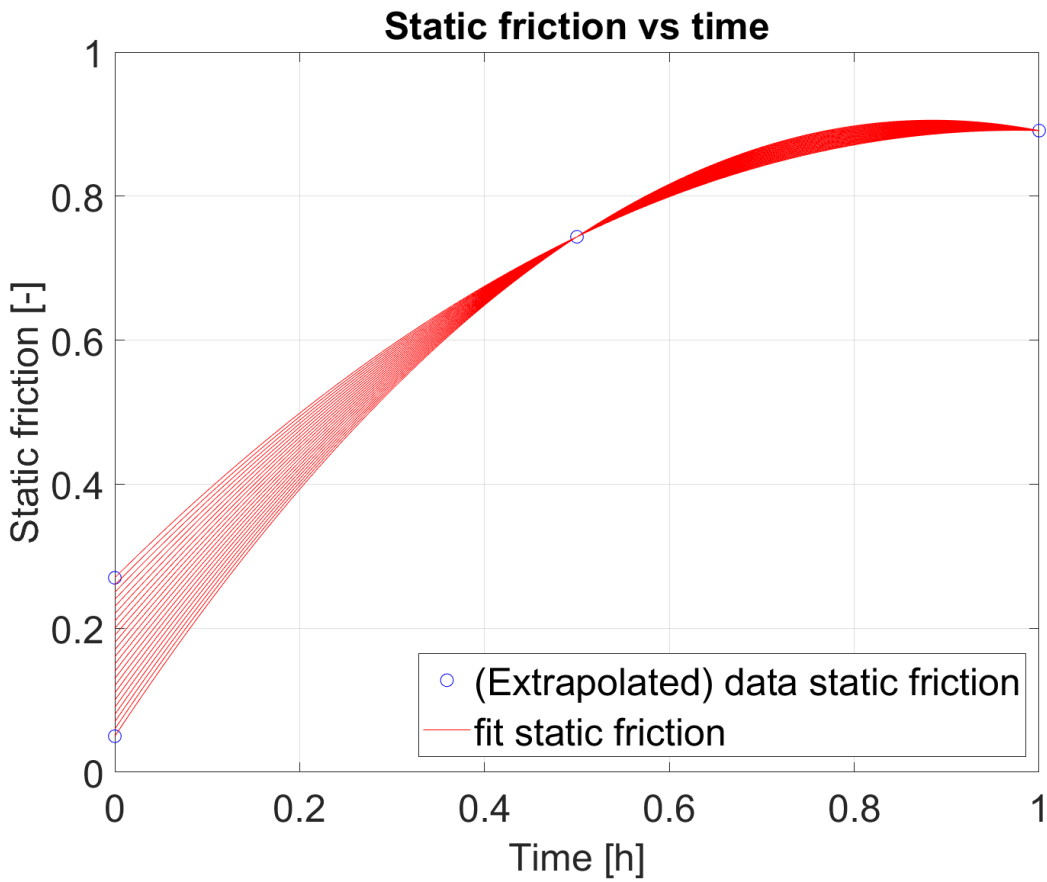


Figure 4.16: Potential fits for static friction vs time Rotation Restriction case

Table 4.10: Results  $\zeta$  analysis for static friction Rotation Restriction case

Static friction [-]	$\zeta$
0.05	-0.565
0.06	-0.563
0.07	-0.562
0.08	-0.560
0.09	-0.558
0.1	-0.556
0.11	-0.554
0.12	-0.553
0.13	-0.551
0.14	-0.548
0.15	-0.546
0.16	-0.544
0.17	-0.541
0.18	-0.539
0.19	-0.537
0.2	-0.534
0.21	-0.531
0.22	-0.529
0.23	-0.526
<b>0.24</b>	<b>-0.522</b>
<b>0.25</b>	<b>-0.519</b>
0.26	-0.516
0.27	-0.512

#### THE RELATIONSHIP FOR ROTATION RESTRICTED CASE

In Equation 4.7 the general form of the equation introduced in Equation 4.2 is changed to an equation that is dependent of  $\zeta_{mean}$  from the experimental data.

$$y(t) = \zeta(\hat{\alpha}t^2 + \hat{\beta}t + \hat{\epsilon}) \quad (4.7)$$

where:

y = Relevant parameter

t = time (h)

$\zeta$  = ratio of alpha and beta from the experimental data (-0.52)

$\hat{\alpha}$  = Coefficient 1 (quadratic)

$\hat{\beta}$  = Coefficient 2 (linear)

$\hat{\epsilon}$  = error

Equation 4.8 and 4.9 show the resulting mathematical expressions for the fits of the static friction and surface energy over time. In Figure 4.17 the graphical representation of the static friction in blue and the graphical representation of the surface energy in red can be seen.

$$static\ friction(t) = 0.52(-1.37t^2 + 2.62t + 0.462) \quad \text{for } 0 \leq t \leq 1 \quad (4.8)$$

$$surface\ energy(t) = 0.52(-14.3t^2 + 27.5t + 5.00) \quad \text{for } 0 \leq t \leq 1 \quad (4.9)$$

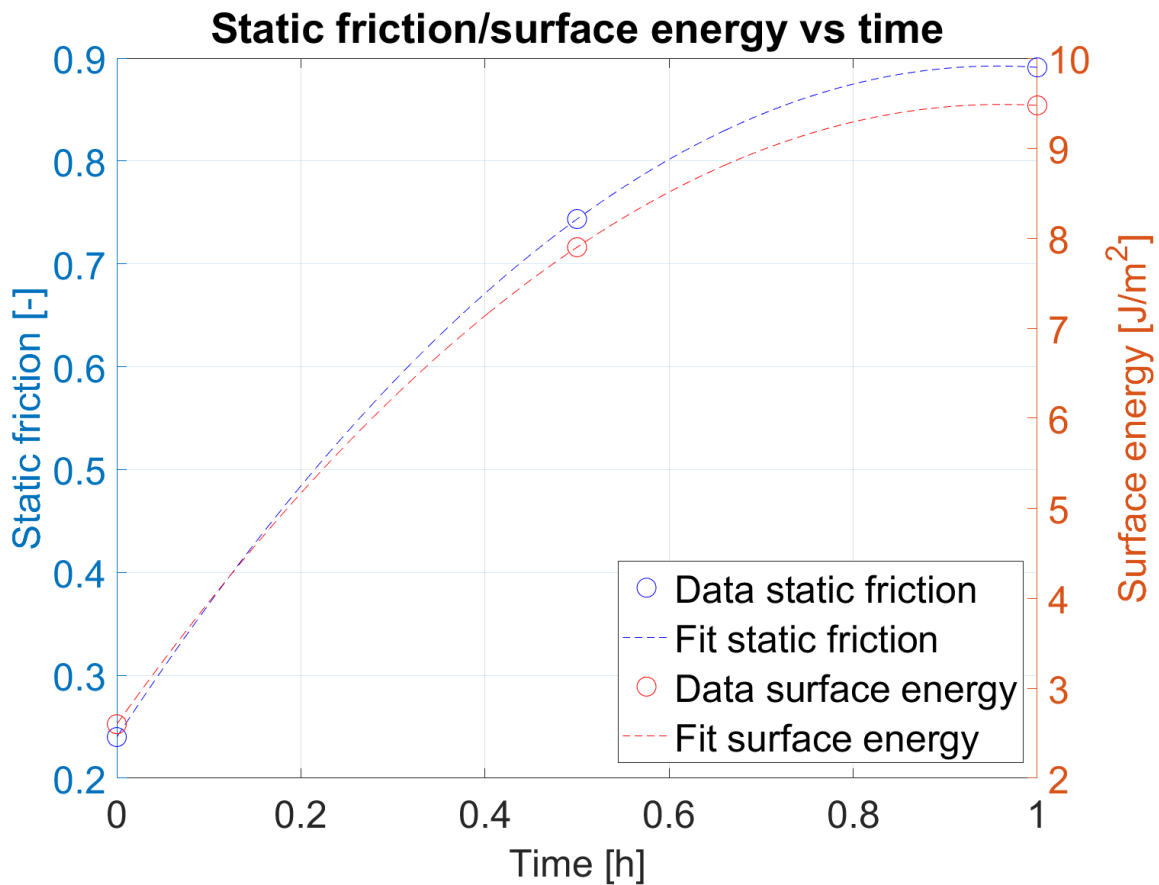


Figure 4.17: Static friction/surface energy vs time fit Rotation Restriction case (scaled)

The found relationship for the static friction and surface energy over time needs to be scaled down by the rules of Mohajeri, to provide the relationships for the particle size of  $\text{NaBH}_4$  in powder form. The scaling factor for the simulations was 7, so the same procedure as described above will be performed with a scaled-down range. Equations 4.10 and 4.11 are the resulting mathematical representations of the static friction and surface energy. In Figure 4.18 the graphical representations can be seen.

$$\text{static friction}_{real}(t) = 0.52(-0.196t^2 + 3.74t) + 0.0659 \quad \text{for } 0 \leq t \leq 1 \quad (4.10)$$

$$\text{surface energy}_{real}(t) = 0.52(-2.05t^2 + 3.94t) + 0.744 \quad \text{for } 0 \leq t \leq 1 \quad (4.11)$$

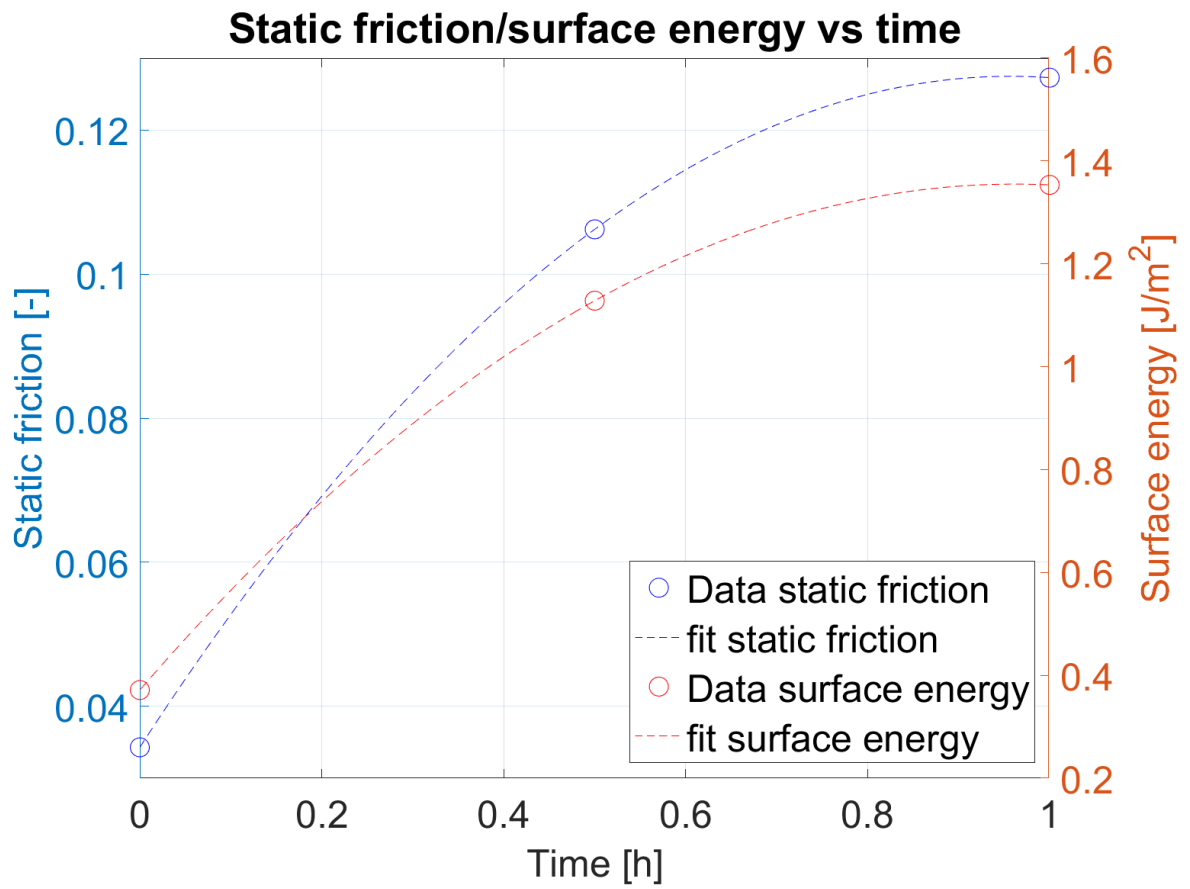


Figure 4.18: Static friction/surface energy vs time fit Rotation Restriction case (unscaled)

### 4.5. CALIBRATION AND VERIFICATION ROLLING MODEL TYPE C CASE

In Figure 4.19 the procedure for the case where Rolling type C is used can be seen. In this case, the surface energy is chosen to be higher due to an increase in forces inside the shear cell. The higher forces can be explained by allowing rotation of the particles [26]. Again, a trend/correlation between the static friction and time and the surface energy and time is searched for and these can be used to instantly create a time-consolidated particle bed.

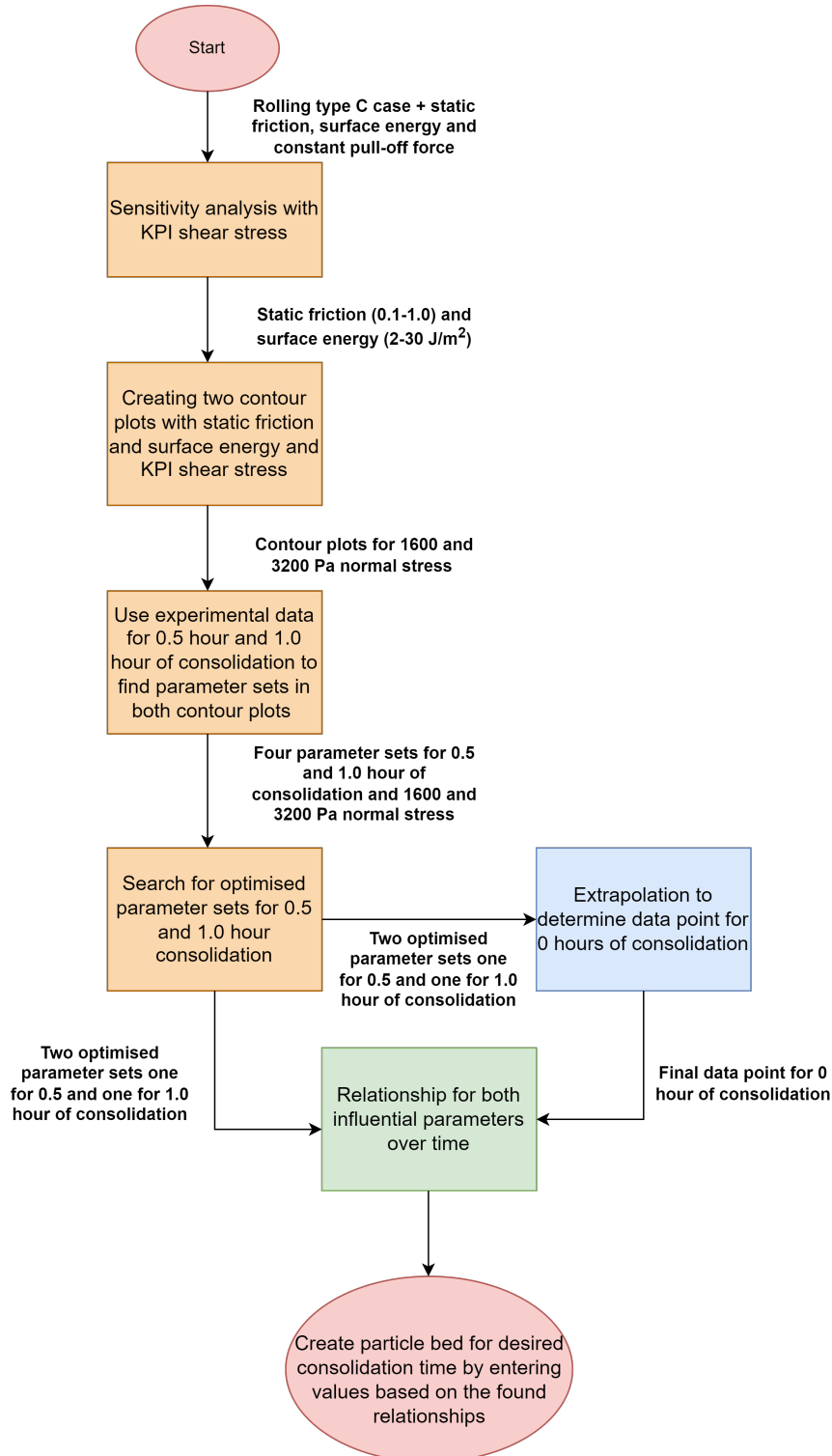


Figure 4.19: Calibration and verification for Rolling type C case

Table 4.11: Calibration range Rolling type C

Parameter	Unit	Values
$\mu_{r,p-p}$	-	0.1, 0.2, 0.4, 0.6, 0.8 and 1.0
$\Delta\gamma$	J/m <sup>2</sup>	2, 6, 10, 14, 18, 22, 26 and 30

#### 4.5.1. RESULTS ROLLING TYPE C AND EXTRAPOLATION

In Appendix F the plots to find the optimised parameter set for the RC case can be seen, the results of this analysis can be seen in Table 4.12.

Table 4.12: Results parameter set optimisation Rolling type C case

Time consolidation [hours]	Static friction [-]	Surface energy [J/m <sup>2</sup> ]
0	non	non
0.5	0.823	8.08
	0.866	26.7
1.0	0.977	27.9
	0.995	6.78

When looking at the results not a similar approach as in Section 4.4 for the RR case can be used for extrapolation of the surface energy. For the static friction the procedure described in 4.4.1 and Appendix E are used. In Figure 4.20 the final results can be seen. The mathematical representation that represents these two curves can be seen in Equation 4.12 and 4.13 and Figure 4.20 shows the graphical representation of these equations.

$$\text{static friction1}(t) = -0.52(1.581t^2 - 3.033t - 0.462) \quad \text{for } 0 \leq t \leq 1 \quad (4.12)$$

$$\text{static friction2}(t) = -0.52(1.420t^2 - 2.723t - 0.577) \quad \text{for } 0 \leq t \leq 1 \quad (4.13)$$

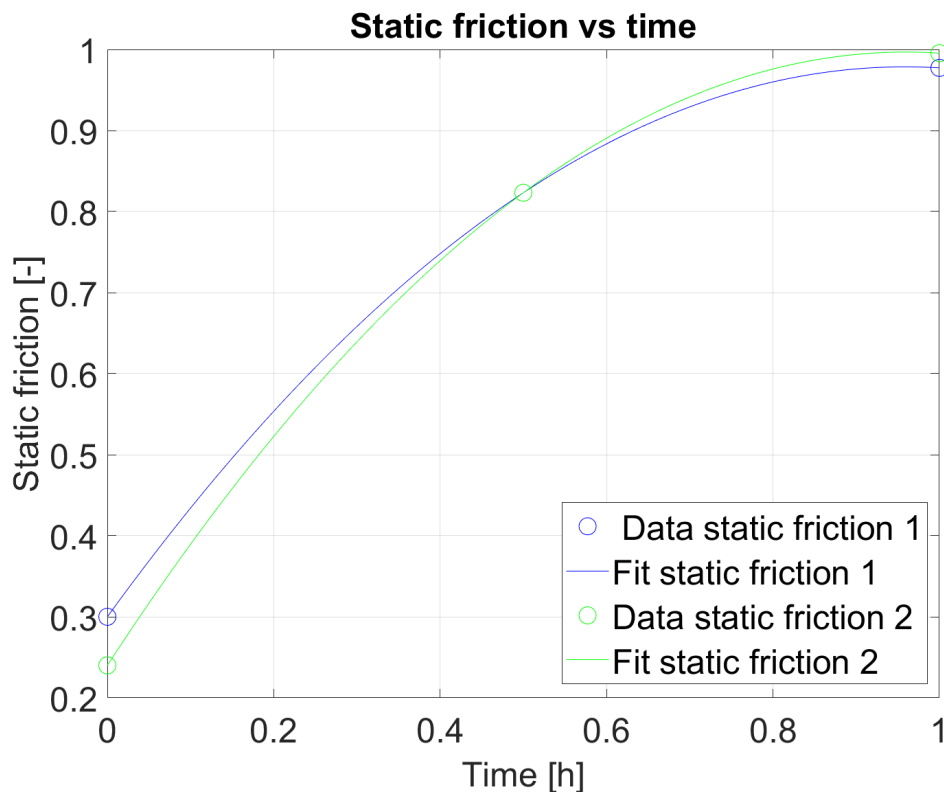


Figure 4.20: Static friction vs time fit Rolling type C case (scaled)

Similarly, to the RR case the constructed two relationships for the static friction over time need to be scaled down by the rules of Mohajeri, to provide the relationships for the particle size of  $\text{NaBH}_4$  in powder form. The scaling factor for the simulations was 7, so the same procedure as described in 4.4.2 are done with a scaled-down range. Equation 4.14 and 4.15 are the resulting mathematical representations of the found relationships for the static friction over time and in Figure 4.21 the graphical representations can be seen.

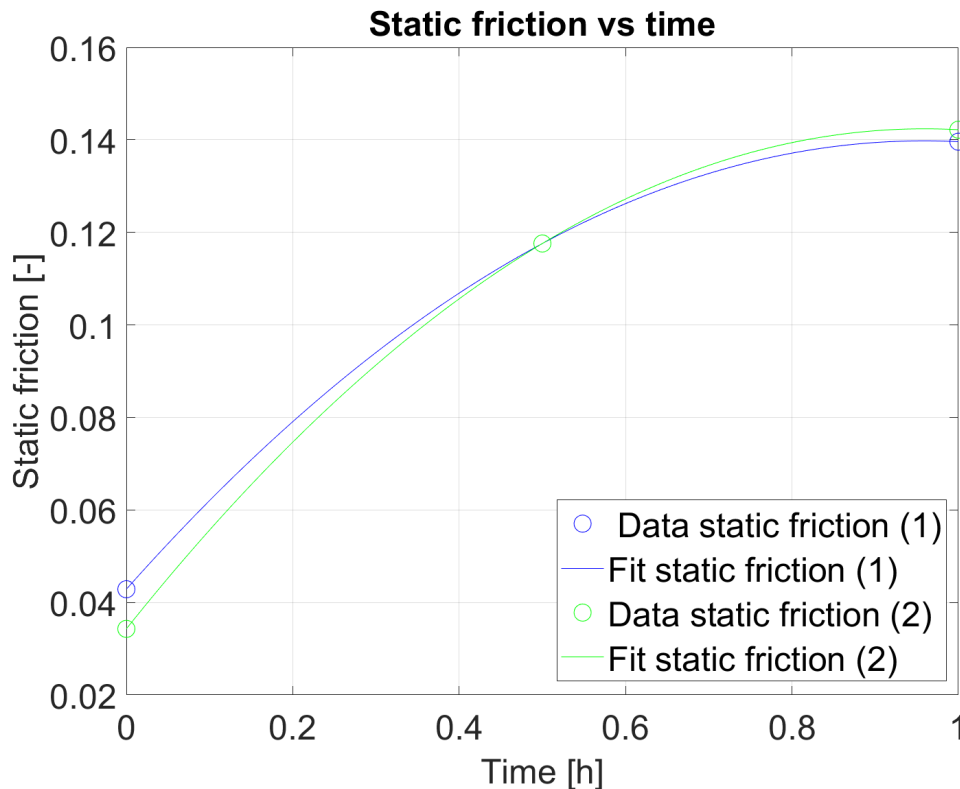


Figure 4.21: Static friction vs time fit Rolling type C case (unscaled)

$$static\ friction1_{real}(t) = -0.52(0.203t^2 - 0.389t - 0.0824) \quad \text{for } 0 \leq t \leq 1 \quad (4.14)$$

$$static\ friction2_{real}(t) = -0.52(0.236t^2 - 0.438t - 0.0659) \quad \text{for } 0 \leq t \leq 1 \quad (4.15)$$

## 4.6. CONCLUDING REMARKS

In this chapter the fifth subquestion: "What is a comprehensive method to capture time consolidation effects on  $\text{NaBH}_4$  using DEM?" is answered, using a DEM model in combination with the EEPA contact model.

In this section a method to model time consolidation is proposed by 5 generic steps. These steps are time consolidation experiments, development of the model, sensitivity analysis, calibration and verification and fitting of the relationship over time. With this relationship, it is possible to instantly create a particle bed that mimics the behaviour of a material after a certain consolidation time. The model that is used is a DEM model that mimics a regular ring shear test. To incorporate time consolidation different input values for the static friction and surface energy can be given to the system. This method is more computationally efficient in comparison to modelling the complete time consolidation process.

$\text{NaBH}_4$  has an irregular particle shape and to model the material as a spherical particle two options are available in the literature and both these two cases are calibrated. Relationships were determined for the static friction and surface energy over time, it should be noted that these relationships are only valid within the

given range of  $0 \leq t \leq 1$  hour of time consolidation. For the RC case, a relationship for the surface energy over time was not found. The results for the RR case show more stable results in comparison to the RC case, similar to the findings of Mohajeri [26]. In the end the relationship needs to be scaled down, because initially the particles were scaled up to reduce the computational expenses. With the found relationships it is possible to instantly create a time-consolidated particle bed.

# 5

## DISCUSSION

In Chapter 4 the static model is calibrated for two cases, rotation restricted and rolling model type C. The results of these two cases together with the results of the time consolidation experiments in Chapter 3 are discussed in Chapter 5. In Section 5.1 the experimental results are discussed, and in Section 5.2 the results of the modelling time consolidation are discussed.

### 5.1. DISCUSSION TIME CONSOLIDATION EXPERIMENT RESULTS

This thesis consists of three main parts, the literature study, time consolidation experiments and DEM simulations. For the experiments, the approach described in [25] was used. Filtering of the data was necessary for smaller normal stresses when using the consolidation bench. This is most likely due to vibrational disruptions during the transfer of the shear cell, which can cause defects in the particle bed and lead to lower shear stress values during the experiments.

Next, the experimental results were analysed for 0, 0.5 and 1.0 hours consolidation. From [25] it is often assumed that the angle of internal friction ( $\phi_t$ ) of the time yield loci is equal to the slope of the linearized yield locus ( $\phi_{lin}$ ). This assumption is made to reduce the number of experiments for construction of the time yield locus. One point is measured and  $\phi_{lin}$  is used to construct the time yield locus. In this study, the experiments show increasing  $\phi_t$  in comparison to the ( $\phi_{lin}$ ) as can be concluded from Table 5.1. When looking at the assumption it should be noted that the assumption is not always applicable for NaBH<sub>4</sub> one should be careful to use this assumption. The number of data is too low to make this conclusion, so more tests should be performed to confirm this observation.

Table 5.1: Angle of internal friction/slope of linearized yield locus (N=3)

Time consolidation [hours]	0	0.5	1.0
$\phi_t / \phi_{lin}$ [°]	38.9	41.4	45.6

From the results of the experiments it can be seen that the cohesion increases rapidly in the first 0.5 hours, but increases with a smaller value after 1.0 hours consolidation as can be seen in Table 5.2. This trend potentially reflects an upper bound for the increase in strength and cohesion of the material, the upperbound is potentially influenced by the initial packing, consolidation stress, voids between the particles and the particle size. Also, when analysing the flow properties of NaBH<sub>4</sub> it shows that the material is free-flowing before consolidation, but after 0.5 hours of consolidation, the material changed into a non-flowing material. This change is captured in a change of  $f f_c$  from 21.4 to 0.88. Again, the change from 0.5 hours to 1.0 hours consolidation is smaller in comparison to the change from no time consolidation to 0.5 hours of consolidation as can be seen from Table 5.2. Therefore, the flowability of NaBH<sub>4</sub> powder form changed rapidly with time consolidation and NaBH<sub>4</sub> is significantly affected by time consolidation.

Table 5.2: Flow properties for different consolidation times (N=3)

Time consolidation [h]	Cohesion [Pa]	Cohesion factor [-]	$\sigma_1$ [Pa]	$\sigma_c$ [Pa]	$\sigma_c$ factor [-]	$ff_c$ [-]
0	49	1	8611	403	1	<b>21.4</b>
0.5	2209	44	8611	9785	24	<b>0.88</b>
1.0	2504	50	8611	12132	33	<b>0.71</b>

In Table 5.3 the results of the cohesion and unconfined yield strength for different moisture levels can be seen. The table shows an increase in both cohesion and unconfined yield strength and when comparing the results of a moisture level 2 % with the result for 0 hours consolidation (and 0 % moisture content) in Table 5.2 it can be noticed that the unconfined yield strength increases with a factor higher than 4. Similarly, the cohesion of these two rows can be compared and an increase with a factor that is higher than 10 shows a significant influence of the moisture content on the bulk properties of NaBH<sub>4</sub>. When comparing the results for the moisture levels in Table 5.3 and the results in Table 5.2 for time consolidation it can be concluded that time consolidation has a higher effect on these bulk properties of NaBH<sub>4</sub> in comparison to moisture (humidity).

5

Table 5.3: Ring shear test results: influence of different moisture levels on NaBH<sub>4</sub> powder (preshear 4 kPa) [38]

Moisture [wt%]	Cohesion [Pa]	$\sigma_c$ [Pa]
2	468 ± 34	1860±73
4	451 ± 49	1813 ±194
6	555±29	2283±129

The time consolidation experiments were performed with the same preshear level 4 kPa, more tests for different preshear levels, more normal stresses, consolidation stresses and consolidation times are necessary to gain more insight into the mechanical behaviour of NaBH<sub>4</sub> before, during, and after time consolidation. The final remark for the experiments is that the experiments were not performed inside a climate chamber and NaBH<sub>4</sub> is affected by humidity and temperature. In Romijn [38] the effect of humidity on the strength of the material is researched, it would be a great opportunity to combine that research and this research and try to set up research conducting the effect of humidity and time consolidation for several moisture levels, consolidation times and consolidation stresses. It is presumed that the effect of humidity in combination with time consolidation has a more severe effect on the material. Experiments to determine the influence of time consolidation should be performed inside a climate chamber to make the humidity and temperature controllable factors.

## 5.2. DISCUSSION DEM MODELLING RESULTS

The time consolidation experiments were necessary to develop a simulation, calibration and verification method, because there was no data for the influence of time consolidation on NaBH<sub>4</sub> found in the literature. In this study two simulation cases are used and the difference between the two simulations is restriction of the rotation (RR) or usage of Rolling type C (RC) as a rolling model. These two options can be used to model irregularly shaped particles as spherical particles in DEM and several researchers successfully used these to model realistic bulk behaviour [26, 51, 58]. A sensitivity analysis was performed and from the analysis, the two most influential parameters were the static friction and surface energy.

For the RR case a relationship was found for both the static friction and surface energy over time. The relationship is valid for the boundary of  $0 \leq t \leq 1$  hours of consolidation. The used fit is a second order polynomial fit. Similarly to the RR case, a relationship for the static friction over time was found for the RC case. However, for the surface energy, this was not found. In Equation 5.1 the general form of the relationship over time can be found. In this case,  $\zeta$  was determined with the time yield loci from the time consolidation experiments, this  $\zeta$  could also be found in the relationship for the static friction for both the RR and RC and for the surface energy for the RR case. The error (starting point) of the fit ( $\epsilon$ ) is the third term in Equation 5.1.

$$y(t) = \zeta(\hat{\alpha}t^2 + \hat{\beta}t + \hat{\epsilon}) \quad \text{for } 0 \leq t \leq 1 \quad (5.1)$$

where:

y = Relevant parameter

t = time (h)

$\zeta$  = ratio of alpha and beta from the experimental data (-0.52)

$\hat{\alpha}$  = Coefficient 1 (quadratic)

$\hat{\beta}$  = Coefficient 2 (linear)

$\hat{\epsilon}$  = error

In Table 5.4 some points are denoted with an \*, these points were determined by using extrapolation, and the other points are determined by finding an optimised parameter set. When comparing the simulation results for the RR and RC case it shows that the results for the RR were more stable, similar to the findings of Mohajeri [26]. Using the RR leads to lower forces and lower computational times. The RR case can therefore be the more suitable option for modelling the irregular shape of the particles with spherical particles.

Table 5.4: Final results Rotation Restriction and Rolling type C cases (scaled)

Parameter	RC			RR		
	0	0.5	1	0	0.5	1
Time consolidation [h]	0	0.5	1	0	0.5	1
	0.30*	0.823	0.977	0.24*	0.744	0.891
Static friction [-]	0.24*	0.866	0.995			
	non	8.085	27.9	2.6*	7.90	9.47
Surface energy [ $J/m^2$ ]	non	26.7	6.78			

\* data points constructed from extrapolation

It should be noted that the relationship that is found is not valid outside the boundaries. When looking at the experiments it is expected that the trend of the data is shown, but for extrapolation to higher levels of static friction and surface energy a smaller scaling factor for the particles is necessary and the relationship would be better captured with an exponential fit. In this thesis the data was limited and therefore it was not possible to fit the data with an exponential fit. An exponential fit might be a better, because the experimental data showed a potential upper bound for the increase in shear stress and cohesion. The data is fitted according to the time consolidation experimental results, so with more data points corresponding to higher consolidation times the better fit is expected to be an exponential fit. The scaling rules from Mohajeri were also used and from these rules, the results that are found should be scaled down by the scaling factor of the particles. In this study, the scaling factor was 7, using the factor changes the results from Table 5.4, but the same relationships from Equation 5.1 can be found. In Table 5.5 the results after downscaling can be seen and the results denoted with an "\*" are extrapolated data points.

Table 5.5: Final results Rotation Restriction and Rolling type C cases (unscaled)

Parameter	RC			RR		
	0	0.5	1	0	0.5	1
Time consolidation [h]	0	0.5	1	0	0.5	1
	0.0429*	0.118	0.140	0.0343*	0.106	0.127
Static friction [-]	0.0343*	0.124	0.142			
	non	1.15	3.99	0.371*	1.13	1.35
Surface energy [ $J/m^2$ ]	non	3.81	0.969			

\* data points constructed from extrapolation

## LIMITATIONS

In this thesis the coefficient of restitution (e) was used from the study of Mohajeri [26] and the rolling friction coefficient ( $\mu_{r,p-p}$ ) was estimated. These two can be incorrect for  $\text{NaBH}_4$  and influence the results. The coefficient of restitution in this study is relatively low which causes low dissipation of energy, with a higher coefficient of restitution higher energy dissipation can cause a higher stress profile through the particle bed.

The higher stress profile results in higher forces between the particles which can result in a higher range of shear stress that can be captured.

Another remark in this research is that the computational time was reduced by reducing the shear modulus. Reduction of the shear modulus can be done according to Lommen [64], but in that study, the performed experiment was an angle of repose test. To see if this assumption can also be made for a RST further research is necessary, for example, the shear modulus can be varied and see how the change affects the output response.

Another remark is that for the simulation the plasticity ratio can also be varied, the plasticity ratio was kept constant during the simulation at 0.75. It was required to use extrapolation to determine the values for 0 hours of consolidation in all the relationships. However, the plasticity ratio can potentially be used to model 0 hours of consolidation, because a plasticity ratio of 0 makes EEPA an elastic model. Before consolidation,  $\text{NaBH}_4$  is a free-flowing material indicated by the experiments and clogging of particles does not occur. Therefore, it can be possible to model this behaviour with a plasticity ratio of 0 or even a different contact model such as Hertz-Mindlin. After time consolidation finding an optimised parameter set with the EEPA model showed results for 0.5 and 1.0 consolidation times, so for time consolidation it is necessary to model  $\text{NaBH}_4$  with EEPA and with the optimised parameter sets the model is calibrated and verified. When looking at the unscaled results in Table 5.5 and more consolidation times are determined a better fit can be found. An exponential curve is expected to be used to capture the relationship, but to confirm this expectation further research needs to be conducted.

Finally, the method proposed in Section 4.1 for modelling time consolidation is used, because there is not a lot of knowledge on modelling time consolidation available in literature. In Section 2.4.2 the only attempt to model time consolidation with a contact model in DEM is described. This model scaled the two most influential parameters the surface energy and the effective Young's modulus linearly to keep a constant ratio accounting for elastic deformation. To take into account the plastic deformation a different ratio between the two is necessary and there is no research performed on that. However, the model accounted for time changes, so taking the knowledge of this model it could be possible in the future to implement time into different contact models to account for time consolidation and also scale the factors accordingly. For  $\text{NaBH}_4$  a second-order polynomial function was found between 0 and 1 hour of consolidation and instantly a time-consolidated particle bed can be created, but as previously mentioned an exponential function is potentially a better fit. This indicates that scaling the parameters according to an exponential fit over time can potentially be a better way for modelling time consolidation effects on  $\text{NaBH}_4$  more accurately. This would not be a quick implementation, because knowledge of how different materials are affected by time consolidation is required.

# 6

## CONCLUSION AND RECOMMENDATIONS

In Chapter 5 the results of this thesis were discussed and with this chapter, the main research question will be answered by using the answers to the subquestions and this thesis is concluded in Section 6.1. The last section, Section 6.2 provides recommendations to improve the proposed DEM model, some potential limitations and interesting research topics concerning both measuring and modelling the influence of time consolidation on  $\text{NaBH}_4$ .

### 6.1. CONCLUSION

The main research question of this thesis is: *How to model the mechanical behaviour of sodium borohydride ( $\text{NaBH}_4$ ) before, during, and after time consolidation using the Discrete Element Method?*

To answer this question several steps were taken, it starts in Chapter 1 with an introduction of the topic and the motivation for this research, an energy transition is required and hydrogen carriers can potentially be used for that.  $\text{NaBH}_4$  shows high potential, but much remains unknown.  $\text{NaBH}_4$  is affected by humidity, stress-history and temperature, but the exact effects are unclear. Therefore, this study focused on stress-history and more specifically time consolidation. Next, the problem definition and research questions were formulated to answer the main research question. Then, the methodology was presented, e.g. how the research questions will be answered, and the chapter closed with an outline of the thesis.

In Chapter 2 the first, second, and third subquestions: "What is time consolidation, and what are the causes and potential results of time consolidation?", "What is a suitable method to measure time consolidation?" and "How can time consolidation be incorporated in DEM modelling?" are answered, with a literature study. In this study, the definition of time consolidation of Schulze is used that time consolidation is: "the increase in strength if bulk solids are stored for a period of time at rest under a compressive stress (e.g. in a silo or an intermediate bulk containers (IBC))". Caking can occur due to time consolidation and the three caking types are amorphous, humidity and mechanical caking. Amorphous caking does not occur for  $\text{NaBH}_4$ , because it is a crystalline material. Both mechanical caking and humidity caking can occur when experiments are performed outside a climate chamber, mechanical caking is caused by powder consolidation. Humidity caking can occur when sorption of water happens, this can cause liquid bridge forming between the particles and this will increase the strength of the material.

To measure the time consolidation effect on a material Schulze's time consolidation experiment can be performed to measure the increase in strength after time consolidation. These tests are performed in Schulze's RST and are performed for  $\text{NaBH}_4$  in powder form.

In the literature no uniform method/contact model is found to model time consolidation. Therefore, from the literature study, the selected contact model is the Edinburgh Elasto-Plastic Adhesive model., because it considers stress-history and with this contact model, a DEM model can be created. As previously mentioned no method was found to model time consolidation, so in this thesis, the proposed method to model time

consolidation is to use the two most influential parameters and artificially change them to instantly create a time-consolidated particle bed for a specific consolidation time.

In Chapter 3 the fourth subquestion: "How does time consolidation affect sodium borohydride?" is answered, with the results of the time consolidation tests. The experiment that is used is the time consolidation test performed with Schulze's RST. From the results, the cohesion, shear stress and unconfined yield stress of NaBH<sub>4</sub> increased after time consolidation. The powder form of NaBH<sub>4</sub> is highly sensible for time consolidation, because the state of NaBH<sub>4</sub> changed from a free-flowing to a non-flowing material after 0.5 hours of consolidation. The time consolidation experiments were not performed inside a climate chamber, which can result in a strength increase of NaBH<sub>4</sub> potentially due to both humidity and mechanical caking.

In Chapter 4 the fifth subquestion: "What is a comprehensive method to capture time consolidation effects on NaBH<sub>4</sub> using DEM?" is answered, by using a generic method of five steps. The DEM model that is used consists of a ring shear test simulation for mimicking the real-life ring shear test, where the time consolidation is an artificial input from the two most influential parameters. With the two most influential parameters it is possible to simulate a particle bed after time consolidation, making it more efficient than modelling the complete time consolidation process. A generic relationship for the static friction and surface energy over time is determined by searching for an optimised parameter set and extrapolation for the RR case. In the second case, the RC case the same generic relationship from equation 5.1 is found for the static friction, but not for the surface energy over time. The results of the RR case are more stable and have two added benefits, a lower computational time and a lower amount of input parameters. Some remarks can be made on these results, the coefficient of restitution and rolling friction coefficient were assumed from previous work and estimated. To obtain accurate results, research into these two parameters is necessary. Also, the shear modulus was reduced significantly from 10<sup>10</sup> to 10<sup>6</sup> Pa, this assumption was made based on the work of Lommen [64], but this work was done for a ledge test. The influence of the shear modulus on the EEPA model and a ring shear test can be performed to see if this assumption can also be used for a ring shear test inside a DEM environment.

In Chapter 5 the results from the time consolidation experiments and the calibration of the DEM model are discussed, it provides some remarks regarding some assumptions made during this thesis. *To answer the main research question: How to model the mechanical behaviour of sodium borohydride (NaBH<sub>4</sub>) before, during, and after time consolidation using the Discrete Element Method? can be done by using the proposed method where a DEM model using EEPA as a contact model is used to capture time consolidation effects. It is possible to artificially change the most influential parameters the static friction and surface energy over the given time range ( $0 \leq t \leq 1$ ) for the RR case and the static friction over time for the RC case and instantly create a time-consolidated particle bed in a simulation. The preferred case is the RR case, because it has the added benefits of lower computational times and lower input parameters.* The found relationships enable the instantaneous creation of a time-consolidated particle bed after a consolidation time within the range  $0 \leq t \leq 1$  and use the relationships in a simulation model of a real-life application for example storing NaBH<sub>4</sub> in a silo.

There are some remarks and opportunity for future research based and these will be discussed in Section 6.2 recommendations.

## 6.2. RECOMMENDATIONS

In this section recommendations for improving the DEM model and further research are made. The recommendations are grouped in recommendations for modelling time consolidation affects of  $\text{NaBH}_4$  and for measuring time consolidation affects of  $\text{NaBH}_4$ .

### RECOMMENDATIONS FOR MODELLING TIME CONSOLIDATION AFFECTS OF $\text{NaBH}_4$

- The first recommendation is related to lower normal stresses. The results were more unstable for a normal stress of 800 Pa and a higher static friction and surface energy. In this thesis, the sensitivity analysis and time step determination were done for a normal stress of 3200 Pa. The recommendation is to perform these two vital steps with the lowest normal stress in the experiments.
- When using this model for higher preshear levels and normal stresses it is expected that the results become more stable due to higher stresses and forces in the particles, so the model is more suitable for higher stress levels.
- $\text{NaBH}_4$  powder is used in this thesis and showed a rapid increase of strength during time consolidation, other materials where this increase is not so rapid might be more suitable using this model, an example is the granular form of  $\text{NaBH}_4$ .
- In this study the coefficient of restitution and rolling friction coefficient were estimated and should be determined by a proper analysis and/or different tests for  $\text{NaBH}_4$  in both granular and powder form.
- Scaling might have a lot of influence on the range of shear stresses in your model, a smaller particle size will have higher shear stress options, making it possible to look at higher consolidation times, when looking at the study of Mohajeri where the scaling rules for EEPA were constructed [26]. A trade-off needs to be made between the computational time and scaling the particles.
- Using the Rotation Restriction model brings the benefit of a lower computational time by about 1.5 times and fewer input parameters, so this is a good option for reducing the computational time and when not a lot of knowledge on your material is available.
- Looking more in-depth into the plasticity ratio to use for example a plasticity ratio of 0 before time consolidation to have EEPA as an elastic model and after time consolidation 0.75 as used in this thesis for the case where there is time consolidation. Also, different values can be looked into for the plasticity ratio.
- In this thesis the shear modulus was scaled down to  $10^6$  similar to the study of Lommen. In that study Lommen concluded that this can be done for an angle of repose test, it should be looked at in more depth if this can also be done for a ring shear test and to what extent.

### RECOMMENDATIONS FOR MEASURING TIME CONSOLIDATION AFFECTS OF $\text{NaBH}_4$

- The time consolidation tests should be performed inside a climate chamber to decouple the effect of humidity and time consolidation on the increase in strength of the material.
- More time consolidation tests should be performed with different preshear levels, consolidation times, repetitions and normal stresses.
- Testing for both granule and powder form of  $\text{NaBH}_4$
- When looking at the different caking mechanisms it becomes difficult to differentiate between humidity and mechanical caking, so it would be possible that humidity conditions and time consolidation cannot be considered separately. Further research into the coupled effect of humidity and time consolidation on  $\text{NaBH}_4$  would give more insight into real-life applications.



**A**

**SCIENTIFIC PAPER**

# MODELLING THE MECHANICAL BEHAVIOUR OF SODIUM BOROHYDRIDE BEFORE DURING AND AFTER TIME CONSOLIDATION USING DEM

A.A. KALPOE, M.C. VAN BENTEN, D.L. SCHOTT

ABSTRACT. Currently, one of the biggest challenges humanity faces is climate change. Reduction of fossil fuels is demanded in the future, hence an energy transition is required. A promising potential alternative fuel is the energy carrier  $\text{NaBH}_4$  that contains hydrogen ( $\text{H}_2$ ). Handling and storing  $\text{NaBH}_4$  provides challenges and the bulk behaviour of  $\text{NaBH}_4$  is not well-known.  $\text{NaBH}_4$  is potentially affected by time consolidation when storing the material inside a silo and to capture the effect on  $\text{NaBH}_4$  a method to model time consolidation using the Discrete Element Method is proposed. To calibrate the simulation model, data is required and to gather data, time consolidation experiments were performed using Schulze's Ring Shear Tester (RST). The shear stress was determined for different consolidation times. Next, the simulation model's two most influential parameters (static friction and surface energy) were selected to calibrate and verify the contact model based on the experimental data. The found relationship of the two parameters over time can be used to instantly create a time-consolidated particle bed after a certain consolidation time, reducing the computational time required to analyse the material behaviour after longer storage periods.

## 1. INTRODUCTION

Currently, climate change is one of the main challenges that humanity is facing. The usage of fossil fuels is causing climate change, hence an energy transition is required [1, 2]. Hydrogen ( $\text{H}_2$ ) can be used as an alternative energy source. One of the biggest emitters is the maritime sector, they are responsible for 3 % of the global greenhouse emissions [3]. The goal is to reduce the emissions by 70 % in 2050 [4]. Nowadays three methods are used for hydrogen storage, compressed, liquefied and cry-compressed [5]. A new promising method is the usage of energy carriers such as  $\text{KBH}_4$  and  $\text{NaBH}_4$ .  $\text{NaBH}_4$  showed high theoretical potential to store hydrogen and can therefore be used as a potential fuel for the future [6].

The chemical properties of  $\text{NaBH}_4$  are well researched, but the bulk behaviour of  $\text{NaBH}_4$  is not known. Initial research by van Bente et al [5] showed that  $\text{NaBH}_4$  is influenced by temperature, humidity and stress history, but the exact influence for different circumstances remains unknown. For handling and storing of the material, this is vital information. When subjecting  $\text{NaBH}_4$  to a normal load during a time period, an increase in material strength can occur, this phenomenon is called time consolidation. In this study, the effect of time consolidation on  $\text{NaBH}_4$  is researched. The goal is to model the mechanical behaviour of sodium borohydride before, during and after time consolidation using the Discrete element method (DEM).

## 2. PROBLEM STATEMENT

In the literature no uniform method for modelling time consolidation was found. The research objective is formulated by using the goal mentioned above. The problem definition of this study is to *Formulate, calibrate and verify a predictive model that mimics the mechanical behaviour of sodium borohydride ( $\text{NaBH}_4$ ) before, during and after time consolidation using the Discrete-element method (DEM)*. With this model it should be possible to model the behaviour of  $\text{NaBH}_4$  when it is subjected to time consolidation.

## 3. LITERATURE REVIEW

According to Schulze [7] time consolidation is "the increase in strength if bulk solids are stored for a period of time at rest under a compressive stress (e.g. in a silo or an intermediate bulk container (IBC))". There is no uniform definition for time consolidation in the literature, so this definition is used in this paper. The result of time consolidation can be clumping of particles together, this phenomenon is called caking. Three types of caking can occur, amorphous, humidity and mechanical caking [8, 9].  $\text{NaBH}_4$  is a hygroscopic crystalline material, so amorphous caking cannot occur. However, humidity and mechanical caking can occur under different circumstances.

Romijn [10] performed several tests to determine the influence of the ambient humidity on the bulk properties of  $\text{NaBH}_4$ . Ring shear tests were performed, and the results show an increase in unconfined yield strength ( $\sigma_c$ ) and cohesion and a decrease of the flowability ( $ff_c$ ) for both the granule and powder form of  $\text{NaBH}_4$  at higher moisture levels. The main conclusion of this research was that the moisture sorption of  $\text{NaBH}_4$  is affected by relative humidity rather than the moisture level of the material.

Measuring the strength of a material can be done by different shear testers, ultimately Schulze's Ring Shear Tester (RST) is used similarly to several researchers [10, 11]. In Figure 1 a schematic overview of the RST can be seen. For time consolidation testing as described in [7] the first procedure is preshearing of the particle bed for a specific preshear stress  $\sigma_{pre}$  followed by subjecting the shear cell to a load. This load is equal to the major principle stress of the material during preshearing e.g. the highest stress in the material and is called the consolidation stress  $\sigma_1$ . After this time the final procedure occurs and is called subsequent shearing where the peak shear stress under a specific normal stress  $\sigma < \sigma_{pre}$  is obtained. With these results time yield loci can be created.

The experimental results consist of several parameters (unconfined yield strength, shear stress etc.), an important property that is looked at is the flowability or flow function of the material and more specifically how the flow function changes for different consolidation times. The flowability is defined as the ratio between  $\sigma_1$  and the unconfined yield stress ( $\sigma_c$ ) presented in Equation 3.1. The classifications for the flow function can be seen in Figure 2.

$$ff_c = \frac{\sigma_1}{\sigma_c} \quad (3.1)$$

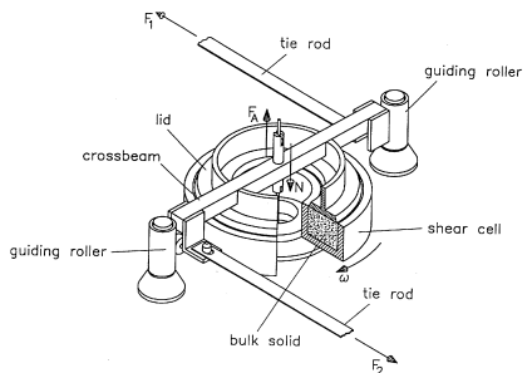


FIGURE 1. Ring Shear Tester [12]

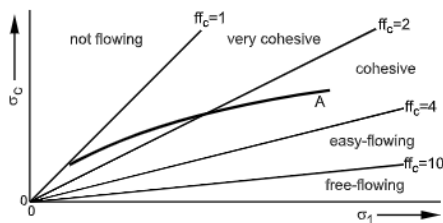


FIGURE 2. Flow function ranges [12]

To model the mechanical behaviour of  $\text{NaBH}_4$  the Discrete Element Method is used. The contact model selected in this paper is the Edinburgh Elasto-Plastic Adhesive (EEPA) model. This model takes into account the stress history and cohesion of the material and is, therefore,

expected to be suitable for modelling time consolidation. The model takes into consideration both plastic and elastic deformation. In figure 3a the graphical representation of the contact model can be seen and in 3b the linear version of the model can be seen. The six parameters that are considered in the simulation model can be seen below:

- Static friction
- Rolling friction
- Coefficient of Restitution
- Plasticity ratio
- Surface energy
- Constant pull-off force

The six parameters mentioned above can be separated into two categories, the independent and dependent parameters of the contact model. The static friction, rolling friction and coefficient of restitution are independent of the contact model and the plasticity ratio, surface energy and constant pull-off force are dependent of the contact model.  $\text{NaBH}_4$  is irregularly shaped and trying to replicate the shapes leads to an unpractical high computational time. Several researchers used two methods to model irregularly shaped materials as spherical shapes and simulate the bulk behaviour [11, 13]. The two methods are usage of a rolling friction model or restricting the rotation of the particles. Both methods will be used, so for the rolling friction, a rolling friction model type C with an estimated value for the rolling coefficient of 0.9 in the first case is used. In the second case, the rotation of the particles is restricted. The coefficient of Restitution and plasticity ratio used in the study of Mohajeri [11] are used in this paper. The remaining three parameters, constant pull-off force  $f_0$ , static friction and surface energy will be used for a sensitivity analysis. From the sensitivity analysis, the two most influential parameters are selected to perform the calibration and verification.

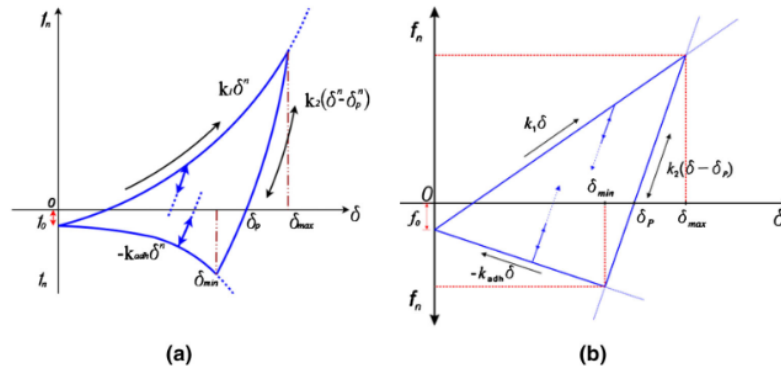


FIGURE 3. Graphical representation of contact model for the normal contact force-displacement function (a) non-linear (b) linear [14]

#### 4. METHODOLOGY

First, a uniform definition, measurement and modelling options for time consolidation need to be gathered. Second, measuring time consolidation is required to gather data on how time consolidation affects  $\text{NaBH}_4$ . Schulze's RST is selected to measure the increase in shear strength of  $\text{NaBH}_4$  after time consolidation. The procedure for time consolidation experiments described by Schulze in [7] will be used. The relevant parameters are the shear stress, flowability, unconfined yield strength, cohesion, shear stress etc. of  $\text{NaBH}_4$ . The shear stress results are used in the next step of the methodology. Third, modelling of time consolidation using a DEM model is proposed in this study. The contact model used to model the interactions between particles is the Edinburgh Elasto-Plastic Adhesive model, this model considers stress-history. The DEM model mimics a regular ring shear test, where preshearing and shear to failure occur. The

experimental procedure for the time consolidation experiments is preshearing, storing under consolidation stress for a certain time and shear to failure. Modelling the storing procedure is computationally expensive, so by changing the most influential parameters of the simulation to create a particle bed that mimics the behaviour after a specific consolidation time, time consolidation can be modelled more efficiently. To select the two most influential parameters a sensitivity analysis is performed. At last, the final result of the paper will be relationships of the two most influential parameters for  $\text{NaBH}_4$  in DEM over time and with these results a particle bed can be created. To determine these relationships, the model is calibrated and verified using the shear stress data gathered from the RST measurements. The found relationships make it feasible to simulate a particle bed after consolidation for a certain period in a practical scenario and this can help design equipment such as a silo.

## 5. TIME CONSOLIDATION EXPERIMENTS

In Figure 4 the yield locus and time yield loci of 0.5 and 1.0 hours of consolidation can be seen. The slope of the time yield locus, the internal angle of friction  $\phi_t$  is often assumed to be similar to the slope of the linearized yield locus  $\phi_{lin}$  to reduce the number of experiments for the time yield locus [7]. One point on the time yield locus is measured and the slope  $\phi_{lin}$  is used to create the time yield locus. In the case of these experiments, the slope angle increases with a higher consolidation time as can be seen from Table 1 which could be an indication that the material acts differently under time consolidation circumstances and the increase in shear stress is higher for higher consolidation times. These results show that the assumption of  $\phi_t$  is equal to  $\phi_{lin}$  is not always valid. However, more trials and experiments should be performed to support that conclusion.

Also, when looking at the cohesion and unconfined yield strength of the material after consolidation a rapid increase for both can be seen in Table 2. For the cohesion, the increase after 0.5 hours of consolidation is up to 44 times in comparison to the cohesion for no consolidation and 50 times for 1.0 hour. Similarly the unconfined yield strength increases by a factor of 24 after 0.5 hours of consolidation and 33 after 1.0 hours of consolidation. It can be noticed that the increase of cohesion and unconfined yield strength becomes smaller when comparing the values of no consolidation and 0.5 hours of consolidation and 0.5 hours, and 1.0 hours of consolidation, indicating that there might be some maximum value for the cohesion and unconfined yield strength for a specific consolidation stress.

The flowability of  $\text{NaBH}_4$  decreased from 21.4 (free-flowing material) to 0.88 after 0.5 hours of consolidation making the material a non-flowing material. This rapid change in bulk behaviour is related to the rapid change in unconfined yield strength making the material not flow out of a silo with only gravitational forces. The results can be influenced by several factors, the first one is the packing of the material. The influence of the packing is related to the voids between the particles. Initial voids between the particles can become smaller during consolidation due to a favourable orientation of particles. The increase in overlapping area causes higher inter-particle forces and a higher  $\sigma_c$  of the material, the opposite can be the case in the following trial and this can cause deviations in the results. This effect is not controllable despite a similar filling process, because it is dependent on the size and the orientation of the individual particles. Another option is the sorption of water, more specifically the contribution of humidity influences. Liquid bridge forming can occur when moisture sorption happens and Romijn [10] showed that a higher moisture content results in a higher shear stress of the material. Therefore, the experiments must be performed inside a climate chamber to capture the influence of only time consolidation. The experiments in this paper are not performed in a climate chamber, so the increase in strength can potentially be caused by both humidity and time consolidation.

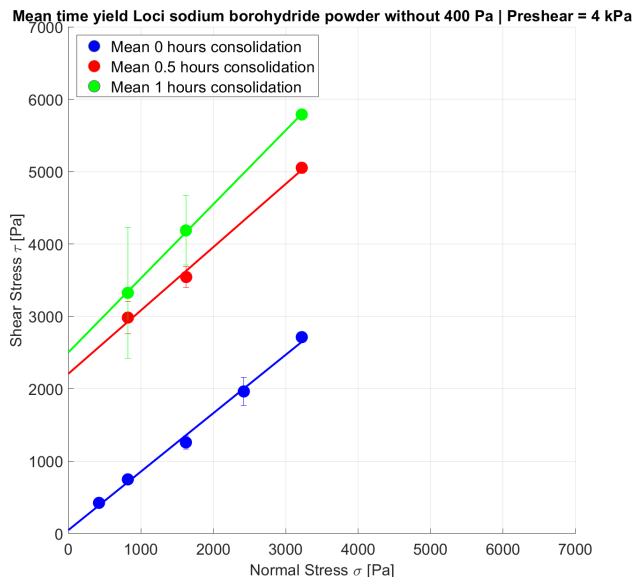


FIGURE 4. Time Yield locus results with a 80 % confidence interval

Table 1: Flowability

Time consolidation [h]	cohesion [Pa]	$\sigma_1$ [Pa]	$\sigma_c$ [Pa]	$\sigma_c$ factor [-]	$ff_c$ [Pa]	$\phi_t / \phi_{lin}$ [°]
0	49	8611	403	1	<b>21.4</b>	38.9
0.5	2209	8611	9785	24	<b>0.88</b>	41.4
1.0	2504	8611	12132	33	<b>0.71</b>	45.6

## 6. TIME CONSOLIDATION MODELLING

The generic flowchart used for modelling time consolidation in this paper can be seen in Figure 5. The calibration and verification step is further elaborated in Figure 6 and consists of two parts. The two parts are finding an optimised parameter set for all consolidation times and extrapolation of the data to determine the data point for no consolidation ( $t = 0h$ ).

In Table 2 the constant parameters for the two cases that are analysed can be seen. In this study, three parameters are used for a sensitivity analysis, static friction, surface energy and constant pull-off force with the ranges presented in Table 3. From the sensitivity analysis, the two most influential parameters static friction and surface energy were found by using a full factorial design. With these two factors, the calibration and verification step was performed and the final result of this step was to find a relationship for the static friction and surface energy over time. The relationships can be used to artificially create a particle bed that mimics a particle bed after a certain consolidation time.

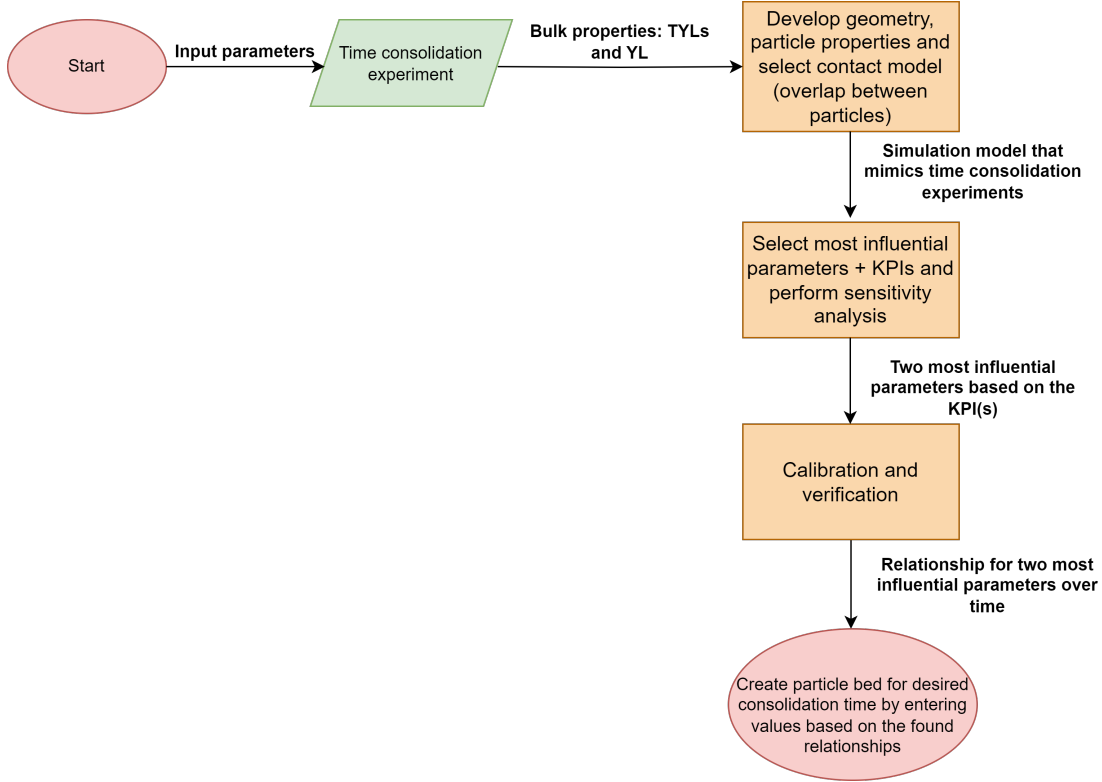


FIGURE 5. Flowchart for modelling time consolidation

Table 2: Constant input parameters in DEM for Rotation Restriction and Rolling model type C cases[11, 15]

Parameter	symbol	unit	value
Shear modulus	$G_p$	GPa	10
Poisson ratio	$\nu$	-	0.28
Particle density	$\rho$	$kg/m^3$	1070
Rolling friction coefficient	$\mu_{r,p-p}$	-	Rotation restriction (RR) / 0.9
Coefficient of static friction (wall-particle)	$\mu_{r,w-p}$	-	0.1
Coefficient of restitution	$e$	-	0.1
Particle shape	$\Psi_p$	-	sphere
Particle size distribution (PSD)	$d_p$	$\mu m$	$289 \pm 94$
Plasticity ratio	$\lambda_p$	-	0.75
Slope exponent	$n$	-	1.5
Tensile exponent	$\chi_{p-p}$	-	7.7

In the calibration verification step for every consolidation time (0,0.5 and 1 hours) an optimised parameter set was searched for. No optimised parameter set was found for no consolidation (0 hour consolidation), so extrapolation is used to determine the data points for no consolidation. The data is extrapolated according to the experimental data. In Figures 7 and 8 the experimental data is fitted with several functions and a second-order polynomial function is selected as the best fit.

Table 3: Variable input parameters in DEM

Parameter	symbol	unit	range
Coefficient of static friction (particle-particle)	$\mu_{r,p-p}$	-	0.1-1.0
Surface energy	$\Delta\gamma$	$J/m^2$	1-100
Constant pull-off force	$-f_0$	N	0.0005-0.05

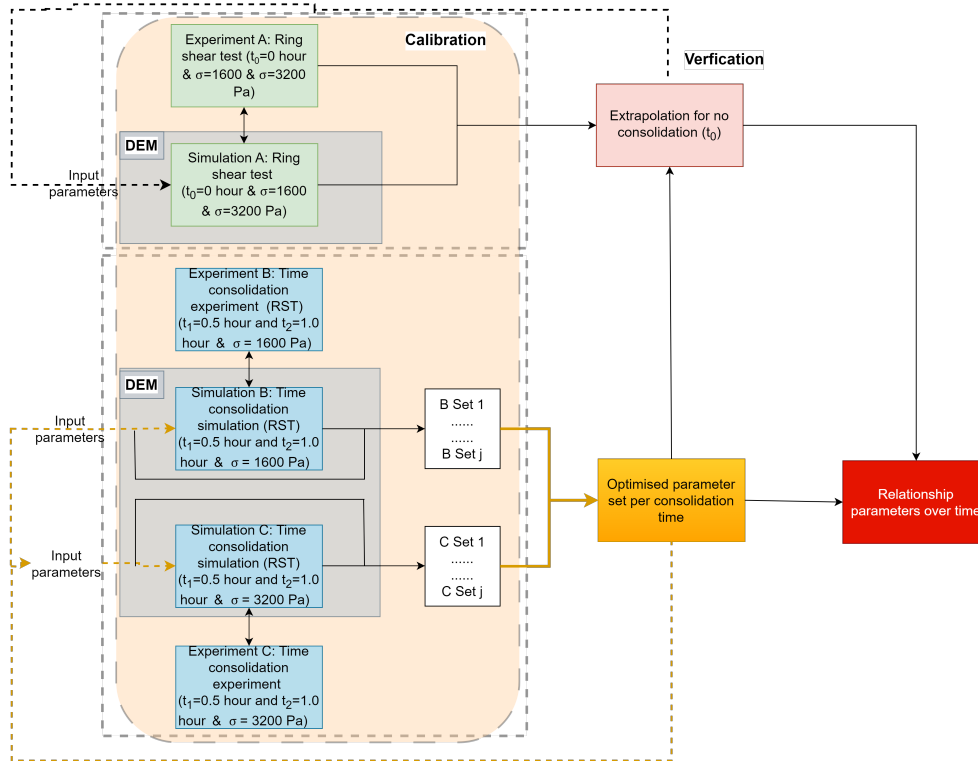


FIGURE 6. Calibration and verification for modelling time consolidation

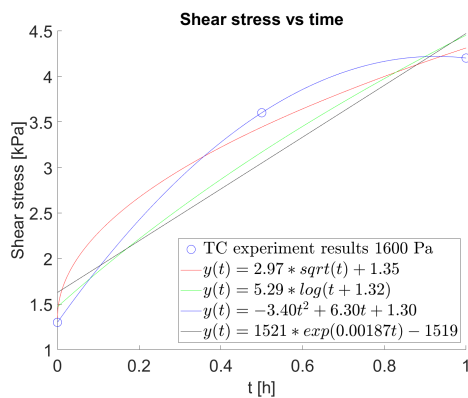


FIGURE 7. Results for fitting experimental data of 1600 Pa normal stress

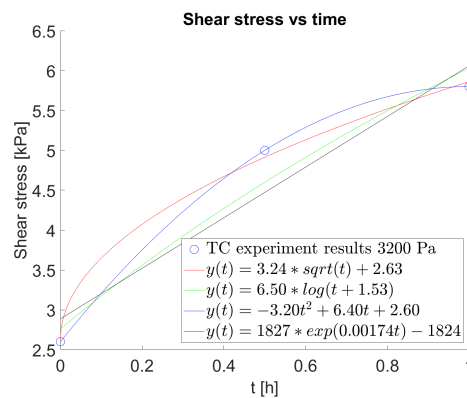


FIGURE 8. Results for fitting experimental data of 3200 Pa normal stress

In Equation 6.1 the generic form for the second order polynomial function can be seen. In Figure 9 the results of both the Rotation Restriction (RR) and Rolling model type C (RC)

cases can be seen. For the surface energy over time in the RC case no relationship similar to Equation 6.1 was found.

$$y(t) = \zeta(\alpha t^2 + \beta t + \epsilon) \quad \text{for } 0 \leq t \leq 1 \quad (6.1)$$

where:

$y(t)$  = Relevant parameter

$\zeta$  = ratio of alpha and beta from the experimental data (-0.52)

$\alpha$  = Coefficient 1 (quadratic)

$\beta$  = Coefficient 2 (linear)

$\epsilon$  = error

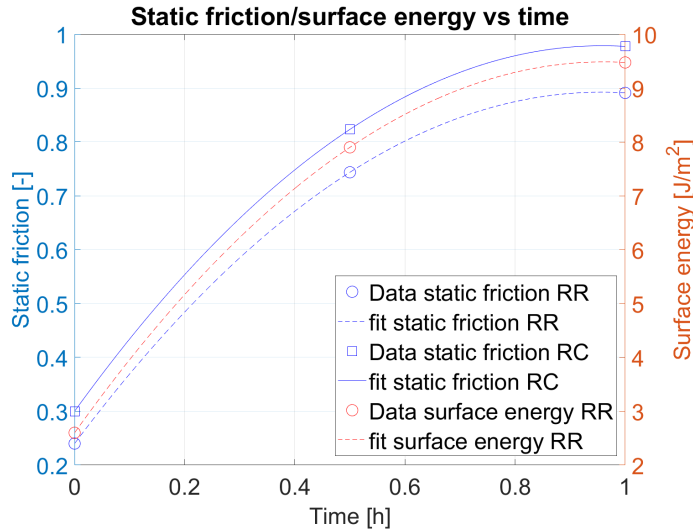


FIGURE 9. Static friction vs time fit rotation restriction case (scaled)

## 7. CONCLUSION

In this paper a generic method for modelling time consolidation is proposed. To model time consolidation experimental data is required and was obtained by performing the time consolidation experiment of Schulze.  $\text{NaBH}_4$  starts as a free-flowing material (before consolidation) and after 0.5 hour consolidation the material becomes non-flowing. Therefore,  $\text{NaBH}_4$  is significantly influenced by time consolidation. Next, modelling of time consolidation is done by using a simulation model of Schulze's RST and the final result is a relationship for the two most influential parameters (static friction and surface energy) over time enabling the instantaneous creation of a time-consolidated particle bed (between 0 and 1 hour). This can be used to create a particle bed in a simulation model for real-life applications that already went through the time consolidation process for example when storing  $\text{NaBH}_4$  in a silo.

## 8. RECOMMENDATIONS FOR FUTURE WORK

Potential future work can be to use the proposed method for modelling time consolidation for different materials or forms of material such as the granular form of  $\text{NaBH}_4$  to confirm the findings and method. More experiments should be performed for different preshear levels, normal stresses, consolidation times, consolidation stresses and repetitions. Next, extrapolation was necessary to determine the shear stress for no consolidation and it might be possible to look at the influence of the plasticity ratio. The plasticity ratio is a value between 0 and 1, where 0 makes EEPA a completely elastic model and 1 a completely plastic model. In Mohajeri's work [11] a plasticity ratio is used to capture the cohesive nature of iron ore and this value is used in

this paper. However, before consolidation the material is a free-flowing material and an elastic model is more suitable to capture that behaviour, so looking at the influence of the plasticity ratio to capture the behaviour before consolidation is a great opportunity for future work. The final recommendation for future work is related to both environmental and time consolidation effects. Romijn [10] studied the effect of moisture and humidity on the strength of  $\text{NaBH}_4$  and saw an increase in strength. In this paper time consolidation showed an even greater effect on the shear stress of  $\text{NaBH}_4$ . A study can be performed to combine the two effects with higher humidity levels and different consolidation times and look into the coupled effect of the two factors humidity and time consolidation.

## REFERENCES

- [1] G.C. Hegerl et al. “Causes of climate change over the historical record”. In: *Environmental Research Letters* 14.12 (2019), p. 123006.
- [2] G. Halkos and E. Gkampoura. “Assessing fossil fuels and renewables’ impact on energy poverty conditions in Europe”. In: *Energies* 16.1 (2023), p. 560.
- [3] Sinai. *How much does the shipping industry contribute to global CO2 emissions?* Website. Visited on 30-11-2023. Nov. 2023.
- [4] IMO. *IMO’s work to cut GHG emissions from ships*. Website. Visited on 30-11-2023. Nov. 2023.
- [5] M.C. van Bente, J.T. Padding, and D.L. Schott. “Towards Hydrogen-Fuelled Marine Vessels using Solid Hydrogen Carriers”. In: *ICBMH 2023: 14th International Conference on Bulk Materials Storage, Handling and Transportation*. 2023.
- [6] F. van Nievelt. “Maritime application of sodium borohydride as an energy carrier”. In: (2019).
- [7] D. Schulze. *Powders and bulk solids*. Springer, 2008.
- [8] P. Thool et al. “Evaluation of Time Consolidation Effect of Pharmaceutical Powders”. In: *Pharmaceutical Research* 39.12 (2022), pp. 3345–3357.
- [9] M. Carpin et al. “Caking of lactose: A critical review”. In: *Trends in Food Science & Technology* 53 (2016), pp. 1–12.
- [10] B. Romijn et al. *Bulk material properties of NaBH4*. Master’s Thesis. 2023.
- [11] M. Mohajeri. “Grabs and Cohesive Bulk Solids: Virtual prototyping using a validated co-simulation”. PhD thesis. PhD thesis, TU Delft. <https://doi.org/10.4233/uuid:b232e542-4881-4b02-8677...>, 2021.
- [12] J. Schwedes. “Review on testers for measuring flow properties of bulk solids”. In: *Granular matter* 5 (2003), pp. 1–43.
- [13] C. Bierwisch et al. “Three-dimensional discrete element models for the granular statics and dynamics of powders in cavity filling”. In: *Journal of the Mechanics and Physics of Solids* 57.1 (2009), pp. 10–31.
- [14] S.C. Thakur et al. “Micromechanical analysis of cohesive granular materials using the discrete element method with an adhesive elasto-plastic contact model”. In: *Granular Matter* 16 (2014), pp. 383–400.
- [15] R. Gaillac, P. Pullumbi, and F. Coudert. “ELATE: an open-source online application for analysis and visualization of elastic tensors”. In: *Journal of Physics: Condensed Matter* 28.27 (2016), p. 275201.

# B

## EXPERIMENTAL CONFIDENCE INTERVALS

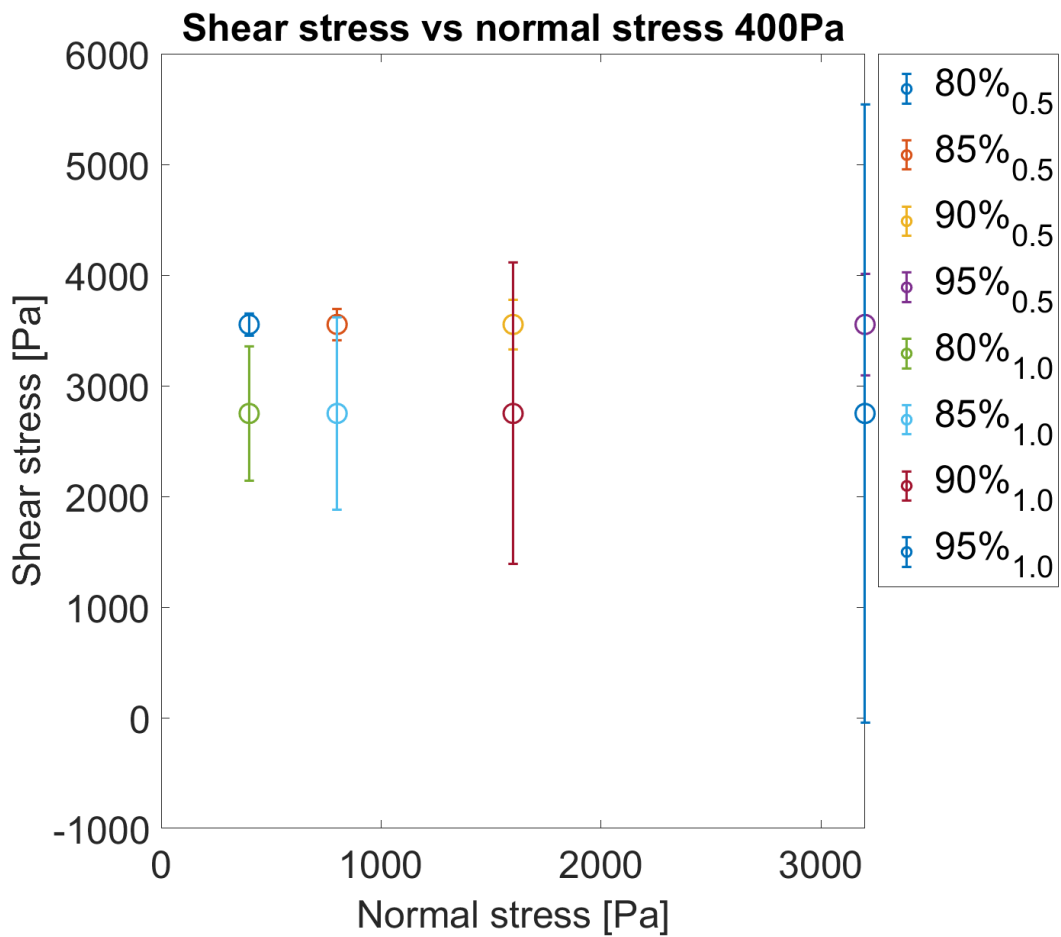


Figure B.1: Shear stress vs normal stress 400 Pa confidence intervals 80-95% for 0.5 and 1.0 hour of consolidation

## B

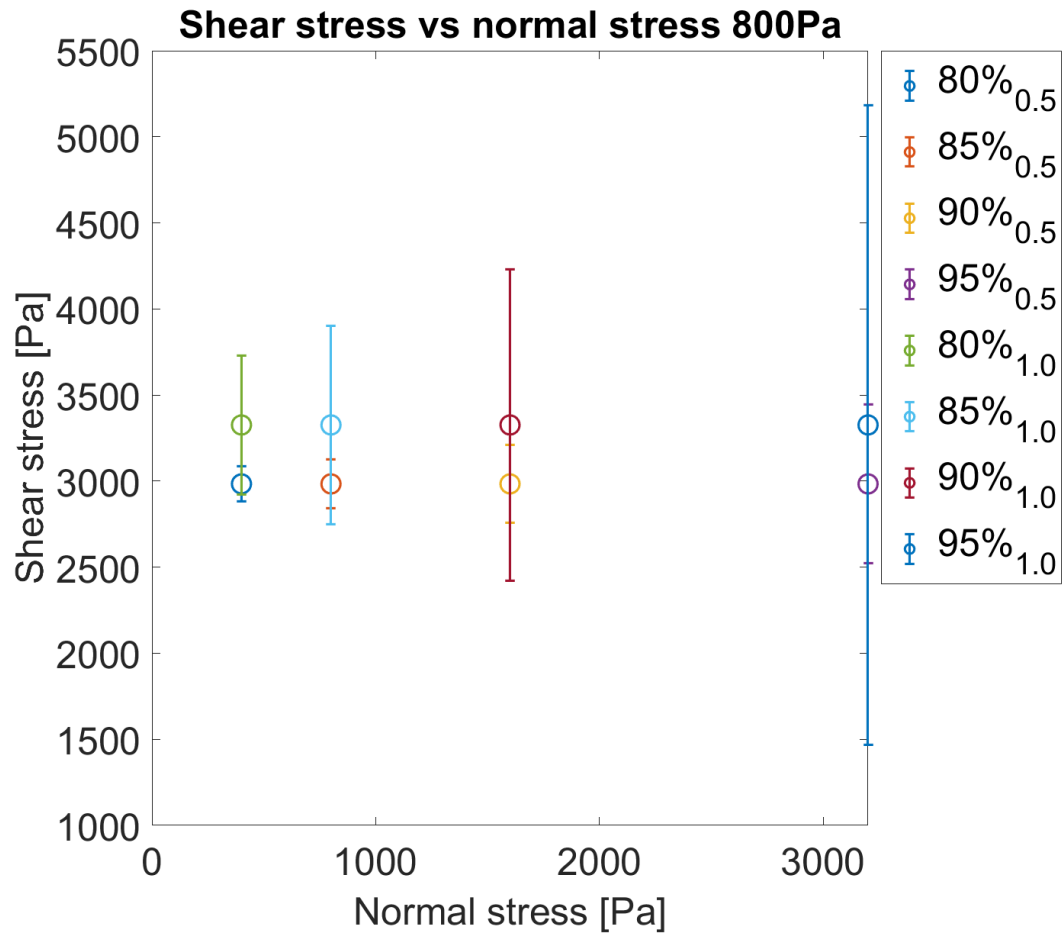


Figure B.2: Shear stress vs normal stress 800 Pa confidence intervals 80-95% for 0.5 and 1.0 hour of consolidation

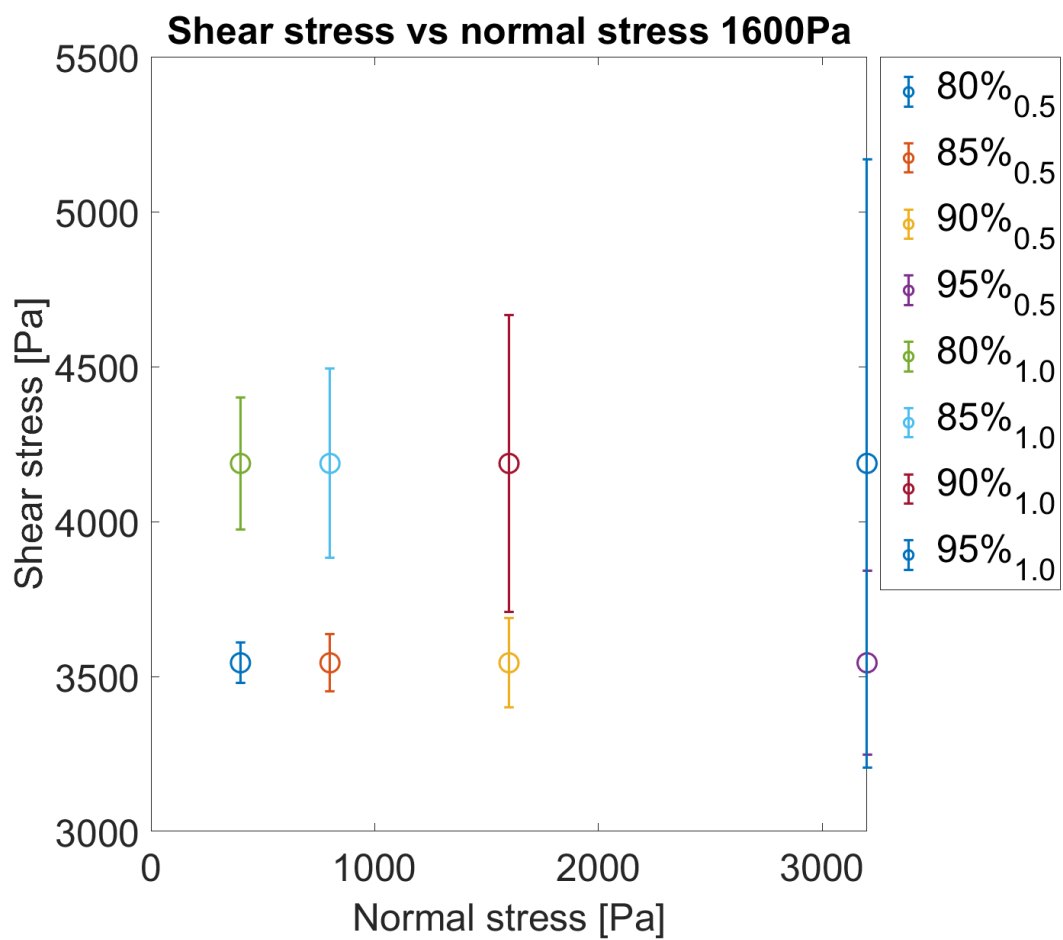


Figure B.3: Shear stress vs normal stress 1600 Pa confidence intervals 80-95% for 0.5 and 1.0 hour of consolidation

## B

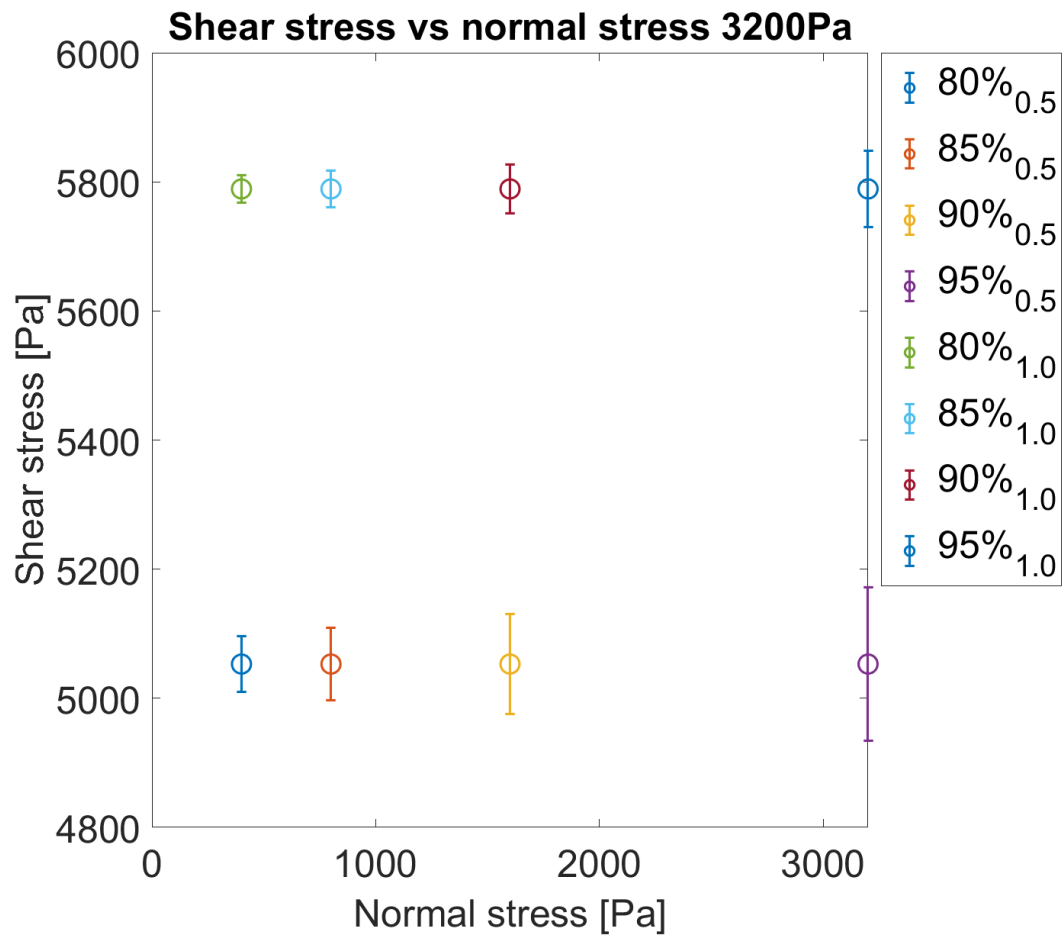


Figure B.4: Shear stress vs normal stress 3200 Pa confidence intervals 80-95% for 0.5 and 1.0 hour of consolidation

# C

## SENSITIVITY ANALYSIS 2

In appendix C the results for the second sensitivity analysis can be seen. From these graphs, it is concluded that the surface energy and the static friction are the most influential factors in the simulation similar to the first sensitivity analysis in Section 4.3.

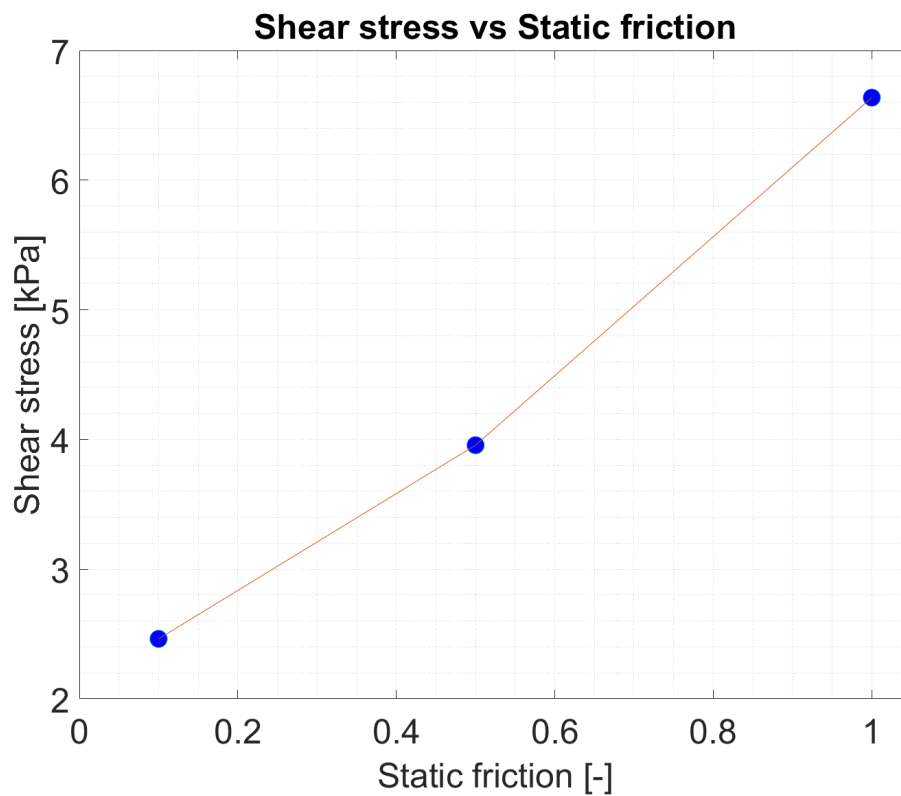


Figure C.1: Shear stress vs static friction (one-factor analysis)

C

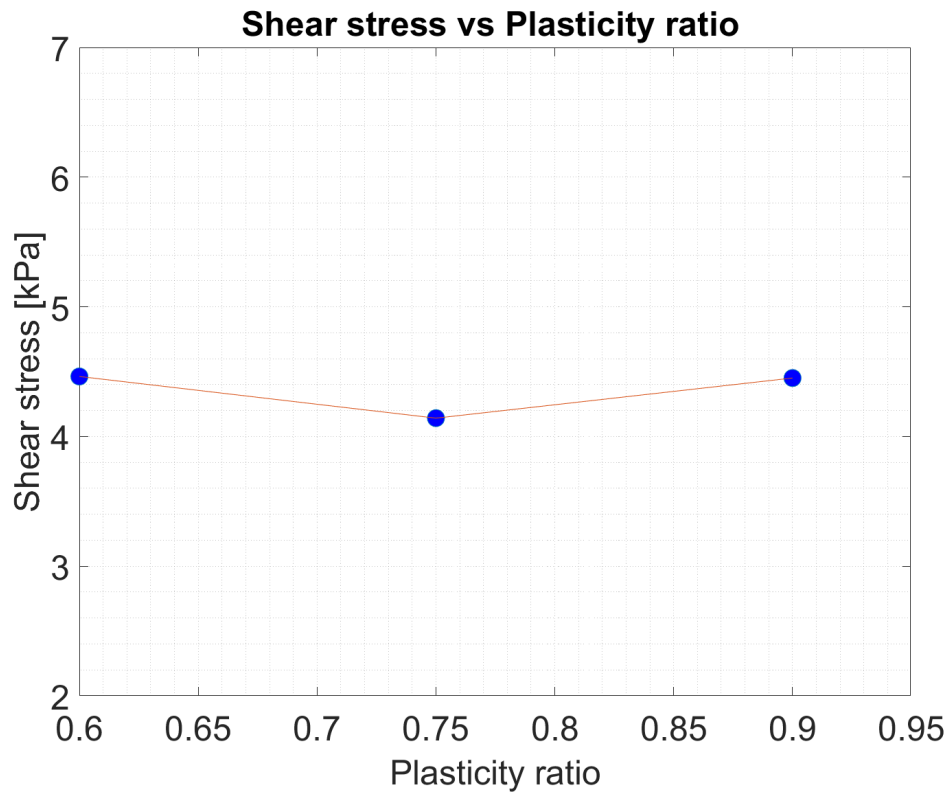


Figure C.2: Shear stress vs plasticity ratio (one-factor analysis)

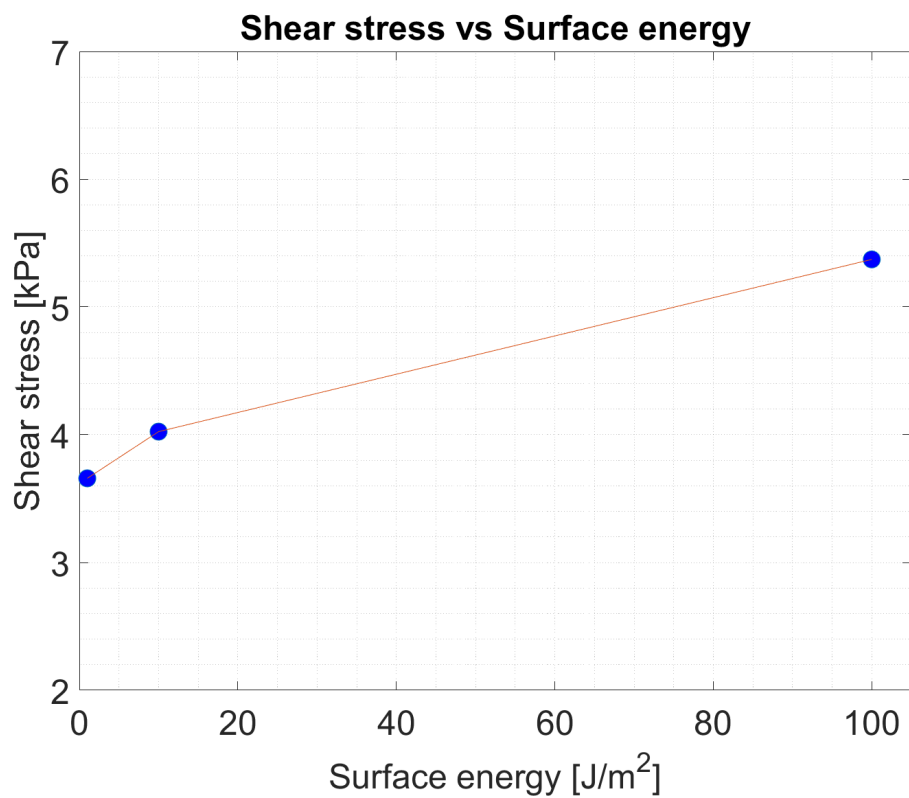


Figure C.3: Shear stress vs surface energy (one-factor analysis)

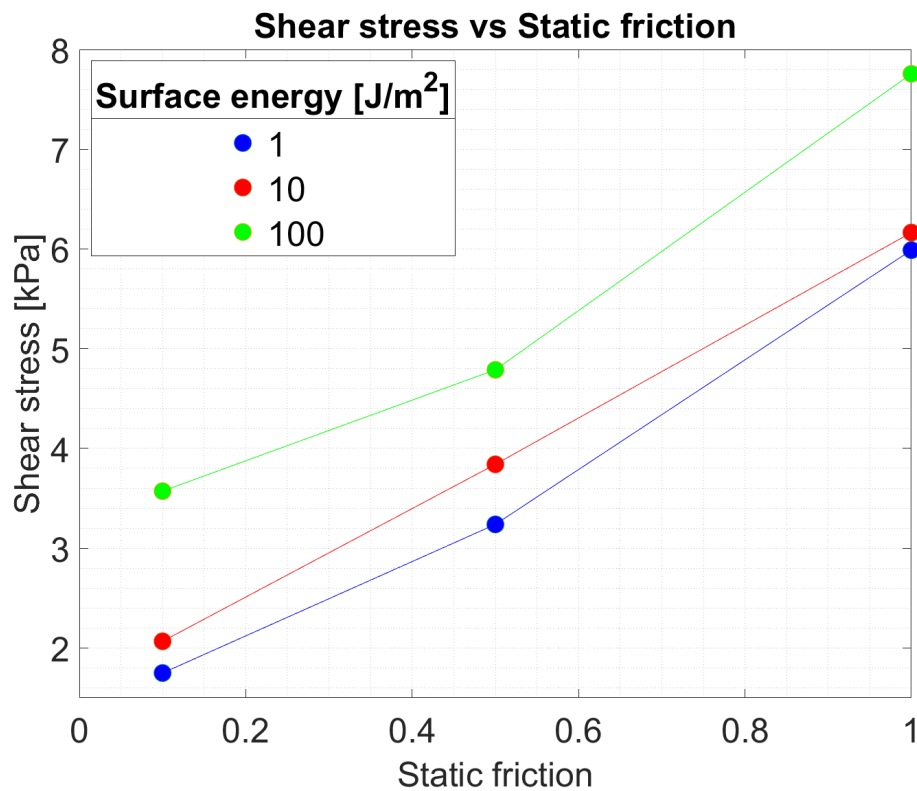


Figure C.4: Shear stress vs static friction and surface energy (two-factor analysis)

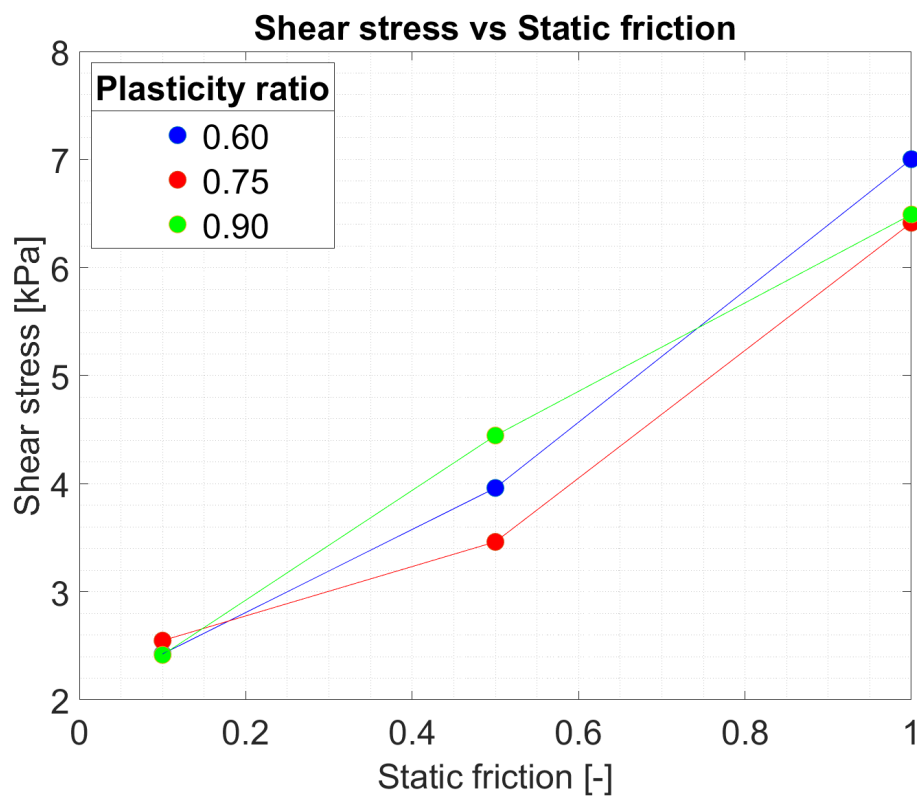


Figure C.5: Shear stress vs static friction and plasticity ratio (two-factor analysis)

C

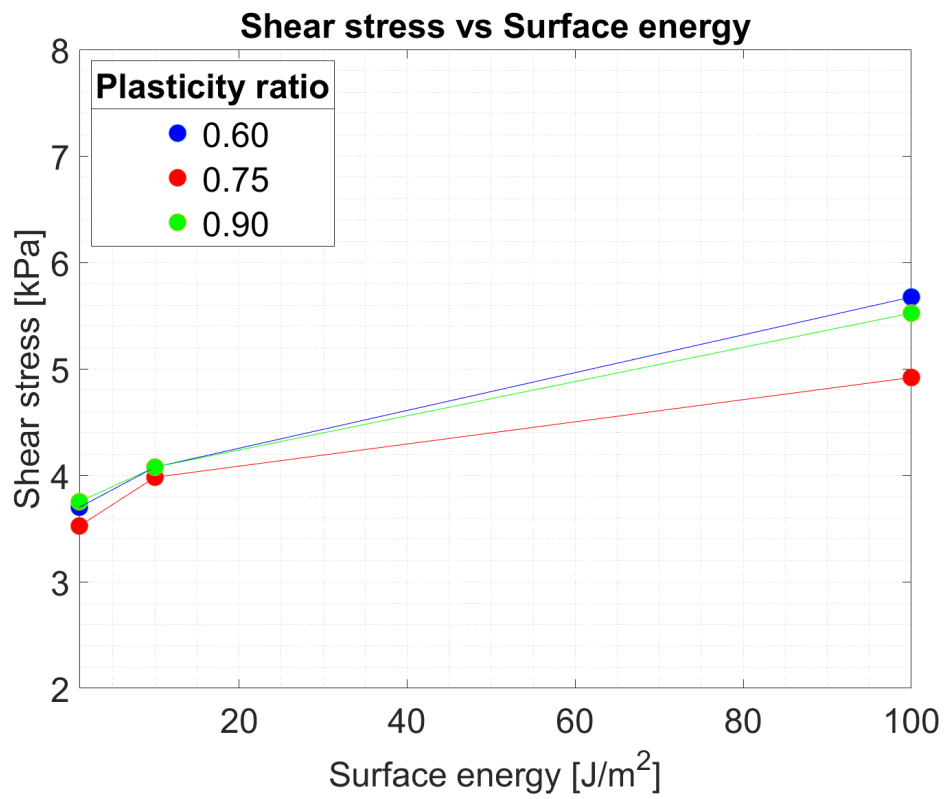


Figure C.6: Shear stress vs surface energy and plasticity ratio (two-factor analysis)

# D

## CONTOUR PLOTS ROLLING TYPE C

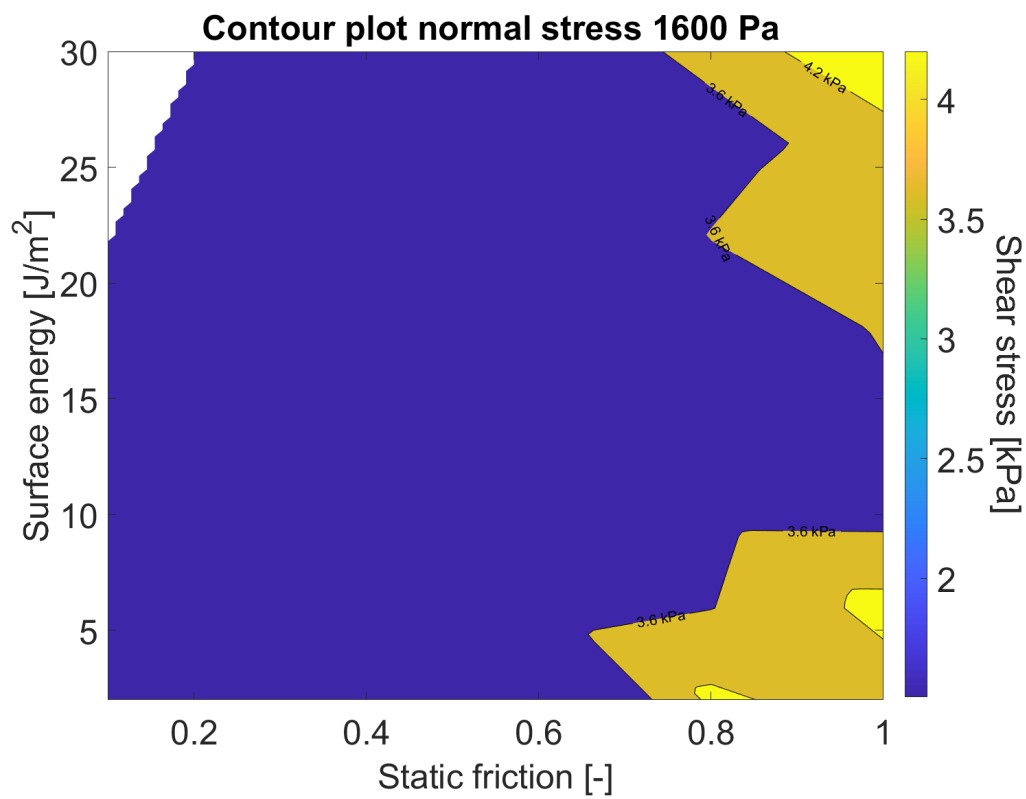


Figure D.1: Contour plot Shear stress for normal stress 1600 Pa Rolling type C case

D

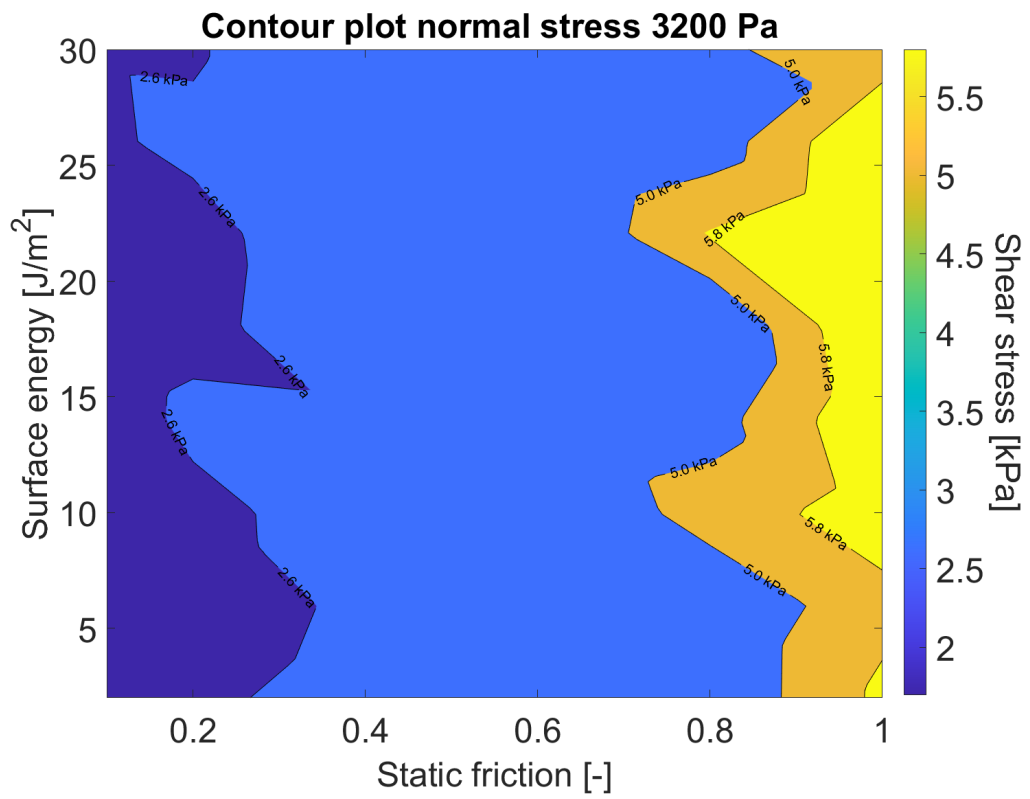


Figure D.2: Contour plot Shear stress for normal stress 3200 Pa Rolling type C case

# E

## RESULTS ROTATION RESTRICTION CASE OPTIMISED PARAMETER SET SEARCH AND EXTRAPOLATION

In Figure E.1 the overlap for 0.5 hours of consolidation can be seen and the final result of the overlap analysis can be seen in Table E.1.

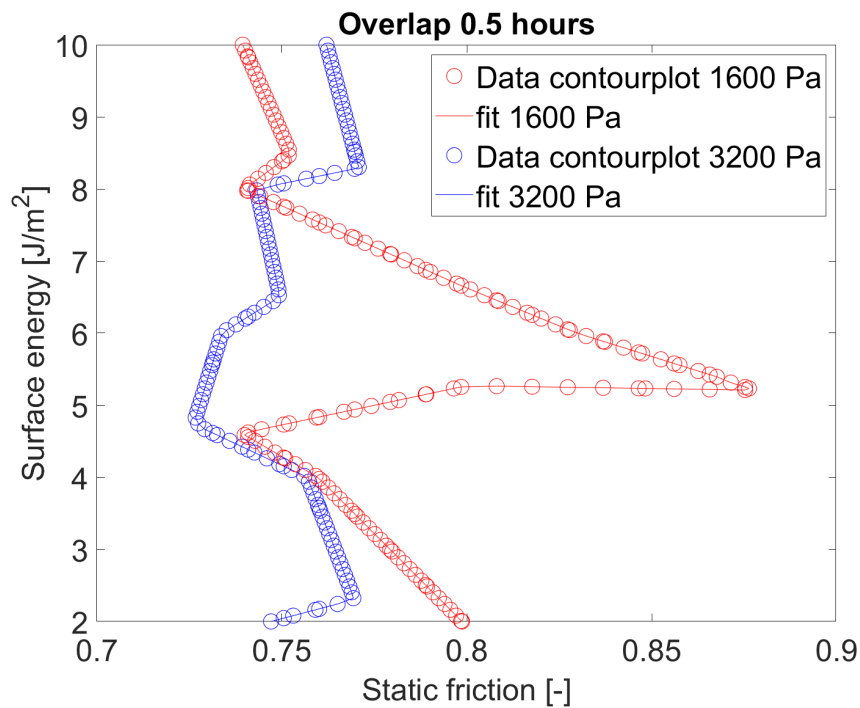


Figure E.1: Surface energy vs static friction parameter set optimisation for 0.5 hour consolidation Rotation Restriction case

Table E.1: Results parameter set optimisation Rotation Restriction case

Time consolidation [hours]	0	0.5	1.0
Static friction [-]	non	0.743564	0.89101
Surface energy	non	7.89899	9.474745

First, the shear stress data for normal stresses 1600 (red) and 3200 (blue) Pa were fitted and the results can be seen in Figure E.2. The form of the fit can be seen in Equation E.1 and the equations for the 1600 and 3200 Pa normal stress can be seen in Equations E.3 and E.4 respectively. The fit that is used is a second order polynomial fit.

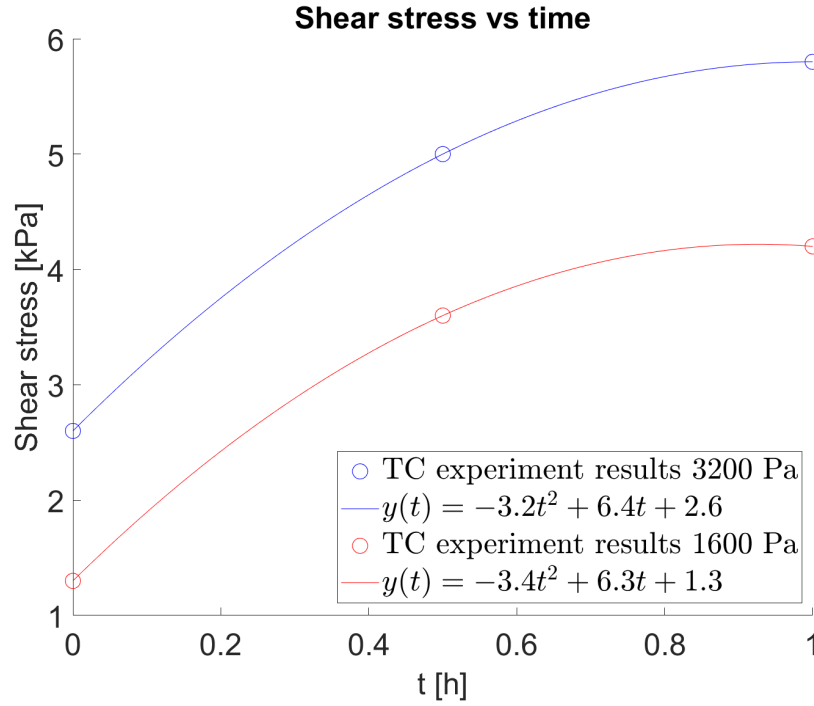


Figure E.2: Shear stress vs time fit for experimental data

$$y(t) = \alpha t^2 + \beta t + C \quad (\text{E.1})$$

$$\zeta = \frac{\alpha}{\beta} \quad (\text{E.2})$$

$$\text{shear stress}_{1600}(t) = -3.4t^2 + 6.3t + 1.3 \quad \text{for } 0 < t \leq 1 \quad (\text{E.3})$$

$$\text{shear stress}_{3200}(t) = -3.2t^2 + 6.4t + 2.6 \quad \text{for } 0 < t \leq 1 \quad (\text{E.4})$$

$$\zeta_{mean} = \frac{\frac{-3.4}{6.3} + \frac{-3.2}{6.4}}{2} = -0.52 \quad (\text{E.5})$$

With these equations a ratio of  $\alpha$  and  $\beta$  is determined. The mean of the ratio's of 1600 Pa and 3200 Pa is used and is equal to 0.52 as can be seen from Equation E.5. With the two datapoints of 0.5 and 1.0 hours of consolidation that can be seen in Table 4.7 and the  $\zeta_{mean} = 0.52$  an extrapolation to find the point for 0 hours of consolidation is performed. The upperbound of the range for the surface energy that will be used is 1 – 5 J/m<sup>2</sup> and are iteratively used to fit the data. In Figure E.3 the result can be seen and for every fit in the figure the ratio  $\zeta$  is determined.  $\zeta_{mean}$  is matched with the results to determine the appropriate fit for the static friction. In Table 4.10 the results can be seen and for a value of  $\zeta = 0.52$  a surface energy 2.6 J/m<sup>2</sup> is required.

Table E.2: Results  $\zeta$  analysis for surface energy Rotation Restriction case

Surface energy [J/m <sup>2</sup> ]	$\zeta$
1.0	-0.55679
1.1	-0.55504
1.2	-0.55323
1.3	-0.55136
1.4	-0.54943
1.5	-0.54744
1.6	-0.54537
1.7	-0.54323
1.8	-0.54102
1.9	-0.53872
2.0	-0.53634
2.1	-0.53387
2.2	-0.5313
2.3	-0.52864
2.4	-0.52586
2.5	-0.52297
<b>2.6</b>	<b>-0.51996</b>
2.7	-0.51682
2.8	-0.51355
2.9	-0.51012
3.0	-0.50654
3.1	-0.5028
3.2	-0.49887
3.3	-0.49475
3.4	-0.49043
3.5	-0.48588
3.6	-0.48109
3.7	-0.47603
3.8	-0.4707
3.9	-0.46506
4.0	-0.45908
4.1	-0.45274
4.2	-0.446
4.3	-0.43882
4.4	-0.43116
4.5	-0.42296
4.6	-0.41418
4.7	-0.40474
4.8	-0.39456
4.9	-0.38356
5.0	-0.37163

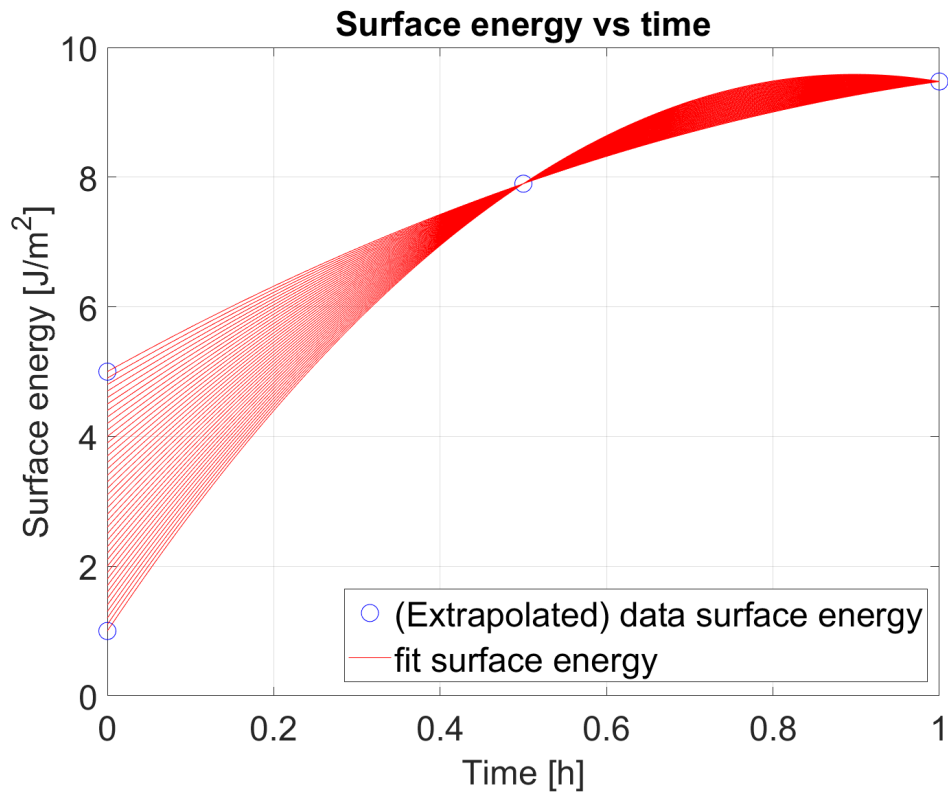


Figure E.3: Surface energy vs time potential fits Rotation Restriction case

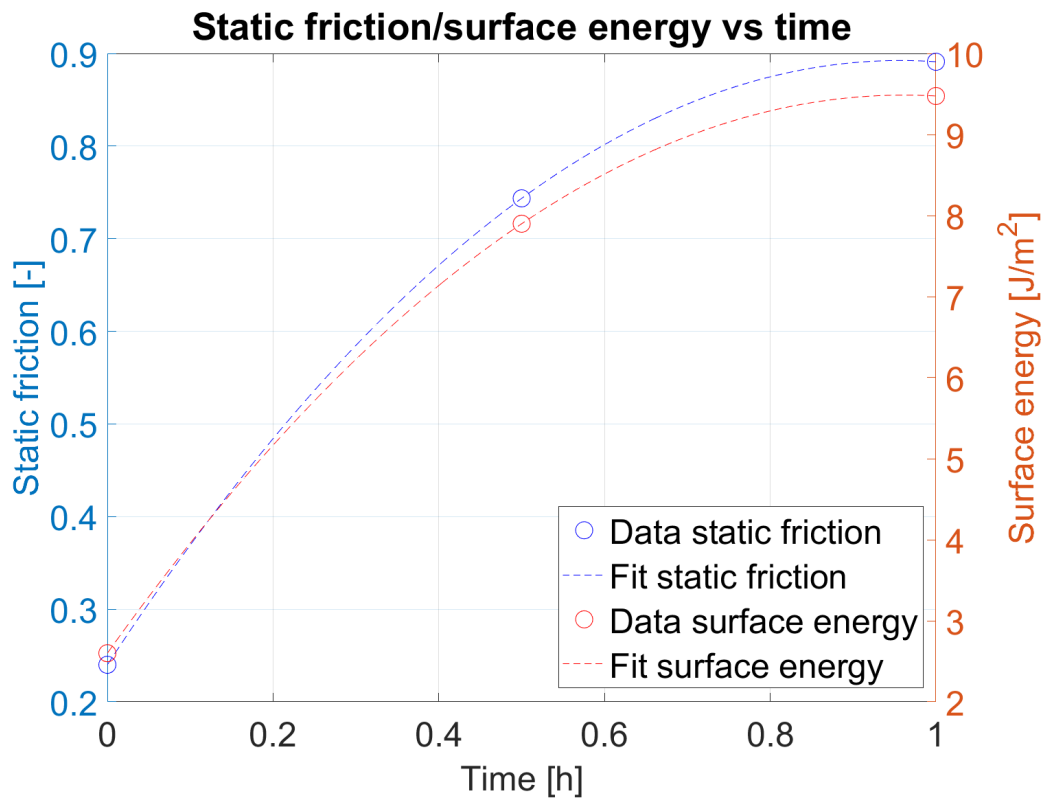


Figure E.4: Static friction/surface energy vs time fit Rotation Restriction case (scaled)

The relationship that can be found by the fit is the one in Equation E.6. The final scaled plot for the surface energy and static friction over time can be seen in Figure E.4.

$$y_{surface}(t) = -0.52(14.32t^2 - 27.54t) - 5 \quad \text{for } 0 < t \leq 1 \quad (\text{E.6})$$



# F

## RESULTS ROLLING TYPE C CASE OPTIMISED PARAMETER SET SEARCH AND EXTRAPOLATION

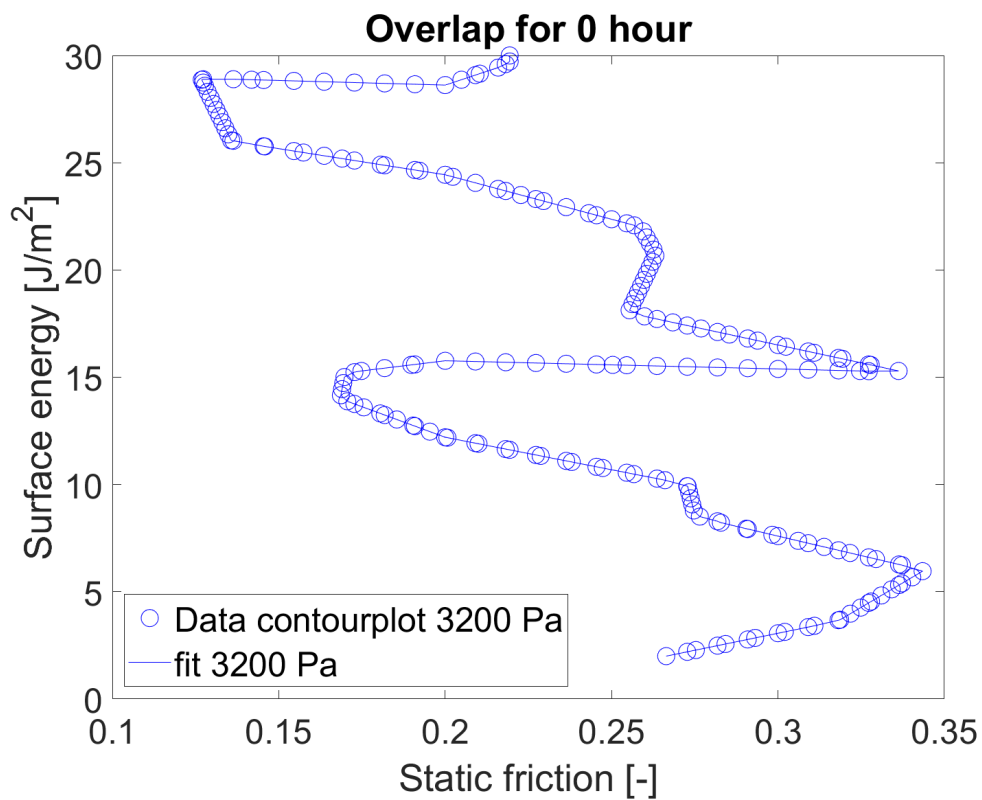


Figure E1: Surface energy vs static friction parameter set optimisation for 0 hour consolidation Rolling type C case

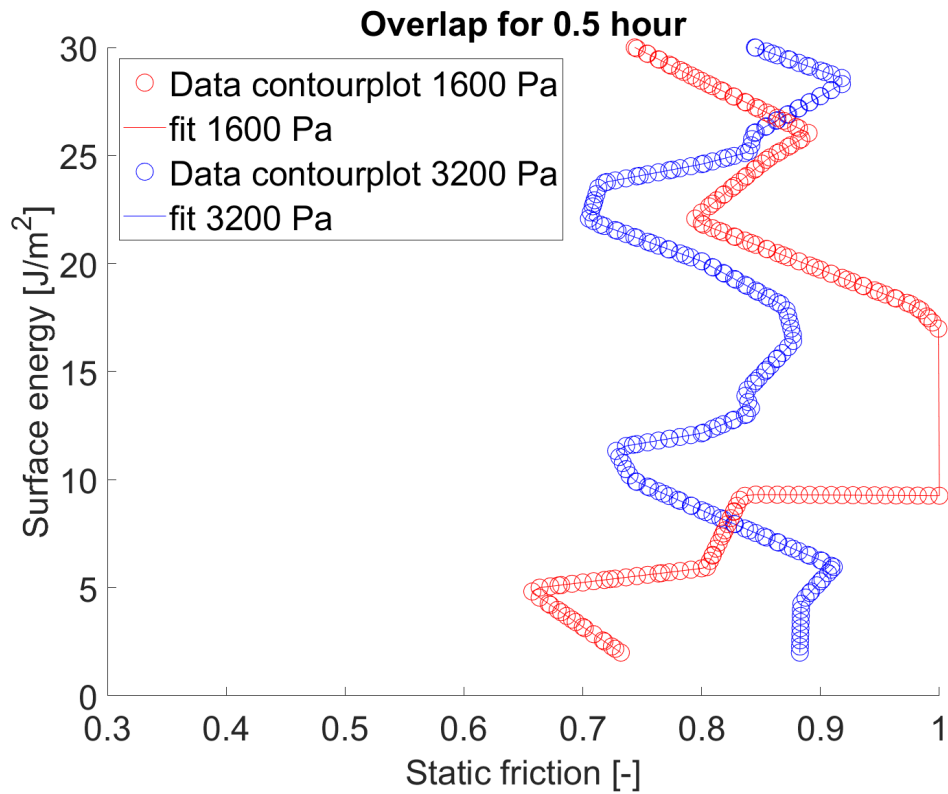


Figure E2: Surface energy vs static friction parameter set optimisation for 0.5 hour consolidation Rolling type C case

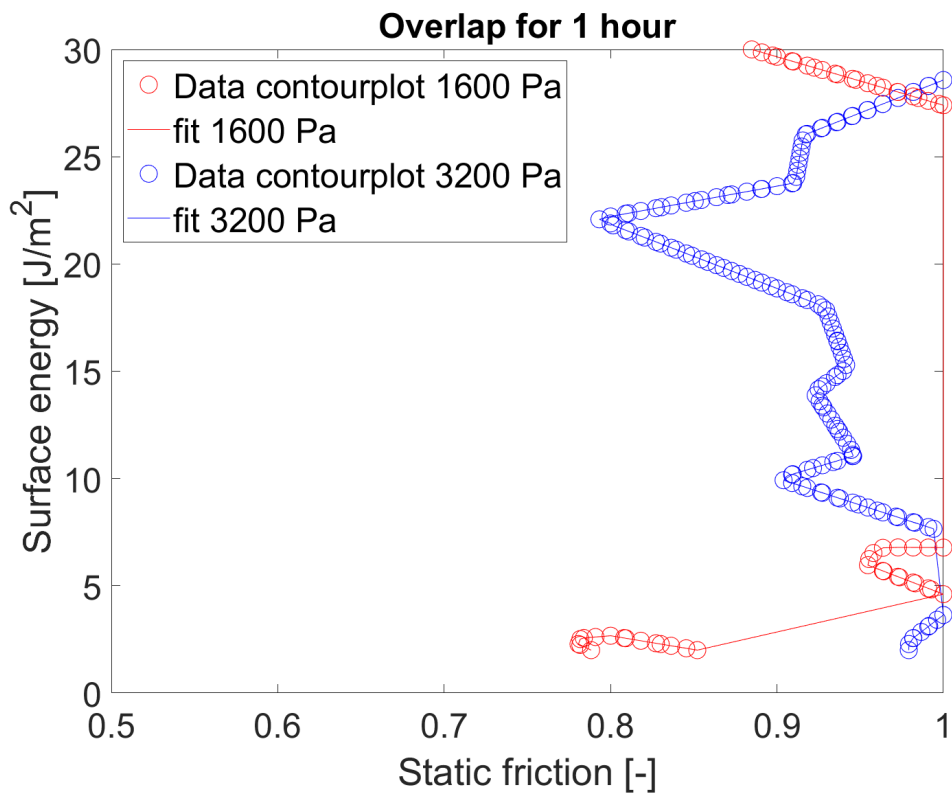


Figure E3: Surface energy vs static friction parameter set optimisation for 1 hour consolidation Rolling type C case

Table E1: Static friction vs time potential fits for Rolling type C case

Static friction [-]	$\zeta$	Static friction [-]	$\zeta$
0.05	-0.55976	0.05	-0.57181
0.06	-0.55824	0.06	-0.57048
0.07	-0.55668	0.07	-0.56911
0.08	-0.55508	0.08	-0.5677
0.09	-0.55343	0.09	-0.56625
0.1	-0.55173	0.1	-0.56475
0.11	-0.54998	0.11	-0.56321
0.12	-0.54817	0.12	-0.56163
0.13	-0.5463	0.13	-0.55999
0.14	-0.54438	0.14	-0.5583
0.15	-0.5424	0.15	-0.55656
0.16	-0.54034	0.16	-0.55476
0.17	-0.53822	0.17	-0.5529
0.18	-0.53603	0.18	-0.55098
0.19	-0.53376	0.19	-0.54899
0.2	-0.53141	0.2	-0.54693
0.21	-0.52898	0.21	-0.5448
0.22	-0.52646	0.22	-0.54259
0.23	-0.52384	0.23	-0.5403
<b>0.24</b>	<b>-0.52113</b>	0.24	-0.53793
<b>0.25</b>	<b>-0.5183</b>	0.25	-0.53546
0.26	-0.51537	0.26	-0.5329
0.27	-0.51232	0.27	-0.53023
0.28	-0.50914	0.28	-0.52746
0.29	-0.50583	0.29	-0.52457
0.3	-0.50238	<b>0.3</b>	<b>-0.52156</b>

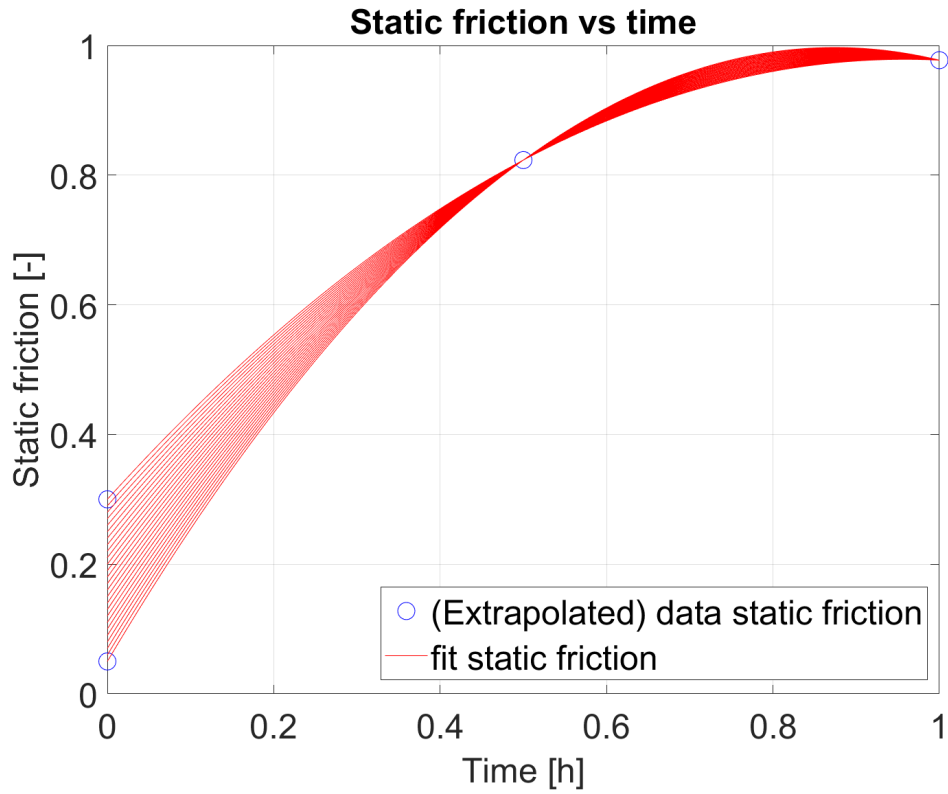


Figure F4: Static friction vs time potential fits for Rolling type C case (optimised parameter set 1)

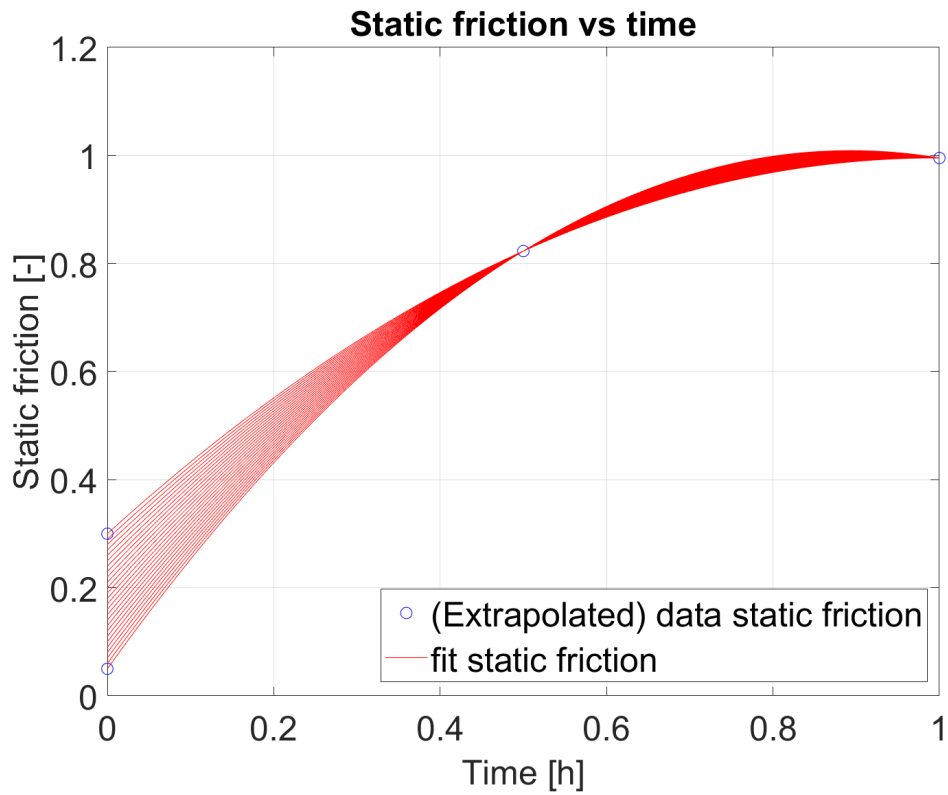


Figure E5: Static friction vs time potential fits for Rolling type C case (optimised parameter set 2)

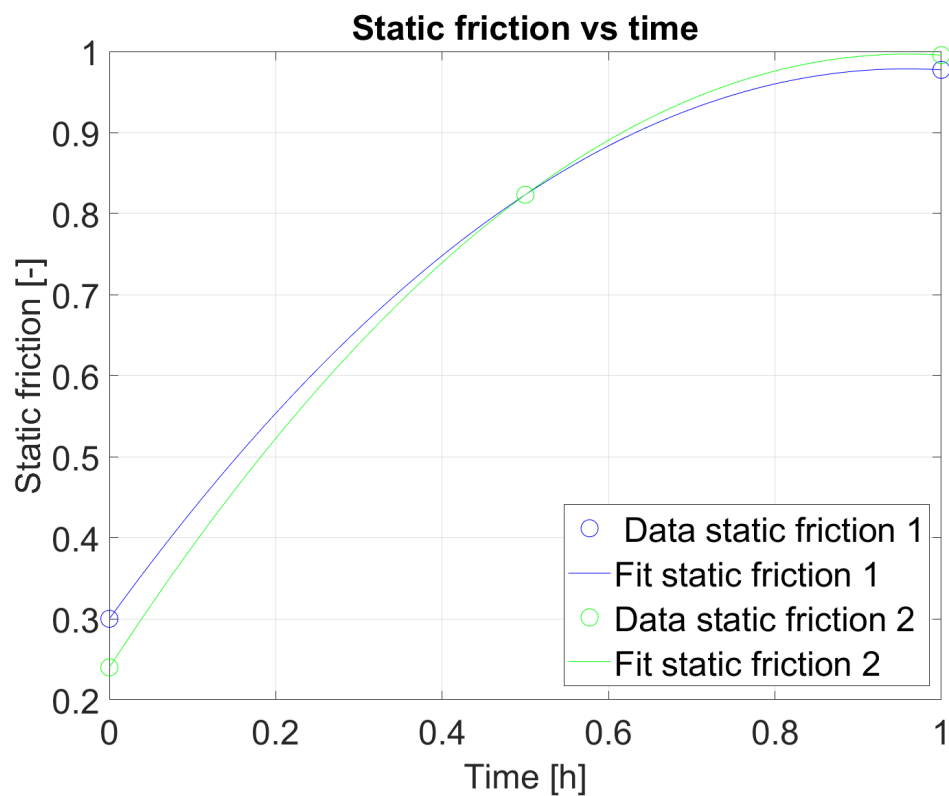


Figure E6: Static friction vs time fit Rolling type C case (scaled)

$$\text{static friction}_1(t) = -0.52(1.581t^2 - 3.033t - 0.462) \quad \text{for } 0 < t \leq 1 \quad (\text{E1})$$

$$\text{static friction}_2(t) = -0.52(1.420t^2 - 2.723t - 0.577) \quad \text{for } 0 < t \leq 1 \quad (\text{E2})$$



## REFERENCES

- [1] Gabriele C Hegerl et al. "Causes of climate change over the historical record". In: *Environmental Research Letters* 14.12 (2019), p. 123006.
- [2] George Halkos and Eleni-Christina Gkampoura. "Assessing fossil fuels and renewables' impact on energy poverty conditions in Europe". In: *Energies* 16.1 (2023), p. 560.
- [3] Sinai. *How much does the shipping industry contribute to global CO2 emissions?* Website. Visited on 30-11-2023. Nov. 2023.
- [4] IMO. *IMO's work to cut GHG emissions from ships*. Website. Visited on 30-11-2023. Nov. 2023.
- [5] Sonal Singh et al. "Hydrogen: A sustainable fuel for future of the transport sector". In: *Renewable and sustainable energy reviews* 51 (2015), pp. 623–633.
- [6] Jose Bellosta Von Colbe et al. "Application of hydrides in hydrogen storage and compression: Achievements, outlook and perspectives". In: *international journal of hydrogen energy* 44.15 (2019), pp. 7780–7808.
- [7] Muhammad Aziz. "Liquid hydrogen: A review on liquefaction, storage, transportation, and safety". In: *Energies* 14.18 (2021), p. 5917.
- [8] MS El-Eskandarany. "Solid-state hydrogen storage nanomaterials for fuel cell applications". In: *William Andrew Publishing: Norwich, NY, USA* (2020), pp. 229–261.
- [9] Henrietta W Langmi et al. "Hydrogen storage". In: *Electrochemical power sources: Fundamentals, systems, and applications*. Elsevier, 2022, pp. 455–486.
- [10] Seyed Ehsan Hosseini. "Chapter 5 - Hydrogen storage and delivery challenges". In: *Fundamentals of Hydrogen Production and Utilization in Fuel Cell Systems*. Ed. by Seyed Ehsan Hosseini. Elsevier, 2023, pp. 237–254. ISBN: 978-0-323-88671-0. DOI: <https://doi.org/10.1016/B978-0-323-88671-0.00003-6>. URL: <https://www.sciencedirect.com/science/article/pii/B9780323886710000036>.
- [11] T Capurso et al. "Perspective of the role of hydrogen in the 21st century energy transition". In: *Energy Conversion and Management* 251 (2022), p. 114898.
- [12] Paul Brack, Sandie E Dann, and KG Upul Wijayantha. "Heterogeneous and homogenous catalysts for hydrogen generation by hydrolysis of aqueous sodium borohydride (NaBH<sub>4</sub>) solutions". In: *Energy Science & Engineering* 3.3 (2015), pp. 174–188.
- [13] Rajasree Retnamma, Augusto Q Novais, and CM Rangel. "Kinetics of hydrolysis of sodium borohydride for hydrogen production in fuel cell applications: A review". In: *International Journal of Hydrogen Energy* 36.16 (2011), pp. 9772–9790.
- [14] DMF Santos and CAC Sequeira. "Sodium borohydride as a fuel for the future". In: *Renewable and Sustainable Energy Reviews* 15.8 (2011), pp. 3980–4001.
- [15] Floris van Nievelt. "Maritime application of sodium borohydride as an energy carrier". In: (2019).
- [16] Hani Nasser Abdelhamid. "A review on hydrogen generation from the hydrolysis of sodium borohydride". In: *international journal of hydrogen energy* 46.1 (2021), pp. 726–765.
- [17] MC van Bente, JT Padding, and DL Schott. "Towards Hydrogen-Fuelled Marine Vessels using Solid Hydrogen Carriers". In: *ICBMH 2023: 14th International Conference on Bulk Materials Storage, Handling and Transportation*. 2023.
- [18] Timothy Lee et al. "Air-Stable Nanoporous Aluminum/Lithium Borohydride Fuel Pellets for Onboard Hydrogen Generation by Hydrolysis with Pure Water". In: *ACS Applied Energy Materials* 4.9 (2021), pp. 9742–9750.
- [19] Tsuneo Imamoto. "Organocerium reagents". In: *Comprehensive organic synthesis* 1 (1991), pp. 231–250.
- [20] HI Schlesinger et al. "Sodium borohydride, its hydrolysis and its use as a reducing agent and in the generation of hydrogen<sup>1</sup>". In: *Journal of the American Chemical Society* 75.1 (1953), pp. 215–219.

- [21] Yakir Nagar et al. "Modeling the mechanical behavior of sodium borohydride (NaBH<sub>4</sub>) powder". In: *Materials & Design* 108 (2016), pp. 240–249.
- [22] Mingyang Chen et al. "Caking of crystals: Characterization, mechanisms and prevention". In: *Powder Technology* 337 (2018), pp. 51–67.
- [23] Prajwal Thool et al. "Evaluation of Time Consolidation Effect of Pharmaceutical Powders". In: *Pharmaceutical Research* 39.12 (2022), pp. 3345–3357.
- [24] E Teunou and JJ Fitzpatrick. "Effect of storage time and consolidation on food powder flowability". In: *Journal of Food Engineering* 43.2 (2000), pp. 97–101.
- [25] Dietmar Schulze. *Powders and bulk solids*. Springer, 2008.
- [26] M Mohajeri. "Grabs and Cohesive Bulk Solids: Virtual prototyping using a validated co-simulation". PhD thesis. PhD thesis, TU Delft. <https://doi.org/10.4233/uuid:b232e542-4881-4b02-8677...>, 2021.
- [27] Shun Zhang et al. "Scaled-up rice grain modelling for DEM calibration and the validation of hopper flow". In: *Biosystems engineering* 194 (2020), pp. 196–212.
- [28] CJ Coetzee. "Calibration of the discrete element method". In: *Powder Technology* 310 (2017), pp. 104–142.
- [29] Jörg Schwedes. "Review on testers for measuring flow properties of bulk solids". In: *Granular matter* 5 (2003), pp. 1–43.
- [30] John W Carson and Harald Wilms. "Development of an international standard for shear testing". In: *Powder technology* 167.1 (2006), pp. 1–9.
- [31] S Kamath, VM Puri, and HB Manbeck. "Flow property measurement using the Jenike cell for wheat flour at various moisture contents and consolidation times". In: *Powder technology* 81.3 (1994), pp. 293–297.
- [32] Ewa Domian and K Poszytek. "Wheat flour flow ability as affected by water activity, storage time and consolidation". In: *International agrophysics* 19.2 (2005).
- [33] EFCE Working Party on the Mechanics of Particulate Solids. *Standard shear testing technique for particulate solids using the Jenike shear cell*. IChemE, 1989.
- [34] Y Venkat Reddy and Sriram Venkatesh. "Flow characteristic evaluation of iron ore for design of bunkers and chutes with different liner materials". In: *Materials Today: Proceedings* 76 (2023), pp. 95–102.
- [35] Michael Röck and Jörg Schwedes. "Investigations on the caking behaviour of bulk solids—macroscale experiments". In: *Powder Technology* 157.1-3 (2005), pp. 121–127.
- [36] A Serkan Çağlı et al. "Flow property measurement using Jenike shear cell for 7 different bulk solids". In: *Proceedings of European Congress of Chemical Engineering (ECCE-6), Copenhagen*. 2007, pp. 16–20.
- [37] Tatum Swize et al. "Impact of shear history on powder flow characterization using a ring shear tester". In: *Journal of pharmaceutical sciences* 108.1 (2019), pp. 750–754.
- [38] B Romijn et al. *Bulk material properties of NaBH<sub>4</sub>*. Master's Thesis. 2023.
- [39] Mélanie Carpin et al. "Caking of lactose: A critical review". In: *Trends in Food Science & Technology* 53 (2016), pp. 1–12.
- [40] Mingyang Chen et al. "Amorphous and humidity caking: A review". In: *Chinese Journal of Chemical Engineering* 27.6 (2019), pp. 1429–1438.
- [41] Igor E Dzyaloshinskii, Efrat M Lifshitz, and Lev P Pitaevskii. "The general theory of van der Waals forces". In: *Advances in Physics* 10.38 (1961), pp. 165–209.
- [42] JJ Fitzpatrick et al. "Glass transition and the flowability and caking of powders containing amorphous lactose". In: *Powder Technology* 178.2 (2007), pp. 119–128.
- [43] Markus Hartmann and Stefan Palzer. "Caking of amorphous powders—Material aspects, modelling and applications". In: *Powder Technology* 206.1-2 (2011), pp. 112–121.
- [44] SW Billings, JE Bronlund, and AHJ Paterson. "Effects of capillary condensation on the caking of bulk sucrose". In: *Journal of Food Engineering* 77.4 (2006), pp. 887–895.
- [45] Arthur W Adamson, Alice Petry Gast, et al. *Physical chemistry of surfaces*. Vol. 150. Interscience publishers New York, 1967.

- [46] Amy M Beaird, Thomas A Davis, and Michael A Matthews. "Deliquescence in the hydrolysis of sodium borohydride by water vapor". In: *Industrial & engineering chemistry research* 49.20 (2010), pp. 9596–9599.
- [47] William R Ketterhagen, Mary T am Ende, and Bruno C Hancock. "Process modeling in the pharmaceutical industry using the discrete element method". In: *Journal of pharmaceutical sciences* 98.2 (2009), pp. 442–470.
- [48] Adham Hashibon et al. "A DEM contact model for history-dependent powder flows". In: *Computational Particle Mechanics* 3 (2016), pp. 437–448.
- [49] Subhash C Thakur et al. "Micromechanical analysis of cohesive granular materials using the discrete element method with an adhesive elasto-plastic contact model". In: *Granular Matter* 16 (2014), pp. 383–400.
- [50] John P Morrissey. "Discrete element modelling of iron ore pellets to include the effects of moisture and fines". In: (2013).
- [51] M Javad Mohajeri, Huy Q Do, and Dingena L Schott. "DEM calibration of cohesive material in the ring shear test by applying a genetic algorithm framework". In: *Advanced Powder Technology* 31.5 (2020), pp. 1838–1850.
- [52] Mohammadjavad Mohajeri, Cees van Rhee, and Dingena L Schott. "Penetration resistance of cohesive iron ore: A DEM study". In: *9th International Conference on Conveying and Handling of Particulate Solids*. 2018, pp. 1–7.
- [53] M Javad Mohajeri, CV Rhee, and Dingena L Schott. "Coarse graining of adhesive elasto-plastic DEM contact models in quasi-static processes". In: *13th International Conference on Bulk Materials Storage, Handling & Transportation*. 2019.
- [54] Jiju Antony. *Design of experiments for engineers and scientists*. Elsevier, 2023.
- [55] Virgil L Anderson and Robert A McLean. *Design of experiments: a realistic approach*. CRC Press, 2018.
- [56] Alisa Vasilenko et al. "Role of consolidation state in the measurement of bulk density and cohesion". In: *Powder technology* 239 (2013), pp. 366–373.
- [57] Lars P Maltby, Gisle G Enstad, and Sunil R de Selva. "Investigation of the behaviour of powders under and after consolidation". In: *Particle & particle systems characterization* 12.1 (1995), pp. 16–27.
- [58] Claas Bierwisch et al. "Three-dimensional discrete element models for the granular statics and dynamics of powders in cavity filling". In: *Journal of the Mechanics and Physics of Solids* 57.1 (2009), pp. 10–31.
- [59] Richard F Gunst and Robert L Mason. "Fractional factorial design". In: *Wiley Interdisciplinary Reviews: Computational Statistics* 1.2 (2009), pp. 234–244.
- [60] Romain Gaillac, Pluton Pullumbi, and François-Xavier Coudert. "ELATE: an open-source online application for analysis and visualization of elastic tensors". In: *Journal of Physics: Condensed Matter* 28.27 (2016), p. 275201.
- [61] Jun Ai et al. "Assessment of rolling resistance models in discrete element simulations". In: *Powder Technology* 206.3 (2011), pp. 269–282.
- [62] SW Lommen. "Virtual prototyping of grabs: co-simulations of discrete element and rigid body models". In: (2016).
- [63] Mustafa Ucgul, John M Fielke, and Chris Saunders. "Three-dimensional discrete element modelling of tillage: Determination of a suitable contact model and parameters for a cohesionless soil". In: *Biosystems Engineering* 121 (2014), pp. 105–117.
- [64] Stef Lommen, Dingena Schott, and Gabriel Lodewijks. "DEM speedup: Stiffness effects on behavior of bulk material". In: *Particuology* 12 (2014), pp. 107–112.
- [65] Corné J Coetzee. "Particle upscaling: Calibration and validation of the discrete element method". In: *Powder technology* 344 (2019), pp. 487–503.
- [66] Shalabh. *Regression analysis*. Indian Institute of Technology Kanpur, 2015.